UNIVERSITÀ DEGLI STUDI DEL PIEMONTE ORIENTALE
"AMEDEO AVOGADRO"

DIPARTIMENTO DI SCIENZE DEL FARMACO

Dottorato di Ricerca in "Scienza delle Sostanze Bioattive"

CHEMICAL AND METABOLIC STABILITY STUDIES OF PROPARGYLAMINE-CONTAINING DRUGS

Coordinatore
Prof. Luigi PANZA

Tutor
Prof. Giorgio GROSA

Candidato
Dott.ssa Rossana CANAVESI

XXVIII Ciclo

TABLE OF CONTENTS

List of abbreviations

AI: 1-(*R*)-aminoindan

AI-EA: 3-(2,3-dihydro-1*H*-inden-1-ylamino)prop-2-enal

Brij 58: polyoxyethylene 20 cetyl ether

CHMA: α-cyclohexylmandelic acid

HLC: human liver cytosol

HLM: human liver microsomes

MS-PROP: (3-[(2-hydroxyethyl)thio]- 2-Propenal)

$NADPNa_2$: Nicotinamide adenine dinucleotide phosphate disodium salt

Oxy: Oxybutynin hydrochloride; (4-(diethylamino)but-2-ynyl (RS)-2-cyclohexyl-2-hydroxy-2-phenyl-acetate hydrochloride

Oxy-DE: *N*-desethyloxybutynin; Benzeneacetic acid, α-cyclohexyl-α-hydroxy-4-(ethylamino)-2-butyn-1-yl ester

Oxy-EK: (3E)-4-(*N*,*N*-diethylamino)-2-oxo-3-buten-1-yl 1-cyclohexyl-1-phenylglycolate

Oxy-HA: Oxybutynin hydroxylamine; Benzeneacetic acid, α-cyclohexyl-α-hydroxy-4-(ethylamino)-4-(hydroxy)-2-butyn-1-yl ester

Oxy-NOs: Oxybutynin *N*-oxides; (diastereomeric **Oxy-NO1** and **Oxy-NO2**): (4-(diethylamino)-but-2-ynyl-(RS)-2-cyclohexyl-2-hydroxy-2-phenylacetate) *N*-oxide

PAPS: 3'-phosphoadenosine-5'-phosphosulfate

RG: Rasagiline mesylate ((1R)-2,3-Dihydro-*N*-2-propynyl-1*H*-inden-1-amine methanesulfonate)

RG-EA: 3-[2,3-dihydro-1*H*-inden-1-yl(prop-2-yn-1-yl)amino]prop-2-enal

RG-NOH: Rasagiline hydroxylamine; [2,3-Dihydro-*N*-hydroxy-*N*-2-propynyl-1*H*-inden-1-amine]

RLM: rat liver microsomes

SG: Selegiline hydrochloride; [methyl(1-phenylpropan-2-yl)(prop-2-yn-1yl)amine]

SG-EA: 3-[methyl(1-methyl-2-phenylethyl)amino]- 2-Propenal

SG-NOs: Selegiline *N*-oxides

TRIS HCl: Tris(hydroxymethyl)aminomethane hydrochloride

UDPGA: uridine-5'-diphosphoglucuronic acid trisodium salt

3OH-AI: 3-hydroxy-1-aminoindan

3OH-RG: 3-hydroxy-*N*-propargyl-1-aminoindan

4OH-AI: 4-hydroxy-1-aminoindan;

4OH-RG: 4-hydroxy-*N*-propargyl-1-aminoindan

6OH-AI: 6-hydroxy-1-aminoindan

6OH-RG: 6-hydroxy-*N*-propargyl-1-aminoindan

7OH-AI: 7-hydroxy-1-aminoindan

7OH-RG: 7-hydroxy-*N*-propargyl-1-aminoindan

CHAPTER 1. Introduction

1.1 CHEMICAL STABILITY STUDIES

Chemical stability of drug molecule is a matter of great concern as it affects the safety and efficacy of the drug product.

The Food and Drug Administration (FDA) and the International Conference on Harmonization (ICH) guidance state the requirement of stability testing data to understand how the quality of a drug substance and drug product changes with time under the influence of various environmental factors.

In particular, the ICH guideline entitled "Stability Testing of New Drug Substance and Products" (ICH Q1A(R2), 2003) states that stress testing is intended to identify the likely degradation products which can in turn help establish the degradation pathways and the intrinsic stability of the molecule and validate the stability indicating power of the analytical procedures used.

Forced degradation or stress testing is undertaken to demonstrate specificity when developing stability-indicating methods, particularly when little information is available about potential degradation products. Besides these studies also provide information about the degradation pathways and degradation products that could form during storage. Forced degradation studies may help facilitate pharmaceutical development as well in areas such as formulation development, manufacturing, and packaging, in which knowledge of chemical behavior can be used to improve a drug product.

Even if the available regulatory guidance provides useful definitions and comments about degradation studies nonetheless it is very general concerning the scope, timing, and best practices for degradation studies. In particular, the issue of how much stress is adequate in stress testing is not addressed specifically. Overstressing a molecule can lead to degradation profiles that are not representative of real storage conditions and perhaps not relevant to method development, hence stress-testing conditions should be realistic and not excessive (Reynolds et al. 2002). It is stated that the testing should include the effect of temperature, humidity (where appropriate), oxidation, photolysis and susceptibility to hydrolysis across a wide range of pH values. However no details are provided about the practical approach towards stress testing, for instance exact experimental conditions regarding temperatures,

duration, extent of degradation, etc. Nevertheless some general indications on how to best conduct forced degradation studies can be found in literature and are here mentioned.

1.1.1 Experimental approach

Forced degradation studies should be conducted whenever a stability-indicating method is required. Studies may need to be repeated as methods, processes, or formulations change.

Forced degradation studies of active pharmaceutical ingredient (API) and drug product (DP) include appropriate solid state and solution state stress conditions (e.g. acid/base hydrolysis, heat, oxidation, and light exposure) in accordance with ICH guidelines.

Since it is advisable that the stress conditions should result in approximately 5–20% degradation of the API, the specific conditions (intensity and duration) used will depend on the chemical characteristics of the API. The stressed sample should be compared to the unstressed sample (control) and the appropriate blank. Finally, a compound may not necessarily degrade under a given stress conditions hence no further stressing is advised in these cases (Alsante et al. 2007).

1.1.2 Degradation conditions

1.1.2.1 Hydrolytic conditions

Hydrolytic reactions are among the most common processes for drug degradation. Hydrochloric acid or sulfuric acid (0.1–1 mol/L solution) for acid hydrolysis and sodium hydroxide or potassium hydroxide (0.1–1 mol/L solution) for base hydrolysis are suggested as suitable reagents for hydrolysis. Studies should be carried out in the solution state. For certain APIs that are partially soluble or insoluble in the described acidic or basic solution, addition of an appropriate co-solvent, may be required to achieve dissolution. Additionally, the sample may be heated for a defined time/temperature to accelerate degradation, depending on the API sensitivity to heat.

1.1.2.2 Oxidation

Oxidation can be carried out under an oxygen atmosphere or in the presence of peroxides. The use of oxygen is a more realistic model. Free radical initiators may be used to accelerate oxidation. Generally, a free radical initiator and peroxide will produce all primary oxidation degradation products observed on real-time stability. Therefore, free radical and/or hydrogen peroxide conditions are strongly recommended at all stages of development.

For solution state stress conditions, dissolve the API utilizing an appropriate solvent, add 5–20 mol% of a free radical initiator at atmospheric pressure. To increase the solubility of oxygen in the solution, the reaction can be performed in a reaction vessel pressurized at 50–300 psi with molecular oxygen. Additionally, the system is heated to accelerate degradation. The temperature depends on the free radical initiator selected.

For peroxide conditions, hydrogen peroxide reagent (up to 3%) can be used. As previously indicated, the addition of an appropriate co-solvent may be necessary, depending on API solubility. Hydrogen peroxide stress testing can be useful in DP studies where hydrogen peroxide is an impurity in an excipient. Solid-state stress conditions may be similarly investigated by placing the API (as is) in suitable closed containers filled with an oxygen headspace versus an argon or nitrogen control headspace. Additionally, the sample may be heated for a defined time/temperature to accelerate degradation, depending on the API sensitivity to heat.

For later stage development compounds when more time and effort can be focused on mechanistic understanding, the following oxidation conditions can be applied. The addition of metal ions to solutions of API can indicate whether there is a tendency for the API to be catalytically oxidized; indeed iron and copper ions are routinely found, as impurities, in APIs and formulation excipients. Transition metal ions can also reduce peroxide to generate hydroxyl radicals in a Fenton-type reaction. In addition, light can also effect oxidation reactions. Light absorbed by a photosensitizer can react with molecular oxygen to form the more reactive singlet oxygen species (Alsante et al. 2007).

1.1.2.3 Thermal/humidity

Solid state stability can be evaluated utilizing accelerated storage temperatures in general greater than 50 °C and > 75% relative humidity. The duration of exposure is dependent on the API sensitivity. If the forced degradation thermal/humidity conditions produce a phase change, it is recommended to also run thermal/humidity conditions below the critical thermal/humidity that produces the phase change.

1.1.2.4 Photostability

The studies should be performed in accordance with ICH photostability guidelines (ICH Q1B, 1996) using Option 1 and/or Option 2. According to the ICH guideline, “the design of the forced degradation experiments is left to the applicant's discretion although the exposure

levels should be justified. The recommended exposures for confirmatory stability studies are an overall illumination of not less than 1.2 million lux hours and an integrated near ultraviolet energy of not less than 200 W-h/m^2.

1.1.3 Drug product

Drug product (DP) degradation cannot be predicted solely from the stability studies of the API in the solid state or solution. The non-active pharmaceutical ingredients can also react with the API or catalyze degradation reactions. Impurities in the excipients can also lead to degradation in the DP not originally observed in the API. For DP formulations, heat, light, and humidity are often used. The DP stress conditions should result in approximately 5–20% degradation of the API or represent a reasonable maximum condition achievable for a given formulation. The specific conditions used will depend on the chemical characteristics of the DP. For a solid DP, key experiments are thermal, humidity, photostability and oxidation, if applicable. For solution formulations, key experiments are thermal, acid/ base hydrolysis, oxidation and photostability. It is recommended to compare stressed samples with unstressed samples and an appropriate blank. For DP studies, the blank sample is an appropriate placebo. The stressed placebo sample will provide information about excipient compatibility. It is advised to take kinetic time points along the reaction pathway for API and DP degradation studies to determine primary degradants and a better understanding of the degradation pathway.

1.1.4 Stability-indicating method development

A stability-indicating method is defined as an analytical method that accurately quantitates the active ingredients without interference from degradation products, process impurities, excipients, or other potential impurities. A method that accurately quantitates significant degradants may also be considered stability-indicating.

Forced degradation should be the first step in method development. If forced degradation studies are performed early, method development and identification of primary degradation products and unknown impurities can be run in parallel (Alsante et al. 2007).

1.2 METABOLIC STABILITY STUDIES

The drug development process involves several steps, from target identification and screening, lead generation and optimization, preclinical and clinical studies to final registration of a drug (Baranczewski et al., 2006). During the preclinical screening stage the main pharmacokinetic, pharmacodynamic, and toxicological properties of the candidate drug are investigated. Accordingly, efforts are being made to reduce attrition of drug candidates during the various stages of their development while bringing safer compounds to market. Among the major reasons for new chemical entities NCEs failure, other than poor clinical efficacy, are serious undesired side effects, adverse drug reactions, and unfavorable drug metabolism and pharmacokinetics (Prakash et al., 2007).

During the past years, pharmaceutical companies have invested and introduced a number of new approaches dedicated to improve the rate of success of development of new drugs. One of the new strategies is an *in vitro* approach for early determination and prediction of drug metabolism of NCEs. The use of *in vitro* methodology in drug metabolism studies has several advantages. First, it allows for determination of metabolic profiles of NCE early in the drug discovery process, and, therefore, this information can be used to guide further modifications of NCE in order to obtain favorable metabolic properties. Secondly, since it is possible to use human enzymes, cells and liver subcellular fraction the data are more relevant for the human *in vivo* situation. Finally, the *in vitro* approach is cost and time effective (Baranczewski et al., 2006).

Metabolism is a biochemical process by which endogenous compounds and xenobiotics (such as drugs) are converted to more hydrophilic (water soluble) entities, which enhance their elimination from the body. In general, metabolites are pharmacologically less active and less toxic than their corresponding parent compound. However, it is not uncommon that biotransformation reactions also lead to undesirable consequences, such as too rapid drug clearance, formation of pharmacologically active metabolites, drug-drug interactions via inhibition or induction of drug metabolizing enzymes, and/or formation of toxic metabolites. Therefore, determination of an NCE's metabolic rate, biotransformation pathways in animals and humans, and pharmacological and toxicological consequences of its metabolites are very critical to pharmaceutical research and compound progression (Prakash et al., 2007).

Biotransformation occurs in many tissues, with the liver as the most important organ, but also the kidneys, skin, lungs, and intestine can be involved. The liver is the largest internal organ

of the human body and is strategically located between the digestive tract and the other parts of the body (Brandon et al., 2003).

1.2.1 Xenobiotics biotransformation

Drug biotransformation is divided into two types of reactions, namely phase I (functionalization) and phase II (conjugation). The biotransformation pathway is mediated by phase I, phase II, or a combination of both.

Phase I include: hydroxylation (aliphatic, aromatic, or nitrogen), epoxidation (aliphatic, aromatic), dealkylation (*O*-, *N*-, or *S*-), deamination, oxidation (*N*-, or *S*-), reduction (nitro, azo, disulfide, keto, aldehyde, olefin), and hydrolysis (amide, ester, carbamate, epoxide). These reactions introduce or unmask a functional group (e.g., –OH, –COOH, $–NH_2$, or –SH) within a molecule to enhance its hydrophilicity. These Phase I reactions are mediated primarily by liver enzymes, such as cytochrome P450 (CYPs), FAD-containing mono-oxygenases (FMOs), monoamine oxidases (MAOs), aldehyde oxidase/xanthine oxidase (AO/XO), alcohol dehydrogenase (ADH), aldo-ketoreductase (AKR), esterases, dehydropeptidase, and epoxide hydrolase (EH).

Phase II biotransformations include: glucuronidation, sulfation, methylation, acetylation, and amino acid (glycine, glutamic acid, and taurine) and glutathione (GSH) conjugation. Phase II reactions are catalyzed by conjugative enzymes, such as UDP-glucuronyltransferase (UGT), sulfotransferase (SULT), glutathione *S*-transferase (GST), *N*-acetyltransferase (NAT), and methyl transferase (*N*-methyl-, thiomethyl-, and thiopurinemethyl-). Glutathione conjugates are further metabolized to cysteine and *N*-acetyl cysteine adducts (i.e., mercapturic acid synthesis). Most phase II reactions result in a concomitant increase in hydrophilicity and decrease in volume of distribution of the metabolized compounds, facilitating their excretion from the body (Prakash et al., 2007). Some of the most important and common enzyme systems involved in drug biotransformation are presented in Figure 1.

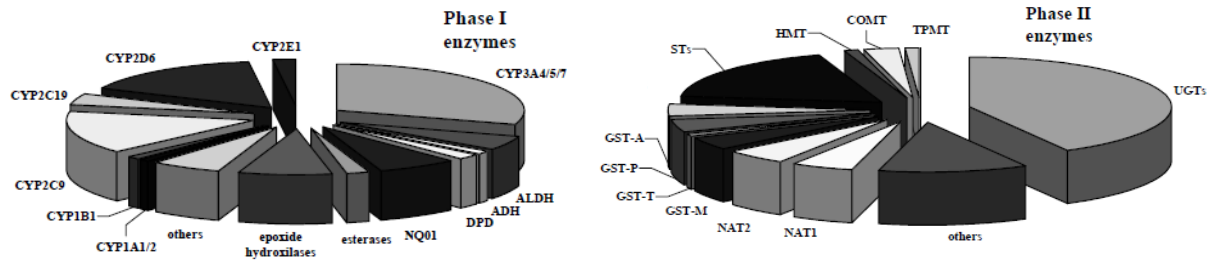

Figure 1. Enzymes involved in phase I and II drugs biotransformation.

Finally it is becoming increasingly apparent that drug transporters (phase III) influence not only the therapeutic efficacy but also the absorption, distribution, and elimination of a drug. The drug transporters are located in epithelial and endothelial cells of the liver, gastrointestinal tract, kidney, blood–brain barrier, and other organs. They are responsible for the transport of most of the commonly prescribed drugs across cellular barriers and thus for the concentration at the target or biotransformation site. Multidrug resistance proteins (MRP; *p*-glycoprotein and others) have been shown to be important in explaining the pharmacokinetics of a drug in man.

1.2.2 Cytochrome P450

Among the phase I enzymatic systems the CYP system is a superfamily of membrane-bound, heme-containing mixed-function oxygenases that are the principal enzyme system for the metabolism of drugs (Figure 1). These enzymes are expressed in many tissues, but are found at the highest levels in liver. CYPs principally function to introduce oxygen into a molecule to increase the hydrophilicity of the product and hence, the ease with which the product can be eliminated from the body. A nomenclature for these enzymes has been developed based on similarities in amino acid sequences. The catalytic activities of CYPs (Figure 2) require molecular oxygen and reducing equivalents from NADPH as summarized by the reaction below reported:

$$ROH + NADPH + O_2 + H^+ \rightarrow ROH + NADP^+ + H_2O$$

The flavoprotein NADPH-cytocrome P450 reductase is associated to the CYPs catalyzing the electron transfer from NADPH to cytocrome P450 through the coenzymes flavin-adenine dicucleotide (FAD) and riboflavin 5'-phosphate (FMN) (Figure 3). In addition, another membrane-bound, heme-containing protein, NADPH-cytocrome b_5 reductase, stimulates the activity of some CYPs towards some substrates.

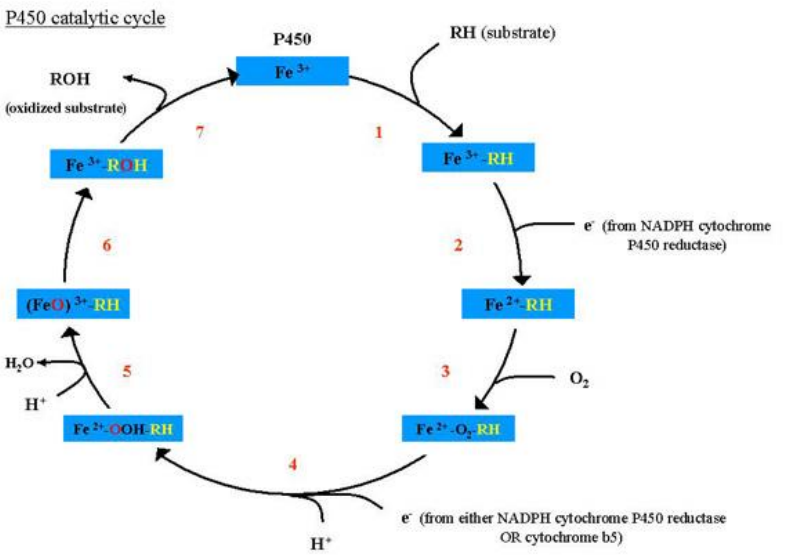

Figure 2. Catalytic cycle of cytocrome P450.

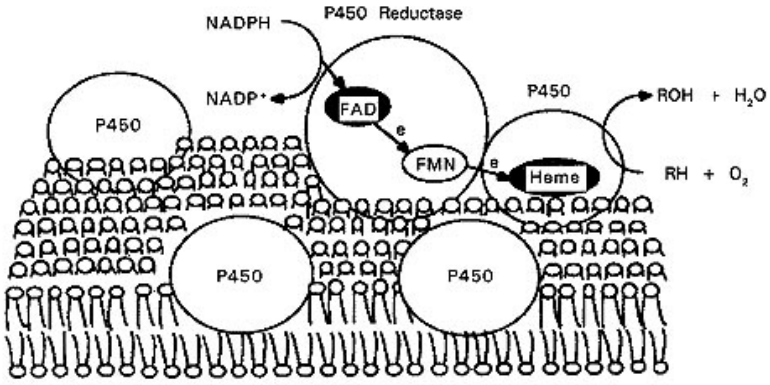

Figure 3. Molecular components constituent of cytocrome P450 system.

There are 11 xenobiotic-metabolizing CYPs that are expressed in a typical human liver (CYP1A2, CYP2A6, CYP2B6, CYP2C8/9/18/19, CYP2D6, CYP2E1, and CYP3A4/5). A relatively limited subset of these enzymes (CYP1A2, CYP2C9, CYP2C19, CYP2D6, and CYP3A4) appears to be most commonly responsible for the metabolism of drugs and associated drug-drug interactions. The relative importance of this subset of enzymes is due to both the mass abundance of these enzymes (e.g., CYP3A4 is the most abundant P450 in human liver at ~30% of total P450) and the preference of these enzymes to bind and/or metabolize chemical structures commonly found in drugs.

Human populations exhibit considerable variability in CYP activity levels. This is due to the fact that some human CYP enzymes are polymorphic, with a significant percentage of populations being deficient in a specific enzyme or having a functional enzyme with an altered amino acid sequence, which can change the kinetics of substrate metabolism. Expression levels of specific CYP enzymes vary substantially among individuals. The levels of other human CYP enzymes (e.g., CYP1A2 and CYP3A4) are induced by certain environmental exposures or drug treatments (Table 1). If an enzyme, which is polymorphic or subject to environmental regulation, is rate-limiting for the elimination of a drug, then substantial interindividual variation in pharmacokinetics is often observed (Crespi and Miller, 1999).

Isoform	Inhibitor	Inducer
CYP1A1	α-Naphtoflavone	Polycyclic hydrocarbons
CYP1A2	Furafylline	Smoking
		3-Methylcholanthrene
		Char-grilled meat
		Rifampicine
CYP2A6	Sulfaphenazole	Pyrazole
		Barbiturates
CYP2B1/2		
CYP2B6	Sertraline	
CYP2C8	Glitazones	Rifampicine
		Barbiturates
CYP2C9	Sulfaphenazole	Rifampicine
		Phenobarbital
CYP2C18/2C19	Ticlopidine	Rifampicine
	Ketoconazole	Carbamazepine
CYP2D6	Quinidine	
	Haloperidol	
CYP2E1	Diethyl-dithiocarbamate	Ethanol
CYP3A4	Ketoconazole	Rifampicine
	Grapefruit juice	Barbiturates
CYP4A11	17-Octadecynoic acid	

Table 1. Common known inhibitors and inducers of the CYP isozyme activity (from Brandon et al. 2003).

1.2.3 In vitro models to study drug metabolism

A key question in human drug biotransformation research is how to make reliable extrapolations from the *in vitro* or *in vivo* model to clinical practice.

Several *in vitro* models have been developed in the past. They are used to obtain early information about biotransformation pathways and to predict drug-drug interactions. The optimal model system depends on a number of factors, such as *in vivo* resemblance, expense, availability of the model, and ethical considerations. *In vitro* data from human and animal models can be used to choose the best *in vivo* model (e.g., mouse, rat, dog) for further testing. In conclusion, it can be stated that an *in vitro* model is always a compromise between convenience and relevance.

1.2.3.1 Liver microsomes

Microsomes can easily be prepared from different tissues, most commonly from the liver of animals and human donors. Therefore, human liver microsomes (HLM) have become a very commonly and widely used *in vitro* model. Liver microsomes consist of vesicles of the hepatocyte endoplasmic reticulum and are prepared by differential centrifugation and thus contain almost only CYP and UGT enzymes (Figure 4).

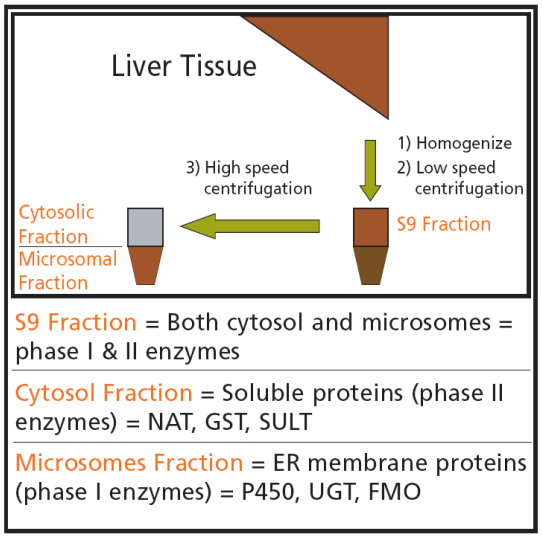

Figure 4. Liver fractions preparation

The enzymatic activities are stable during prolonged storage of the microsomes. In order to reflect the standard proportion of the enzymes in human or animal livers, liver microsomes from different donors are usually pooled. By supplementing the liver microsomes with

appropriate cofactors and other reaction components, it is possible to investigate and distinguish between CYPs, flavin-containing monooxygenase (FMO) and glucuronosyltransferase (UGT) activities.

The major advantages of microsomes are low costs, simplicity in use, and they are one of the best-characterized *in vitro* systems for drug biotransformation research. However, some major drawbacks exist. It should be noted that results obtained with microsomes cannot be used for quantitative estimations of *in vivo* human biotransformation, because CYPs and UGTs are enriched in the microsomal fraction and there is no competition with other enzymes (e.g., NAT, GST, and SULT) with the consequence that metabolites formed in intact liver could be unnoticed.

1.2.3.2 Liver cytosol fractions

The liver cytosolic fraction contains the soluble phase II enzymes, e.g., NAT, GST, and SULT. It is obtained by differential centrifugation of whole-liver homogenate, like microsomes (Figure 4). For the catalytic activity of the phase II enzymes, addition of exogenous cofactors, e.g., acetyl coenzyme A (acetyl CoA), dithiothreitol (DTT), and acetyl CoA regenerating system for NAT, 3'-phosphoadenosine-5'-phosphosulfate (PAPS) for SULT, and glutathione (GT) for GST, is necessary.

The main advantage of cytosol fraction is the presence of only three enzymes at higher concentrations compared to human liver S9 fraction. The biotransformation capacity of NAT, SULT, and GST can be studied separately or in combination depending on the cofactors added. A disadvantage is that only the soluble phase II enzymes are present in the liver cytosol fraction and that therefore the UGTs, which are located on the endoplasmic reticulum, metabolic pathways cannot be investigated with this model.

1.2.3.3 Liver S9 fractions

The liver S9 fraction contains both microsomal and cytosolic fractions. Like microsomes, a NADPH-regenerating system or NADPH solution is required to supply the energy demand of the CYP enzymes, as well as for the catalytic activity of phase II enzymes, addition of exogenous cofactors is necessary.

Compared with microsomes and cytosol, S9 fractions offer a more complete representation of the metabolic profile, by performing both phase I and phase II activities. In some cases with

S9 fractions, metabolites that are not produced by either the cytosolic fraction or the microsomal fraction alone are formed.

1.2.3.4 Human CYP and UGT supersomes (baculovirusinsect-cell-expressed)

Insect cells lack endogenous CYP and UGT activity and, therefore, microsomes, which consist of vesicles of the hepatocyte endoplasmic reticulum, of human CYP- or UGT transfected insect cells can be a useful tool in human biotransformation studies. Since the expression is baculovirus mediated, microsomes of these cells are sometimes referred to as baculosomes, but more often as supersomes™. The availability of specifically expressed human CYPs and UGTs in supersomes allows the investigation of the contribution of a single metabolic enzyme to the biotransformation pathway of the compound under investigation. At present all common human CYPs, coexpressed with NADPH-cytochrome P450 reductase and optionally cytochrome b_5, and UGTs are offered in supersomes™. A control experiment, an incubation with nontransfected supersomes, must always be conducted. NADPH-regenerating system or NADPH is required to supply the energy demand of the CYPs as well as UDPGA for the UGT activity has to be added as a cofactor. A major advantage of supersomes is that they can be used to study not only isozyme-specific drug biotransformation, but also drug–drug interactions. In the past few years the development of new CYP and UGT supersomes™ has increased considerably. The different genotypes of the CYP isozymes (e.g., CYP2C9*1, CYP2C9*2, and CYP2C9*3) are now also commercially available (https://www.corning.com). Hence, the influence of different polymorphisms on the drug biotransformation pattern also can be studied.

A disadvantage is that, in UGT supersomes, the UGT active site is shielded behind a hydrophobic barrier, resulting in latency of glucuronidations. However, this disadvantage can be overcome by using a pore-forming agent, alamethicin.

1.2.3.5 Hepatocytes

Primary hepatocytes

Primary hepatocytes are a popular *in vitro* system for drug biotransformation research due to their strong resemblance of in vivo human liver. Human liver is mainly obtained from patients that undergo partial liver resection, e.g., because of liver metastasis.

Cultured hepatocytes

Once isolated, hepatocytes can be held in suspension, in which case they remain viable for only a few hours, or they can be maintained in monolayer culture for a maximum of 4 weeks. Both cultured hepatocytes and suspensions of primary hepatocytes have repeatedly proven to be powerful tools to analyze the specific metabolic profile of a variety of drugs with good *in vitro–in vivo* correlations However, it has been widely recognized that cultured hepatocytes are subject to a gradual loss of liver-specific functions, with special reference to a decreased CYP expression. This loss is different for the specific CYP isoforms; for some isoforms it becomes evident after a few days of culture (CYP 2E1 and CYP 3A4), while others remain nearly unaffected by the isolation and culturing processes (CYP 1A2 and CYP 2C9). An advantage of isolated hepatocytes compared to liver slices and perfused liver is the possibility of cryopreservation. Indeed cryopreserved hepatocytes have been shown to retain the activity of most phase I and phase II enzymes. A disadvantage is the lack of liver nonhepatocyte cells. Although hepatocytes account for the vast majority of the liver volume (about 80%), other cells such as Kupffer cells may be necessary for cofactor supply. Another problem encountered with human hepatocytes, as with human liver microsomes, is the considerable interindividual variation (Brandon et al., 2003).

1.3 PROPARGYLAMINE-CONTAINING DRUGS

1.3.1 Neurodegenerative disorders

Parkinson's disease (PD) and Alzheimer's disease (AD) are conditions constituting part of the broad cluster of diseases commonly referred to as neurodegenerative disorders (ND).

A classical feature of these diseases is the transient loss of neuronal cells in the brain due to apoptosis triggered by one of many factors including genetic, endogenous and environmental ones. Although each disease has its own molecular mechanisms and clinical manifestations, some general pathways might be recognized in different pathogenic cascades. They include protein misfolding and aggregation, oxidative stress and free radical formation, metal dyshomeostasis, mitochondrial dysfunction, and phosphorylation impairment, all occurring concurrently (Cavalli et al., 2008).

The multifactorial nature of NDs suggests that targeting any single mechanistic site will not result in successful retardation of the disease progression and many "single-site-targeting" drugs have failed to render sufficient neuroprotective and/or neurorestorative activity. The use of drugs aiming to a single receptor or enzymatic system is thus insufficient for treatment of these multifactorial diseases (Zindo et al., 2015).

It is now widely accepted that a more effective therapy would result from the use of multitarget-directed ligands (MTDLs) able to intervene in the different pathological events underlying the etiology of neuronal disorders. To obtain novel MTDLs, a design strategy is usually applied in which distinct pharmacophores of different drugs are combined in the same structure to afford hybrid molecules. In principle, each pharmacophore of these new drugs should retain the ability to interact with its specific site or sites on the target and, consequently, to produce specific pharmacological responses that, taken together, should slow or block the neurodegenerative process (Cavalli et al., 2008).

The last few decades have seen increasing research interest and exploration of the neuroprotective ability of compounds bearing propargylamine function seen in selegiline and rasagiline. The propargylamine moiety is now known to play an important role in providing the neuronal and mitochondrial protective properties inherent in these compounds and other reported activities ascribed to this moiety in literature include antiapoptotic and amyloid-β (Aβ) aggregation inhibition. These features of the propargylamine moiety have led to its incorporation into structures of many drug-like compounds designed for neuroprotection to afford resultant molecules with broader therapeutic profiles that may potentially meet the curative needs of multifactorial NDs (Zindo et al., 2015).

1.3.2 Alzheimer's Disease (AD)

Alzheimer's disease (AD) stands out among neurodegenerative disorders as the fourth leading cause of death and the most common cause of acquired dementia in the elderly population, afflicting more than seven million people worldwide (Cavalli et al., 2008).

The predominant clinical manifestation is progressive memory deterioration and changes in brain function, including disordered behaviour and impairment in language and comprehension, which progressively worsen over 5–10 years. Most of these cognitive symptoms result from a depletion of basal forebrain cholinergic neurons leading to decreased cholinergic neurotransmission. Besides the cognitive deficits, patients frequently exhibit neuropsychiatric symptoms such as depression, psychosis and agitation.

From the histopathological viewpoint, two characteristic hallmarks accompany these features: the neurofibrillary tangles (NFT) which are intracellular fibrillar deposits mainly composed of the microtubule-associated protein tau, and the senile plaques (SP), formed by deposition of the aggregated amyloid-β peptide (Aβ). Although the pathogenesis of AD is not yet fully understood, it is a multifactorial disease triggered by several factors, including excessive protein misfolding and aggregation, oxidative stress and free radical formation, mitochondrial dysfunction, metal dyshomeostasis, excitotoxic and neuroinflammatory processes. In addition to the cholinergic dysfunction, disturbances in other neurotransmitter systems such as the monoaminergic have also been reported to account for AD symptoms (Bolea et al., 2012).

Of the above-mentioned hypotheses, the cholinergic one is the oldest and it has also had the strongest influence on the development of clinical treatment strategies, which led to the introduction of the acetylcholinesterase inhibitor (AChEI) tacrine (1), donepezil (2), galantamine (**3**) and rivastigmine (**4**) (Figures 5).

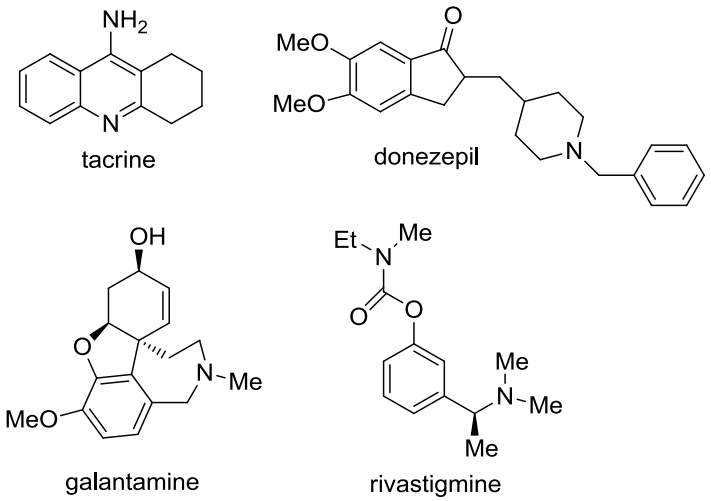

Figure 5.

These drugs have become the standard for AD therapy and, although beneficial in improving cognitive, behavioral, and functional impairments, they seem unable to address the molecular mechanisms that underlie the pathogenic processes.

1.3.3 Parkinson's disease (PD)

Parkinson's disease (PD) is the second most common neurodegenerative disorder. Like AD, it is currently an incurable disease. The available pharmacological therapies are unable to arrest or reverse the neurodegeneration associated with PD.

PD is characterized by the progressive loss of dopaminergic neurons in the substantia nigra pars compacta and other subcortical nuclei and by the presence of intraneuronal aggregates known as Lewy bodies (LBs), which are enriched in filamentous α-synuclein and other proteins that are often ubiquitinated. Depletion of dopamine (DA) causes dysregulation of the motor circuits that project throughout the basal ganglia, resulting in the clinical manifestations of PD, which include tremor, bradykinesia, rigidity, and postural instability. However, additional neurotransmitter systems are also involved in PD and, consequently, nonadrenergic, serotoninergic, and cholinergic neurons are also lost. This loss is responsible for nonmotor symptoms, such as cognitive decline, sleep abnormalities, and depression, which dominate the later stages of PD (Cavalli et al. 2008).

The crucial molecular step of PD pathogenesis is the formation of LBs, whose key constituent is represented by α-synuclein, a cytoplasmic soluble protein that contains a highly amyloidogenic domain within its mid-region. In pathogenic conditions, α-synuclein misfolds

and is converted into pathological oligomers and higher-ordered aggregates, which fibrillize and deposit into LBs as β-pleated sheets. Therefore, maintaining α-synuclein in the native and soluble random coil conformation, and consequently preventing α-synuclein-mediated neuron toxicity, emerges as a clear goal of innovative disease-modifying PD therapies. Moreover treatment with antioxidants might theoretically be of benefit in preventing neurodegeneration.

Despite an increased understanding of the molecular causes of PD, current PD therapies are based mainly on exogenous replacement of DA within the striatum. This improves the symptoms but without halting the progression of the neurodegenerative process or reversing the neuronal degeneration. Furthermore, although PD also involves degeneration of non-dopaminergic neurons, the treatment of the resulting predominantly non-motor features remains a challenge. Depletion of striatal DA from the loss of nigral projections is the main target for the currently available drugs. The classes of compound that still hold a prominent position in current anti-PD drug discovery are reported in Table 2.

Mechanism of action	**Drugs**
DA precursor (prodrug)	L-dopa
COMT inhibition	Entacapone, Tolcapone
MAO-B inhibition	Selegiline, Rasagiline
Dopaminergic receptor agonism (ergot derivative)	Bromocriptine, Pergolide, Cabergoline, Lisuride
Dopaminergic receptor agonism (non-ergot derivative)	Ropinirole, Pramipexole, Piribedil
Muscarinic receptor antagonism	Biperiden, Triexyphenidyl, Metixene
Ion channel blockade	Amantadine
Peripheral dopa decarboxylase inhibition	Benserazide, Carbidopa

Table 2.

Levodopa (L-dopa) is the key compound in the treatment of PD, acting as a precursor of DA. However, besides offering only symptomatic relief for patients, this drug shows substantial side effects at the high doses required for therapeutic action.

Certain other available drugs, like MAO-B (selegiline and rasagiline) and COMT (entacapone and tolcapone) inhibitors, are used mainly with L-dopa, since they alter the *in vivo* metabolism of DA by increasing its plasma half-life. Anticholinergic compounds (such as

biperiden, triexyphenidyl) were among the first drugs used for PD therapy, since they were intended to correct the imbalance between DA and acetylcholine (ACh) brain levels. More recent therapeutic approaches to PD are represented by nicotine, anti-inflammatory agents, melatonin, selenium, iron chelators, and vitamins A, C, and E.

As previously mentioned, none of these therapies are able to arrest or reverse the progression of PD probably because these compounds treat only the symptoms of the disease rather than tackling the actual molecular PD causes. Moreover, the currently available drugs have been shown to interact with a single molecular target, instead of confronting the multifactorial nature of PD neurodegeneration.

1.3.4 Monoamine oxidase

Monoamine oxidase (MAO, E.C.1.4.3.4) is a flavin-containing enzyme that catalyses the oxidative deamination of a wide range of biogenic and xenobiotic amines, including dopamine (DA), noradrenaline, adrenaline, tyramine, serotonin (5-HT). This enzyme is known to exist in two isoforms namely MAO-A and MAO-B, which show different selectivities for substrates and inhibitors. The enzyme is inserted in the outer mitochondrial membrane, and is widely distributed in the body tissues, with a high degree of expression in the gastro-intestinal tract and liver, as well as neuronal tissue, and nearly all other organs. Monoamine oxidase A and B catalyze the oxidation of primary, secondary, and some tertiary amines to their corresponding aldehyde, hydrogen peroxide and ammonia (in case of primary amines) or a substituted amine (in case of secondary and tertiary amines) in a reaction shown below:

$$RCH_2NH_2 + H_2O + O_2 \rightarrow RCHO + NH_3 + H_2O_2$$

Selective inhibitors for MAO-A have been shown to be effective antidepressants, whereas MAO-B inhibitors are useful for the treatment of Parkinson's disease. The neuroprotective effect of monoamine oxidase inhibitors (MAOIs) in these disorders may result not only from the increased amine neurotransmission, but also from prevention of neurotoxic product formation, which promotes reactive oxygen species (ROS) generation and may ultimately contribute to increased neuronal damage. Despite some disadvantages found in using MAOIs in clinical practice, such as hepatotoxicity and the so-called ''cheese-effect'', which describes the hypertensive crisis produced by the consumption of tyramine-rich food, especially cheese.

MAO enzymes remain in the focus of drug design targeting neurodegenerative disorders. Nevertheless, it seems at present unlikely that the neuroprotective activities of MAOIs are exclusively related to the ability to decrease the production of free radicals and toxic aldehydes via the inhibition of enzymatic activity. With regard to this, several studies have suggested that they are rather related to the anti-apoptotic properties of the propargyl group present in these molecules (Bolea et al., 2014).

1.3.5 Propargylamines

Propargylamines are molecules containing a propargyl moiety that typically inhibits MAO-B including the well characterized compounds selegiline (l-deprenyl), rasagiline and PF9601N (Fig. 6).

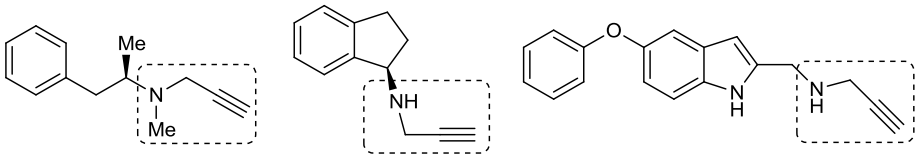

Selegiline **Rasagiline** **PF9601N**

Figure 6. Propargylamine-derived MAOIs (the propargylamine moiety is highlighted with dotted lines)

While selegiline was the first selective MAO-B inhibitor used clinically for the treatment of Parkinson's disease, rasagiline and PF9601N belong to a second generation of MAO-B inhibitors that, unlike selegiline, do not generate amphetamine derivatives when metabolized. Since these compounds possess anti-apoptotic properties independent from their ability to inhibit MAO-B, diverse mechanisms have been suggested to be involved in the neuroprotective properties of propargylamine-containing compounds (Fig. 7).

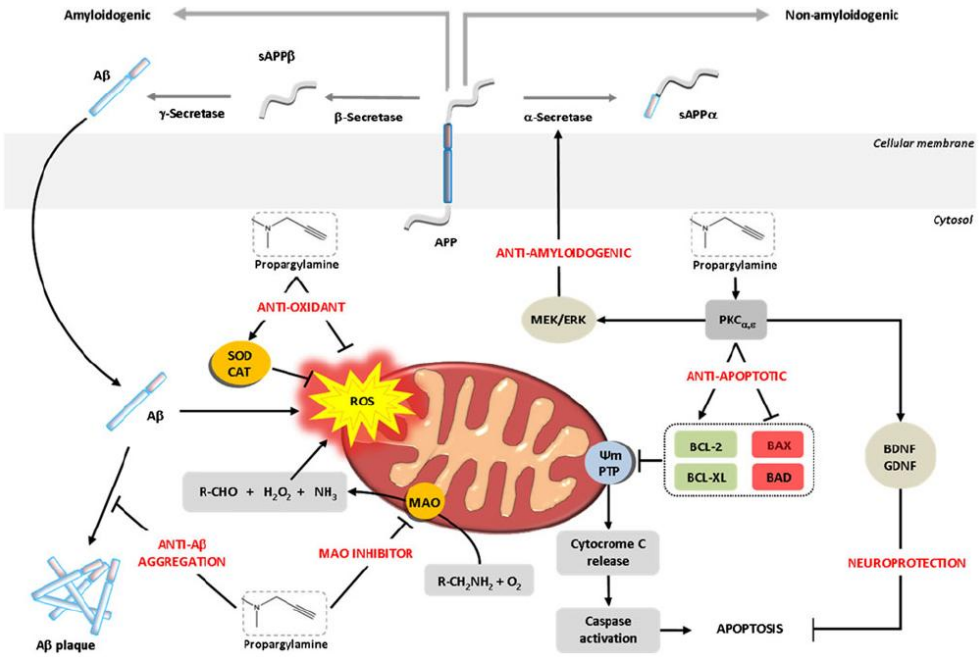

Figure 7. Schematic representation of the sites of action of propargylamine-derived compounds as potential targets for AD treatment figure taken from Bolea et al. (2014)

One of these mechanisms involves a significant antioxidant potency arising from the increase in the activities of superoxide dismutase (SOD) and catalase (CAT) enzymes, besides the prevention of the MAO reaction products formation, which are potentially neurotoxic since they contribute to oxidative stress and the formation of ROS. Moreover, the anti-apoptotic activity of these molecules has been attributed to their ability to prevent the fall in mitochondrial membrane potential (Ψm) and the blockade of the permeability transition pore (PTP) opening as a consequence of the up-regulation of Bcl-2 family protein and activation of protein kinase C (PKC) and mitogen-activated protein kinase (MAPK). These pathways may be additionally involved in the effect of propargylamines on the enhanced release of the non-amyloidogenic α-secretase form of soluble amyloid precursor protein (sAPPα), which precludes the formation of amyloid derivatives promoting the non-amyloidogenic pathway of APP processing. Further neuroprotective effects have been related to the induced increase in the expression of neurotrophic factors such as BDNF and GDNF (Bolea et al., 2014).

1.3.6 Multitarget-directed ligands (MTDLs) strategy

The advent of MTDL approach has now seen many researchers develop a number of compounds that can potentially confer neuroprotection by acting simultaneously on different receptors and target sites implicated in NDs. This approach has yielded a wide amount of interesting MTDLs to halt NDs: some examples of propargylamine-derived compounds as promising neuroprotective agents are here mentioned.

1.3.6.1 MAO/AChE inhibitor

A successful approach of combined MAO/AChE inhibition came from the combination of the carbamate moiety of rivastigmine (figure 5) with the indane scaffold present in the MAO-B inhibitor rasagiline (figure 6), leading to the compound ladostigil (Fig. 8) (Sterling et al., 2002).

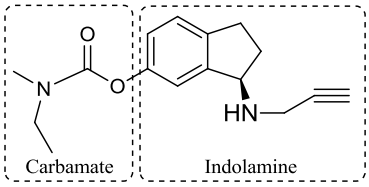

Ladostigil

Figure 8.

Ladostigil is able to inhibit both AChE and butyrylcholinesterase (BuChE) for a longer time than the parent compound rivastigmine. In addition, ladostigil selectively inhibits brain MAO-A and MAO-B resulting in an increase in noradrenaline, dopamine and serotonine levels, and thus exerting an antidepressant action. Ladostigil has also been shown to retain the neuroprotective and anti-apoptotic properties observed in the parent compound and propargylamine-derived rasagiline. Besides, ladostigil also possesses a cognition enhancing activity and is the most advanced MTDL on its category as demonstrated by the promising results obtained from a phase 2 clinical trial.

1.3.6.2.MTDLs targeting MAO and iron

It has been reported that iron contributes to Aβ aggregation, which in turn contributes to neuronal degeneration through the induction of oxidative stress. A link between high iron concentration and MAO activity and their involvement in ROS production has also been

reported. To address these problems, Youdim and collaborators have developed compounds with a bi-functional action on iron chelation and MAO inhibition obtained by combining the iron-chelating and antioxidant scaffold of VK28 with the *N*-propargylamine moiety of rasagiline. The most interesting compounds obtained were **M30** and **HLA20** (Fig. 9) possessing iron-chelating activity similar to that of VK28, but holding higher brain permeability.

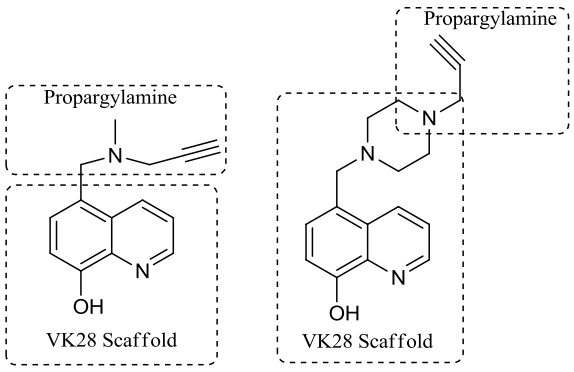

M30 **HLA20**

Figure 9.

M30 and **HLA20** possess neuroprotective properties comparable to rasagiline and potently inhibit the iron induced membrane lipid peroxidation features. More importantly, **M30** has been shown to selectively inhibit brain MAO (A and B) enzymes and to increase serotonin, dopamine and adrenaline neurotransmission, which confers to this multipotent compound an antidepressant action besides preventing the potentiation of tyramine-induced cardiovascular activity. Interestingly, **M30** inhibits the Aβ aggregation induced by metals and reduces Aβ formation (Bolea et al., 2014).

1.3.7 Conclusions

The complex pathogenesis and etiology of neurodegenerative diseases make it clear that drugs targeting a single receptor or enzymatic system will not result in successful retardation and treatment of these multifactorial diseases. This is even more evident in that drugs used in the symptomatic treatment of these diseases fail to render sufficient neuroprotective and/or neurorestorative activity. The advent of MTDL approach has however seen the development of compounds that combine symptomatic treatment and neuroprotection in one molecule by acting simultaneously on different receptors and target sites implicated in NDs.

Compound bearing the propargylamine function have received significant attention based on the neuroprotective ability observed for the MAO-B inhibitors selegiline and rasagiline. This has led to its incorporation into many drug-like compounds designed for neuroprotection and to afford molecules with broader therapeutic profiles to potentially meet the curative needs of the multifactorial NDs.

1.4 REFERENCES

Alsante, K., Ando, A., Brown, R., Ensing, J., Hatajik, T., Kong, W., & Tsuda, Y. (2007). The role of degradant profiling in active pharmaceutical ingredients and drug products. *Advanced Drug Delivery Reviews*, *59*(1), 29–37.

Baranczewski, P., Stańczak, A., Sundberg, K., Svensson, R., Wallin, Å., Jansson, J., Garberg, P., Postlind, H. (2006). Introduction to *in vitro* estimation of metabolic stability and drug interactions of new chemical entities in drug discovery and development. *Pharmacological Reports*, *58*, 453–472.

Bolea, I., Gella, A., & Unzeta, M. (2013). Propargylamine-derived multitarget-directed ligands: fighting Alzheimer's disease with monoamine oxidase inhibitors. *Journal of Neural Transmission*, *120*(6), 893–902.

Brandon, E. F. A., Raap, C. D., Meijerman, I., Beijnen, J. H., & Schellens, J. H. (2003). An update on *in vitro* test methods in human hepatic drug biotransformation research: pros and cons. *Toxicology and Applied Pharmacology*, *189*(3), 233–46.

Cavalli, A., Bolognesi, M. L., Minarini, A., Rosini, M., Tumiatti, V., Recanatini, M., & Melchiorre, C. (2008). Multi-target-directed ligands to combat neurodegenerative diseases. *Journal of Medicinal Chemistry*, *51*(3), 347–372.

Crespi, C. L., & Miller, V. P. (1999). The use of heterologously expressed drug metabolizing enzymes-state of the art and prospects for the future. *Pharmacology & Therapeutics*, *84*(2), 121–31.

ICH Harmonized Tripartite Guidelines Q1B (1996). Stability Testing: Photostability Testing of New Drug Substances and Products

ICH Harmonized Tripartite Guidelines Q1A (R2) (2003). Stability Testing of New Drug Substances and Products.

Prakash, C., Shaffer, C. L., Nedderman, A. (2007). Analytical strategies for identifying drug metabolites. *Mass Spectrometry Reviews*, *26*(2), 340–369.

Reynolds, D. W., Facchine, K. L., Mullaney, J. F., Alsante, K. M., Hatajik, T. D., & Motto, M. G. (2002). Available Guidance and best practices for conducting forced degradation studies. *Pharmaceutical Technology*.

Sterling, J., Herzig, Y., Goren, T., Finkelstein, N., Lerner, D., Goldenberg, W.,Weinstock, M. et al. (2002). Novel Dual Inhibitors of AChE and MAO Derived from Hydroxy Aminoindan and Phenethylamine as Potential Treatment for Alzheimer 's Disease. *Journal of Medicinal Chemistry*, *45*, 5260–5279.

Zindo F.T., Joubert J., M. S. F. (2015). Propargylamine as functional moiety in the design of multifunctional drugs for neurodegenerative disorders: MAO inhibition and beyond. *Future Med. Chem.*, *7*(5), 609–629.

CHAPTER 2. Aim of the work

Chemical stability studies were performed on both drug substance and drug product to guarantee their efficacy, quality and safety and fulfill the requirements of regulatory authorities. In this area, forced degradation studies provide useful data to support: the intrinsic stability of the drug molecule, through the identification of possible degradants and the corresponding degradation pathways, and the development and validation of stability-indicating analytical procedures.

On the other hand, metabolic stability studies were performed on drugs to identify the metabolites arising from phase I and phase II reactions while delineating the corresponding metabolic pathways; these studies have become an integral part of the drug discovery/development process while playing a role also in post-marketing phase. Since drug metabolites may have intrinsic pharmacological activity or display specific toxicity, their knowledge is relevant for both pharmacokinetic, pharmacodynamic and for toxicokinetics. Generally, in academic research, chemical and metabolic stability studies were not conducted in an integrated manner being preferably done from researchers having different expertise. However, since the intrinsic stability of drugs can be strictly related to its metabolic stability, the integration of both aspects of stability could be conveniently performed defining a unique chemical and metabolic stability space.

In this work the chemical and metabolic stability of three propargylamine-containing drugs, whose structures are reported in the Figure 1, were studied.

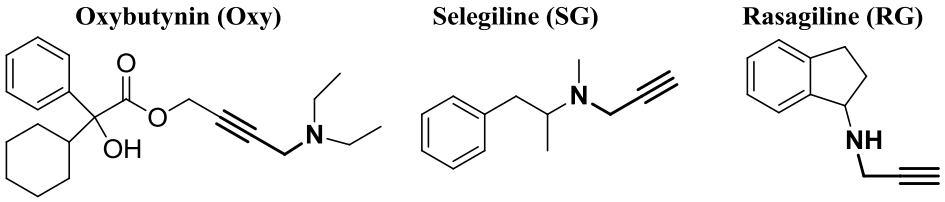

Figure 1.

The interest regarding this class of drugs arises from the analyses in the course of stability studies performed on new formulations of oxybutynin hydrochloride (**Oxy**), a tertiary propargylamine used for the management of urinary frequency, urgency and incontinence in neurogenic bladder disorders. During the study, a new and unprecedented degradation product

was identified in topical formulations, whose structure and mechanism of formation has been determined through a forced degradation study. These results prompted us to extend the study of chemical and metabolic stability to other propargylamine-containing drugs. Selegiline (**SG**, tertiary and H-terminated propargylamine) and rasagiline (**RG**, secondary and H-terminated propargylamine), MAO-B inhibitors used in the treatment of Parkinson's Disease, were included in the panel of compounds to increase the chemical diversity of propargylamine moiety.

To face the analytical tasks, required in performing the chemical and metabolic stability studies, LC-DAD-UV and LC-ESI-MS/MS techniques were employed: the analytical methods were developed to allow both qualitative and quantitative determination of analytes. Moreover, the new degradation products showing in their structure the presence of a structural alert were assessed for genotoxic potential evaluation; similarly, the new metabolites will be assessed for their potential pharmacodynamic activity.

CHAPTER 3. New insights in oxybutynin chemical stability: identification in transdermal patches of a new impurity arising from oxybutynin *N*-oxide rearrangement

3.1 INTRODUCTION

Oxybutynin hydrochloride (4-(diethylamino)but-2-ynyl (RS)-2-cyclohexyl-2-hydroxy-2-phenyl-acetate hydrochloride, **Oxy**) is an antimuscarinic drug which is used for the management of urinary frequency, urgency and incontinence in neurogenic bladder disorders and in idiopathic detrusor instability (Kennelly, 2010). With **Oxy** being the first choice in treating urinary incontinence, different types of formulations are at present available on the market: immediate and extended release tablets, oral solutions, syrup and solution for intravesical administration. Alternatively, to mitigate the systemic adverse effects occurring during the therapy, **Oxy** *free base* was employed in topical formulations such as adhesive patch (Kentera™) and gel (Gelnique™) (Shaw et al., 2007). Indeed oxybutynin is associated with a high incidence of systemic side-effects, including dry mouth, constipation, blurred vision, dryness of the eyes, palpitations, drowsiness, dizziness and esophageal reflux (Lose et al., 2001).

From a structural point of view **Oxy** is characterized by the presence of a tertiary propargylamine moiety and a carboxyester function; as a consequence, the chemical stability of **Oxy** has been investigated (Miyamoto et al., 1994), demonstrating the formation of a single hydrolytic degradation product, namely α-cyclohexylmandelic acid (**CHMA**). The formation of **CHMA** was also observed by Wagieh et al. (2010) and El-Gindy (2005) during the stress studies performed in acidic and alkaline conditions. Moreover, **CHMA** was the only degradation product included in the list of specified impurities in both the **Oxy** monographs of the European and United States Pharmacopoeias (EP 8, 2013; USP 38, 2015). In accordance with this scenario, a literature survey showed that the stability indicating analytical methods (Wagieh et al., 2010; El-Gindy, 2005; De Schutter et al., 1988) for the determination of **Oxy** in drug substance and drug product take into account **CHMA** as the only degradation product. Interestingly, even if De Shutter et al. (1988) noted the formation of several minor peaks in the chromatogram of **Oxy** treated with hydrogen peroxide in severe conditions, no degradation product arising from oxidation has been identified so far. At first sight this is not

surprising, because oxybutynin is mainly used as hydrochloride salt and the corresponding protonated amino group is scarcely prone to oxidation. However, due to its better lipophylicity and permeability, **Oxy** *free base* is used in the new topical formulations: in that case the unionized tertiary amine can be more easily oxidized with the potential formation of degradation products.

These considerations, combined with the observation of an unknown impurity during oxybutynin adhesive patch analysis, prompted us to reinvestigate the **Oxy** chemical stability, focusing our attention on the oxidative degradation pathway.

In this report, we elucidated the chemical fate of **Oxy** in oxidative conditions showing the formation of the corresponding diastereomeric *N*-oxides (**Oxy-NO1** and **Oxy-NO2**) and an unprecedented degradation product (**Oxy-EK**), whose structure and mechanism of formation were discussed. Finally, **Oxy-EK** synthesis was described, allowing us to propose it as the indicator of stability for the oxidative degradation in stability studies and, at the same time, to evaluate its potential mutagenic effects.

3.2 EXPERIMENTAL

3.2.1. Reagents and chemicals

Methanol (HPLC grade), tetrahydrofuran (THF), ammonium acetate, iron (III) trichloride hexahydrate, copper sulphate, pentahydrate, hydrogen peroxide solution (30% *w/w)*, *N*,*O*-dimethylhydroxylamine hydrochloride acetoxyacetyl chloride, ethynylmagnesium bromide (0.5 M in THF), 4,4'-azobis-(4-cyanovaleric acid) (**ACVA**), α-cyclohexylmandelic acid (97%), ninhydrin, histidine, tryptophan, biotin, 2-nitrofluorene (**2NF**), 2-aminoanthracene (**2AA**), sodium azide (**SA**), 9-aminoacridine (**9AA**) and methyl methanesulfonate (**MMS**), bacteriological agar, nutrient broth, nutrient agar were supplied by Sigma-Aldrich (St. Louis, MO, USA). Water (HPLC grade) was obtained from Milli-Q reverse osmosis system (Millipore Co., Billerica MA, USA). Column chromatography was performed on silica gel 60 (230-400 mesh ASTM Merck). TLC was carried out on plates with a layer thickness of 0.25 mm (silica gel 60 F254; Merck); when necessary, they were visualized after spraying with ninhydrin reagent. **Oxy** (potency: 99.3%), was obtained as gift sample from Pharmafar S.r.l. (Torino, Italy); Kentera™ transdermal patches (lot n° 356861C; exp. date: 11/2013 and lot n° 818002A exp. date: 09/2016; Nicobrand Ltd, Coleraine, Northern Ireland), were purchased from local pharmacy. The S9 fraction (the liver postmitochondrial supernatant of rats treated

with the mixture phenobarbital/β-naphthoflavone to induce the hepatic microsomal enzymes) was supplied and certified by Moltox (Molecular Toxicology, Boone, NC, USA).

3.2.2. Instrumentation and chromatographic conditions

3.2.2.1 LC-UV analyses

A Shimadzu HPLC system, consisting in two LC-10AD *Vp* module pumps and a DGU-14-A on-line vacuum degasser, was used. The analyses were carried out on a Luna C18(2) (150 x 4.6 mm I.D., 5μm d_p; Phenomenex, Torrance, CA, USA) column. The isocratic mobile phase (flow rate 1.2 ml/min) was composed of eluant A ammonium acetate buffer (20 mM pH=5.7) and eluant B methanol, being the A:B ratio 25:75 (*v/v*). The eluants A and B were filtered through a 0.45 μm PVDF membrane filter prior the use. A SIL-10AD *Vp* autosampler was used for the injection of samples (20μl). The SPD-M10A *Vp* photodiode array detector was used to detect **Oxy** and the degradation products **CHMA, Oxy-NOs** at 210 nm and **Oxy-EK** at 311 nm. A LCsolution 1.24 software was used to process the chromatograms. All the analyses were carried out at room temperature.

3.2.2.2 LC-MS/MS analyses

A Thermo Finningan LCQ Deca XP Plus system equipped with a quaternary pump, a Surveyor AS autosampler, a Surveyor PDA detector and a vacuum degasser was used for LC-MS analysis (Thermo Electron Corporation, Waltham, MA, USA).

The analysis were performed on a Luna C18(2) (150 x 4.6 mm I.D., 5μm d_p; (Phenomenex, Torrance, CA, USA) column maintained at 35°C. The mobile phase (flow rate 0.8 ml/min) was composed of eluant A: ammonium acetate buffer (pH 5.7; 10 mM) and eluant B: methanol, using an isocratic mode being 20:80 the ratio A:B; the sample injection volume was 20 μl. The eluate was injected into the electrospray ion source (ESI) with a splitting of 40% and the MS and MS/MS spectra were acquired and processed using the Xcalibur® software (Thermo Electron Corporation, Waltham, MA, USA). The operating conditions of the ion trap mass spectrometer in positive ion mode were as follows: spray (source) voltage, 5.30 kV; source current, 80 μA; capillary temperature, 350 °C; capillary voltage, 23.00 V; tube lens offset, 40.0 V; multipole 1 offset, -5.75 V; multipole 2 offset, -7.00 V; sheath gas flow (N_2), 60 Auxiliary Units; sweep gas flow (N_2): 6.0 A. U. Data were acquired both full

scan and MS/MS product ion scan modes using mass scan range *m/z* 105 to 500, optimizing the collision energy at 30%.

3.2.2.3 Spectroscopic analyses

^{1}H and ^{13}C experiments were performed at 298K on a JEOL Eclipse ECP 300 FT MHz spectrometer (Jeol Ltd. Tokyo, Japan) operating at 7.05T. Chemical shifts are reported in part per million (ppm). FT-IR experiments were performed on AVATAR 370 FT-IR (Thermo Fisher Scientific, Madison WI, USA) spectrophotometers.

3.2.3 Forced degradation study of Oxy

The degradation study in solution was done at 1 mg/ml **Oxy** concentration. For the acidic degradation study, **Oxy** was dissolved in 0.5 N HCl and the solution was left in the dark at 50°C for 24 h. The degradation in alkaline conditions was done in 0.01 N NaOH in presence of methanol/water 50/50 and the solution was left in the dark at 50°C for 30 minutes.

The oxidative degradation was studied, protecting the samples from light, using the following protocols:

a) **Oxy** was dissolved in 3% (*v*/*v*) H_2O_2 in acetate buffer (pH 4.5) and the solution was left at room temperature (r.t.) for 24h.
b) **Oxy** was dissolved in 3% (*v*/*v*) H_2O_2 in 50/50 water/methanol mixture (8 mL) in the presence of sodium hydrogen carbonate (100 mg): the solution was left at r.t. for 4h.
c) **Oxy** was dissolved in acetate buffer (pH=4.5) in the presence of 1.5 mM Cu^{2+} or Fe^{3+} and left at r.t. for 4h.
d) To a solution of **Oxy** in 50/50 methanol/water, the radical initiator **ACVA**, previously dissolved in water (1 mg/ml) in the presence of sodium hydrogen carbonate, was added. The mixture of reaction (**ACVA**: 1 mM final concentration) was stored at 60 °C for 24h.

The thermal and photodegradation were studied by testing **Oxy** and **Oxy** *free base*. In particular, for thermal degradation, the samples were stored for 18 h at 60 °C in a hot air oven. Photodegradation was carried out, at r.t., by exposing a thin layer (10 mg) of **Oxy** or **Oxy** *free base* to daylight and UV-light (365 nm) for 15 days and 4 hours respectively.

3.2.3.1 Sample preparation

Before LC-UV and LC-MS/MS analyses, acidic and alkaline samples were first neutralized by addition of a suitable amount of sodium phosphate dibasic and diluted phosphoric acid (8.5% *w/v*) respectively, and then diluted with mobile phase. The other stressed samples were dissolved or tenfold diluted in mobile phase only; finally, solid samples were dissolved in mobile phase to attain ~0.1 mg/ml concentration. For comparison purposes a freshly prepared aqueous solution of **Oxy** (~1 mg/ml) was diluted and analyzed as above.

3.2.3.2 Procedure for the analysis of transdermal patch

After removal of the protective film (Kentera™ 36 mg/39 cm^2), the patch was transferred into a Falcon™ conical tube and extracted by sonication (SweepZone Technology Quantrex S200) with methanol (3x20ml). The combined methanolic extracts were evaporated to small volume under reduced pressure and then transferred and diluted in a 20 ml volumetric flask with methanol/water 75/25. The solution was analyzed with LC-UV and LC-MS/MS. To evaluate the role of the extraction conditions on the chemical stability of **Oxy**, the procedure was repeated on a sample of **Oxy** *free base*.

3.2.3.3. Accelerated stability study of transdermal patch

The stability study was performed in a Binder-KBF-115 constant climate chamber (Binder GmbH, Tuttlingen Germany). Drug product (Kentera™ transdermal patch) packaged in the container closure system used for marketing was stored using the following condition: 40°C±2°C/75% RH±5%, t= 6 months.

3.2.4. Isolation and purification of Oxy-EK

To a solution of **Oxy** (500 mg, 1.27 mmol) in 5 ml of water, 240 mg of sodium hydrogen carbonate 5 ml of methanol and 5 ml of 30% *w/w* hydrogen peroxide were added. The mixture was reacted, under stirring at r.t., for 3h monitoring by TLC analysis (eluant: CH_2Cl_2/MeOH 9:1). At the end of the reaction, methanol was evaporated under reduced pressure. The aqueous residue was extracted (3x15 ml) with CH_2Cl_2. The pooled organic layers were washed with brine, dried over anhydrous sodium sulphate, filtered and evaporated in vacuo to dryness. The pale-yellow oily residue was left overnight at r.t. and then purified by column chromatography using dichloromethane/methanol 98/2 as eluant to give pure **Oxy-EK** (88 mg, 19% yield; 94% purity by HPLC assay).

ESI-MS: calculated for $C_{22}H_{31}NO_4$ *M*= 373.48; Found *m/z* = 374 $[M+H]^+$ and *m/z* = 396 $[M+Na]^+$

FT-IR: (KBr): 3515, 2932, 2852, 1727, 1646 cm^{-1}.

^{1}H-NMR and ***^{13}C-NMR (*$CDCl_3$*)***: for comparison purposes the spectra of **Oxy-EK** and **Oxy** *free base* were reported in the Table 1.

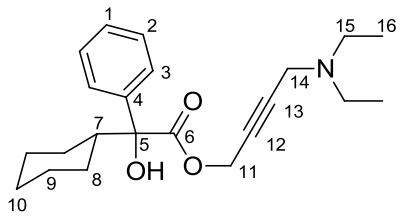

Oxy free base

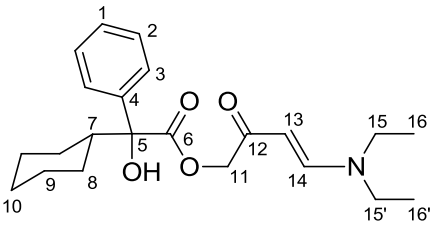

Oxy-EK

#	^{1}H-NMR	^{13}C-NMR	#	^{1}H-NMR	^{13}C-NMR
1	7.24 tt (7.2, 1.4)	127.4	**1**	7.24 tt (7.2, 1.2)	127.4
2	7.31 tt (7.4, 1.7)	126.0	**2**	7.34 tt (7.4, 1.5)	126.3
3	7.62 bd	128.0	**3**	7.70 dd (8.4, 1.3)	128.2
4	---	140.5	**4**	---	140.9
5	3.61 s (OH)	81.0	**5**	3.72 s (OH)	81.2
6	---	174.9	**6**	---	175.2
7	2.23 m	46.1	**7**	2.30 (m)	46.0
8	1.80-1.05 m	27.2, 26.3 (x2), 26.2, 25.4	**8**	1.83-1.10 m	27.4, 26.4 (x2), 26.3, 25.6
9			**9**		
10			**10**		
11	4.81 dt (15.3, 1.8) 4.69 dt (15.3, 1.8)	54.2	**11**	4.68 d (15.3) 4.57 d (15.3)	69.0
12	---	82.6, 77.9	**12**	---	189.7
13	---		**13**	4.82 d (12.5)	89.4
14	3.40 t (1.8)	40.9	**14**	7.63 d (12.6)	152.2
15	2.44 q (7.2)	47.3	**15** **15'**	3.23 q (7.2) 2.92 q (7.1)	50.5 42.7
16	1.01 t (7.2)	12.8	**16** **16'**	1.16 t (7.1) 1.00 t (7.1)	14.7 11.5

Table 1.

3.2.5. Synthesis of Oxy *free base*

To a solution of oxybutynin hydrochloride (600 mg, 1.5 mmol) in water, 15.5 ml of sodium hydroxide 0.1N were added. The aqueous layer was extracted with dichloromethane. The organic solution was washed with brine, dried over anhydrous sodium sulphate, filtered and evaporated in vacuo to dryness obtaining a pale yellow oily product (477 mg, 89% yield).

ESI-MS: calculated for $C_{22}H_{31}NO_3$ *M*= 357,49; Found *m/z* = 358 $[M+H]^+$

3.2.6 Synthesis of degradation products

*3.2.6.1 Synthesis of 4-(diethylamino)-2-oxy-but-3-enyl(RS)-2-cyclohexyl-2-hydroxy-2-phenylacetate (**Oxy-NO2**)*

To a solution of **Oxy** (500 mg, 1.27 mmol) in 5 ml of water, 240 mg of sodium hydrogen carbonate 5 ml of methanol and 5 ml of 30% *w/w* hydrogen peroxide were added. The mixture was reacted and extracted following the same procedure reported in the paragraph 3.2.4; however the purification was performed immediately after the extraction, using dichloromethane/methanol 90/10 as eluant, giving **Oxy-NO2** (193 mg; 40% yield; purity ~70% HPLC).

ESI-MS: calculated for $C_{22}H_{31}NO_4$ *M*= 373.48; Found *m/z* = 374 $[M+H]^+$ and *m/z* = 396 $[M+Na]^+$

*3.2.6.2 Stability of **Oxy-NO2***

Two aliquots (~100 mg) of freshly prepared **Oxy-NO2** were stored, separately, in a refrigerator at -20°C and at room temperature. The LC-UV analysis was carried out at 0, 1, 2, 24, 48h by weighing and dissolving in 50 ml of methanol an appropriate amount of the samples.

*3.2.6.3 Synthesis of 2-[methoxy(methyl)amino]-2-oxoethyl acetate (**1**)*

N,O-Dimethylhydroxylamine hydrochloride (4.8 g, 49.2 mmol) was dissolved in freshly prepared anhydrous dichloromethane (40 ml) and acetoxyacetyl chloride (6.3 ml, 59.6 mmol) was added dropwise maintaining the reaction at 0°C under nitrogen. Triethylamine, (13.6 ml, 98.1 mmol) was then added dropwise removing the gas generated from the reaction flask. The reaction mixture was stirred under nitrogen for 3h while the temperature rose to r.t. Finally, the reaction was quenched by adding 20 ml of methanol obtaining a clear solution. After concentration to dryness, the residue was diluted with ice-cold freshly prepared anhydrous THF and the white salt was filtered under vacuum and washed with dry THF. The filtrates were combined and concentrated under reduced pressure to give a yellow oil (8.2 g, quantitative yield).

***ESI-MS** m/z162 $[M+H]^+$.*

*3.2.6.4 Synthesis of 2-oxobut-3-yn-1-yl acetate (**2**)*

To a solution of compound **1** (2-[methoxy(methyl)amino]-2-oxoethyl acetate; 8.0 g, 49.6mmol) in freshly prepared anhydrous THF (30 ml), ethynylmagnesium bromide (100 ml, 0.5 M in THF) was added dropwise at -78 °C. The mixture was stirred for 7 h while the temperature rose to r.t. After partial concentration under reduced pressure, the reaction mixture was poured into 40 ml of ice-cold *o*-phosphoric acid (20%) and the organic phase diluted with diethyl ether. The aqueous layer was separated and extracted twice with diethyl ether. The combined organic layers were washed with brine, dried over anhydrous sodium sulfate, filtered and evaporated under reduced pressure obtaining a yellow oil. The crude product was directly used for the next step of the synthesis.

*3.2.6.5 Synthesis of (3E)-4-(diethylamino)-1-hydroxybut-3-en-2-one (**3**)*

a) To a solution of compound **2** (2-oxobut-3-yn-1-yl acetate; 6.4 g, 51 mmol) in anhydrous THF (30 ml), diethylamine (10.5 ml, 102 mmol) was added dropwise and the mixture was stirred overnight at r.t.

Evaporation under reduced pressure of the mixture gave a yellow oil which was analyzed by TLC (dichloromethane/methanol 9:1, visualization with ninhydrin) obtaining two spots having R_f 0.70 and 0.62 respectively).

b) The residue was suspended in a mixture of 2 ml of saturated sodium carbonate solution and about 50 ml of methanol and vigorously stirred for 2h at r.t. After the evaporation of methanol under reduced pressure, the aqueous residue was extracted three times with dichloromethane. The combined organic layers were washed with brine, dried over anhydrous sodium sulfate, filtered and evaporated under reduced pressure. The crude residue was purified by column chromatography using dichloromethane–methanol 9:1 as eluant to give compound **3** as yellow oil (1.1 g, 6.8 mmol, 13% yield).

ESI-MS *m/z 158* $[M+H]^+$.

^{1}***H-NMR*** *(300 MHz,* $CDCl_3$*)* δ *7.67(d, J=12.6 Hz, H-olefinic), 4.99(d, J=12.6 Hz, H-olefinic), 4.16(s,* CH_2*), 3.67(s, OH), 3.15(s,* $2CH_2$*), 1.17(s,* $2CH_3$*).*

*3.2.6.6 Synthesis of (3E)-4-(*N,N-*diethylamino)-2-oxo-3-buten-1-yl 1-cyclohexyl-1-phenylglycolate (**Oxy-EK**)*

To a suspension of α-cycloexylmandelic acid (801 mg, 3.4 mmol) in anhydrous toluene (30 ml), triethylamine (1.2 ml, 8.5 mmol) was added under nitrogen. Subsequently, a solution of isobutyl chloroformate (532 µl, 4.1 mmol) dissolved in a few ml of anhydrous toluene, was added dropwise and the resultant white suspension was stirred at 60°C for 1.5h; then compound **3** (700 mg, 4.4 mmol) was added and the reaction mixture was stirred at 100 °C for 3h and then at 70°C overnight. The reaction mixture was slightly diluted with ethyl acetate and quenched by the addition of 10% aqueous sodium hydrogen phosphate solution. The organic layer was washed with brine, dried over anhydrous sodium sulfate, filtered and evaporated under reduced pressure giving a crude oil which was first purified by column chromatography using dichloromethane/methanol 98:2 as eluant and then by a second column using petroleum ether/2-propanol 9:1 as eluant to give **Oxy-EK** as a pale yellow oil (389 mg, 1.0 mmol, 29 % yield, 95% purity by HPLC assay).

ESI-MS: calculated for $C_{22}H_{31}NO_4$ *M*= 373.48; Found *m/z* = 374 $[M+H]^+$ and *m/z* = 396 $[M+Na]^+$.

(The scheme of **Oxy-EK** synthesis is reported in the Figure 9).

3.2.7. Evaluation of the mutagenic effects of Oxy-EK and Oxy

(This study was carried out in collaboration with the Department of Physiology and Pharmacology "V. Erspamer", Sapienza University, Rome)

Experiments were carried out on different *Salmonella typhimurium* and *Escherichia coli* strains, according to Di Sotto et al. (2013). Taking into account that bacteria are unable to metabolize inactive chemicals via cytochrome P450, an exogenous metabolic activation system S9 was also included in the Ames test.

3.2.7.1. Bacterial strains

A set of different strains, *Salmonella typhimurium* TA1535 (hisG46 chl1005 rfa1001), TA1537 (hisC3076 chl1007 rfa1003), TA1538 (hisD3052 chl1008 rfa1004), TA98 (hisD3052 chl1008 rfa1004 pKM101), and TA100 (hisG46 chl1005 rfa1001 pKM101), and *Escherichia coli* WP2uvrA (trpE65 uvrA155) and WP2uvrA/R (trpE65 uvrA155 pKM101), was used. The strains TA1535, TA1537 and TA1538 were supplied by Department of Pharmacy and Biotechnology, University of Bologna (Italy), while TA98, TA100, WP2uvrA and

WP2uvrA/R were provided by the Research Toxicological Centre (Pomezia, Rome, Italy). After confirmation of the genotypes by the Strain Check Assay (Di Sotto et al., 2014), the permanent cultures of each strain were prepared and then frozen. The working cultures, prepared from the permanent ones, were incubated overnight (16 h) at 37 °C, to reach a concentration of approximately 1×10^9 bacteria/ml. In each experiment the number of viable cells for each strain was determined according to Ames et al. (1975). Viability of the tested strains TA1535, TA1537, TA1538, TA98, TA100, WP2uvrA and WP2uvrA/R, expressed as viable cells/plate, was of 275.1±8.7, 343.7±14.2, 236.5±11.7, 240.0±13.1, 209.0±9.5, 371.5±12.9 and 319.0±15.5, respectively.

3.2.7.2. Preliminary assays

Preliminarily, the solubility of **Oxy-EK** and **Oxy** in the final mixture was assessed. Insolubility was defined as the formation of a precipitate of the substance in the final mixture under the test conditions and evident to unaided eye (Di Sotto et al., 2014).

Starting from the highest soluble concentration, different concentrations of the substances (dilution factor from 1:2 to 1:5) were tested for the cytotoxicity, in order to find the highest concentration to study in the mutagenicity test. A cytotoxic effect was evaluated as a reduction (> 30%) in the number of revertant colonies and as a change in the auxotrophic background growth (background lawn), in comparison with the control plates (Di Sotto et al., 2014). To perform the test, solutions of test substances (50 µl) were added to an overnight culture (100 µl) and S9 mixture or phosphate buffer (0.1 M; 500 µl). The mixture was pre-incubated under shaking at 37 °C for 30 min, then it was added with top agar (2 ml) containing 10% of histidine/ biotin (0.5 mM) for *S. typhimurium* strains, and 10% of tryptophan (0.5 mM) for E. coli strains; finally it was poured onto a minimal agar plate. After incubation at 37 °C for 48 h, the plates were examined, the background lawn was observed and the bacterial colonies were scored.

3.2.7.3. Mutagenicity assay

The mutagenicity was assayed by the pre-incubation method (Di Sotto et al., 2014), starting from the highest non-toxic concentration (1:1.4 dilution factor). The vehicle DMSO (2% *v/v*) was used as negative control. The mutagens SA (1 µg/plate for TA1535 and TA100), 9AA (50 µg/plate for TA1537), 2NF (2 µg/plate for TA1538 and TA98), MMS (500 µg/plate for WP2uvrA and WP2uvrA/R), 2AA (1 µg/plate for TA1538, TA98 and TA100 and 10 µg/plate for TA1535, TA1537, WP2uvrA and WP2uvrA/R), were used as positive controls, in order to verify the bacteria susceptibility to a known genotoxic damage. The experiments were repeated at least twice and each concentration was tested in triplicate. To perform the test, an overnight culture (100 µl) was added to the solutions of the samples tested (50 µl) plus S9 mixture or phosphate buffer (0.1 M) (500 µl). The mixture was gently vortexed in a sterile tube then was incubated under shaking at 37 °C for 30 min. After the pre-incubation, the tubes were added with top agar (2 ml) containing 10% of histidine/biotin (0.5 mM) for *S. typhimurium* strains, and 10% of tryptophan (0.5 mM) for *E. coli* strains, then were gently vortexed and poured onto a minimal agar plate. The plates were incubated at 37 °C for 72 h and then examined. The histidine- or tryptophan-independent revertant colonies and the viable cells were scored and the bacterial background lawn was observed. A positive response in the mutagenicity assay was defined as an increase (at least two-fold above the vehicle) in the histidine- or tryptophan-independent revertant colonies (Di Sotto et al., 2014).

3.2.7.4 Statistical analysis

All values are expressed as mean ±SE. The one-way analysis of variance (one-way ANOVA), followed by Dunnett's multiple comparison post test, was used to verify the significance of a positive response. A P value <0.05 was considered statistically significant. Statistical analysis was performed with GraphPad Prism™ (Version 4.00) software (GraphPad Software, Inc., San Diego, California, USA).

3.3 RESULTS AND DISCUSSION

3.3.1 Forced degradation study of Oxy by LC-UV analysis

In the course of the stability studies carried out during the development of new **Oxy** formulations and their comparison with those currently marketed, the presence of a degradation product in transdermal patch was observed with its structure unknown. To address the problem, a reinvestigation of the chemical stability of **Oxy**, using the stress conditions required by international guidelines (ICH, 2003), was undertaken. The hydrolysis of **Oxy** in alkaline and acidic solutions has been previously reported in the literature (Miyamoto et al., 1994) showing the formation of **CHMA** as degradation product. Accordingly, in our protocol the formation of **CHMA** (t_R= 2.1 min) in 0.01 N NaOH or 0.5 N HCl solutions as the only degradation product was observed (Figure 1a, 1b): its structure was confirmed by comparison of its retention time with that of **CHMA** reference standard (Figure 1c).

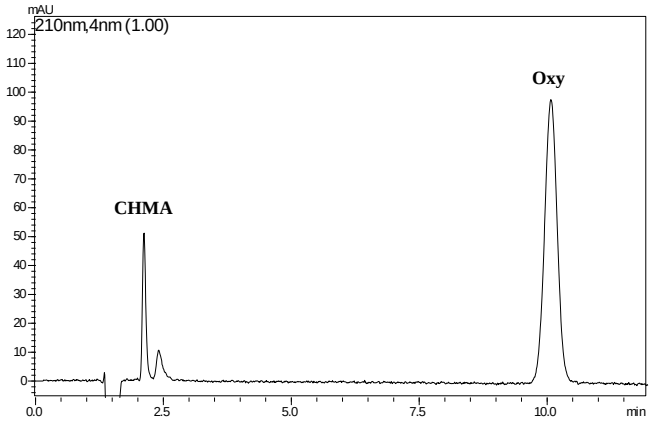

Figure 1a. LC-UV chromatogram of oxybutynin in 0.01N NaOH solution (t= 30 min at 50°C).

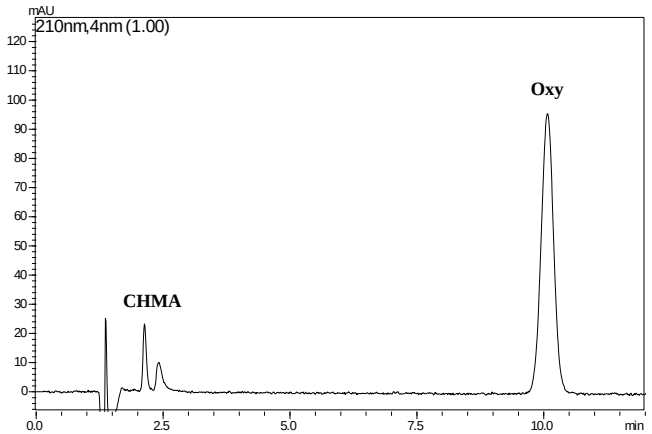

Figure 1b. LC-UV chromatogram of oxybutynin in 0.5N HCl solution (t= 24h at 50°C).

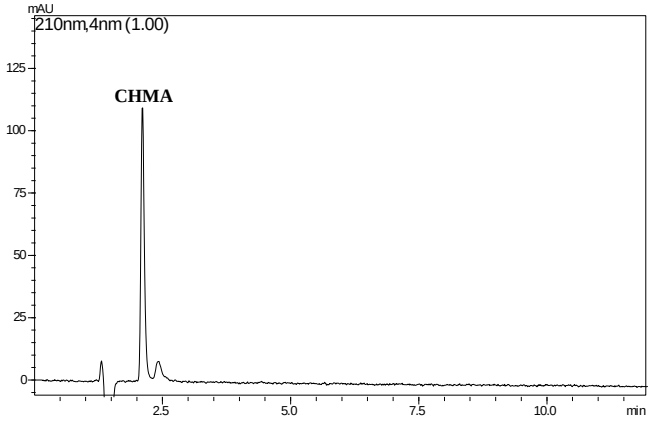

Figure 1c. LC-UV chromatogram of CHMA solution.

To evaluate the stability of **Oxy** in oxidative stress testing, four sets of experiments were performed. In the presence of hydrogen peroxide (pH= 4.5), demonstrating that no degradation occurred over 24 hours (data not shown). On the contrary, in alkaline conditions (pH~8), two degradation products, **Oxy-NO2** (t_R= 3,9 min) and **Oxy-EK** (t_R= 6.6 min), were observed in the LC-UV chromatogram reported in the Fig. 2-A1. It is worth noting that, differently from **Oxy** and **Oxy-NO2**, the intensity of the **Oxy-EK** peak dramatically increases when the analytes were detected a higher wavelength (i.e. 311 nm) Fig. 2-A2; that feature indicates the presence of a new chromophoric group in its structure. Moreover, neither **Oxy-NO2** nor **Oxy-EK** were formed in the alkaline solution in the absence of hydrogen peroxide ruling out their possible formation by hydrolysis. When the oxidative degradation was studied in the presence of the radical initiator **ACVA**, the formation of the peak of **Oxy-EK** was again observed (Fig.2-B) while the peak of **Oxy-NO2** was absent. Differently, **Oxy** did not undergo degradation in the presence of the transition metals Fe^{3+} and Cu^{2+} (data not shown): possibly, this could be due to the acidic conditions of the assay (pH= 4.5) favouring the protonated form of tertiary amine. The formation of **Oxy-EK** was also observed in thermal degradation of **Oxy** *free base* performed at 60 °C (Fig. 2-C) whereas **Oxy** in the same conditions did not (data not shown). Finally, the photodegradation was also studied, exposing **Oxy** or its free base to daylight and 365 nm UV-light, without observing the formation of degradation products (data not shown). These data showed that the assay in the presence of radical initiator allowed a better representation of Oxy oxidative degradation. Indeed, while hydrogen peroxide is a facile ‘‘two-electron’’ oxidant for amines this reaction does not involve peroxy radicals (Boccardi, 2005). On the other hand, it is recognized that the main

oxidative pathway in pharmaceutical solid dosage forms involves free radical chain reactions in which peroxy radical, $ROO^{\cdot}$, is the oxidant (Boccardi, 2005).

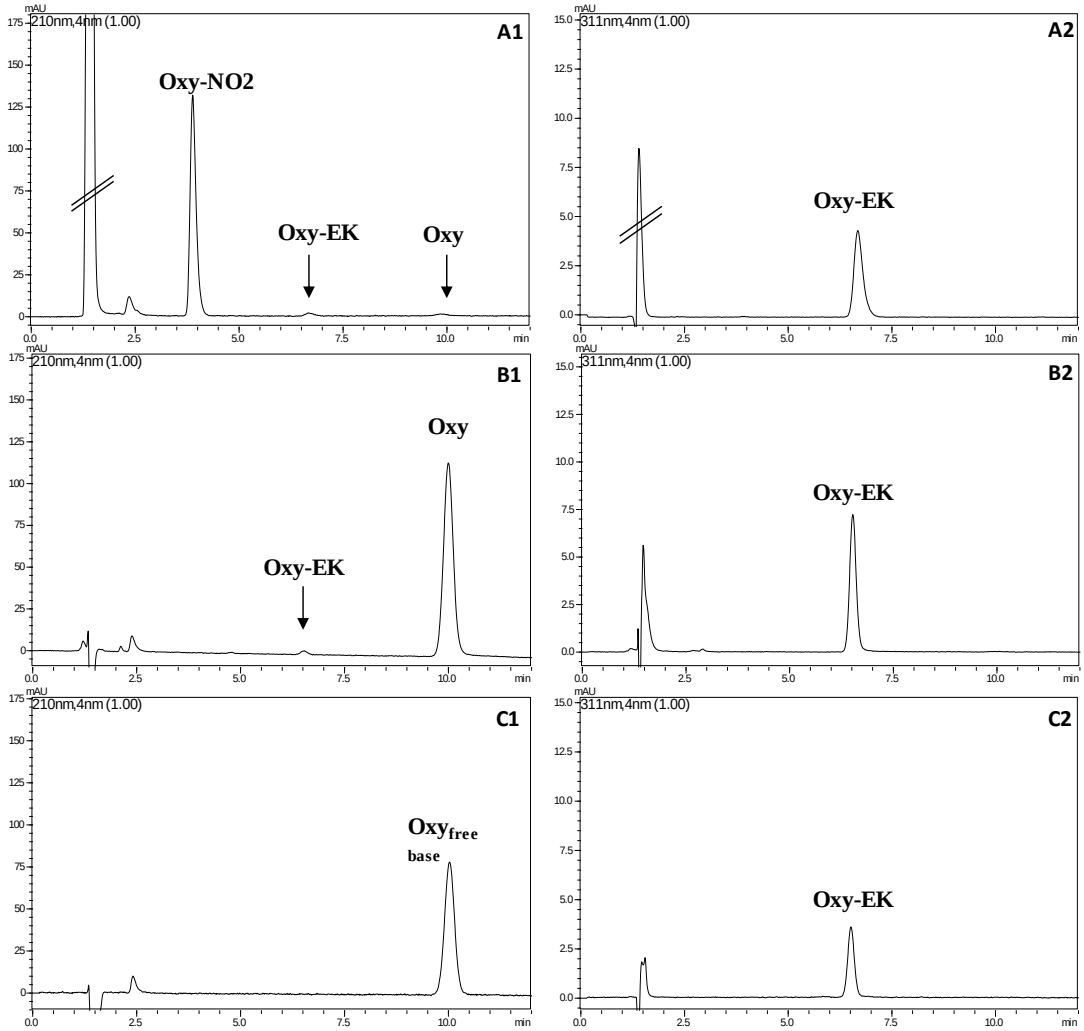

Figure 2. A1) LC-UV chromatogram (λ_a=210 nm) of **Oxy** in 3% H_2O_2 alkaline solution (t= 4h); A2) LC-UV chromatogram (λ_a=311 nm) of **Oxy** in 3% H_2O_2 alkaline solution (t= 4h). B1) LC-UV chromatogram (λ_a=210 nm) of **Oxy** in presence of radical initiator (t= 24h); B2) LC-UV chromatogram (λ_a=311 nm) of **Oxy** in presence of radical initiator (t= 24h). C1) LC-UV chromatogram (λ_a=210 nm) of **Oxy** *free base* in oven at 60°C (t= 18 h);. C2) LC-UV chromatogram (λ_a=311 nm) of **Oxy** *free base* in oven at 60°C (t= 18 h).

3.3.2. Structural characterization of degradation products by LC-ESI-MS/MS analysis

In order to obtain information on the structures of the degradation products, the hydrogen peroxide-treated sample was analyzed by LC-ESI-MS/MS. Interestingly, three degradation products were observed in the full mass chromatogram: **Oxy-NO1**, **Oxy-NO2** and **Oxy-EK**. They showed the same protonated molecule at *m/z* 374, (+16 Da with respect to **Oxy** *free base*) (Fig. 3) indicating the insertion of an oxygen atom in the structure of oxybutynin.

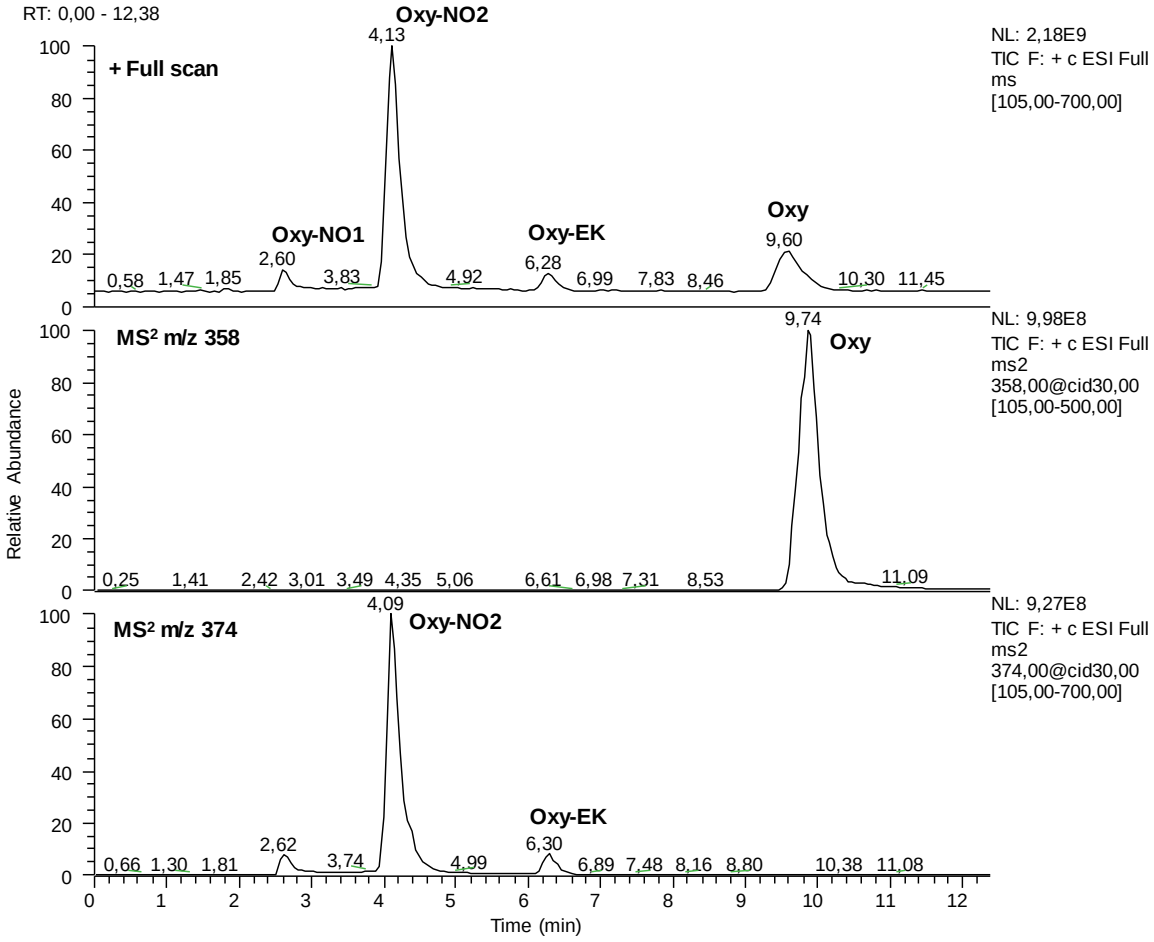

Figure 3. LC-MS chromatogram of **Oxy** in 3% H_2O_2 alkaline solution (t= 4h).

In particular, the presence of the tertiary amine function suggested that **Oxy-NO1** and **Oxy-NO2** are the diastereomeric *N*-oxides of oxybutynin: indeed their MS/MS spectra showed the same fragment ions although with different intensity pattern (Fig. 4).

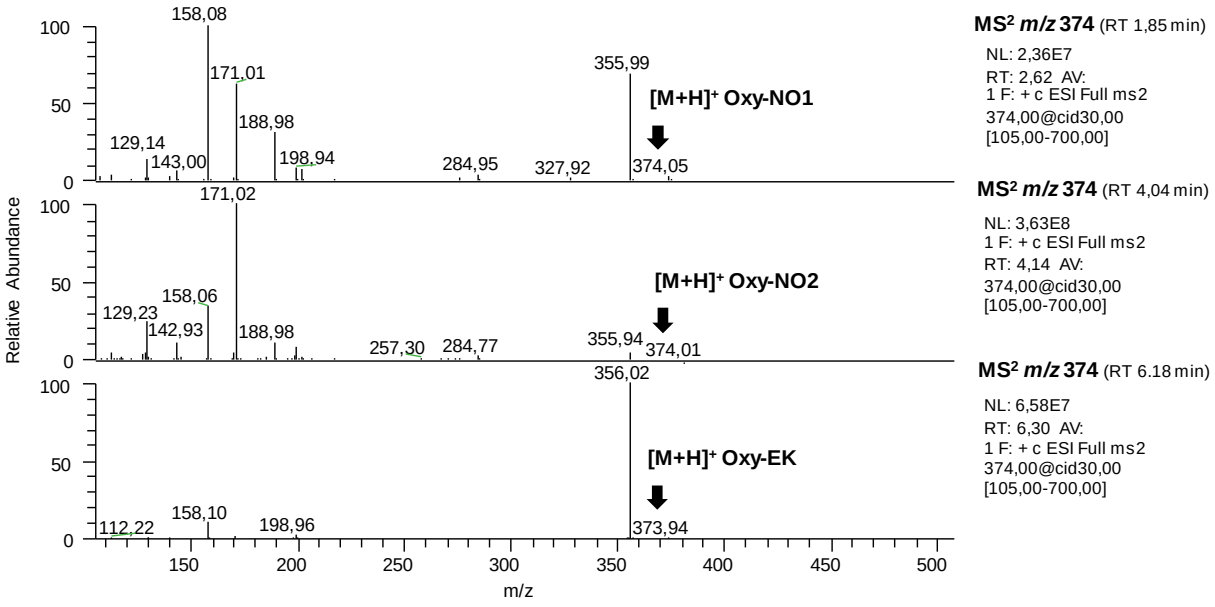

Figure 4. LC-MS^2 fragmentation patterns of **Oxy-NO1**, **Oxy-NO2** and **Oxy-EK**

The preparation of a synthetic standard was performed using hydrogen peroxide as oxidant followed by an immediate purification to avoid or at least mitigate its degradation. In any case the most abundant **Oxy-NO2** could be only isolated, being its mass spectral and chromatographic properties identical to those of the degradation product found in the transdermal patch and in the forced degradation study. **Oxy-NO2** was quite unstable undergoing, at room temperature, degradation leading to the formation of **Oxy-EK** as showed in the LC-UV chromatogram (Fig. 2-A). However when it was stored at -20°C the rate of degradation significantly decreased (Figure 5).

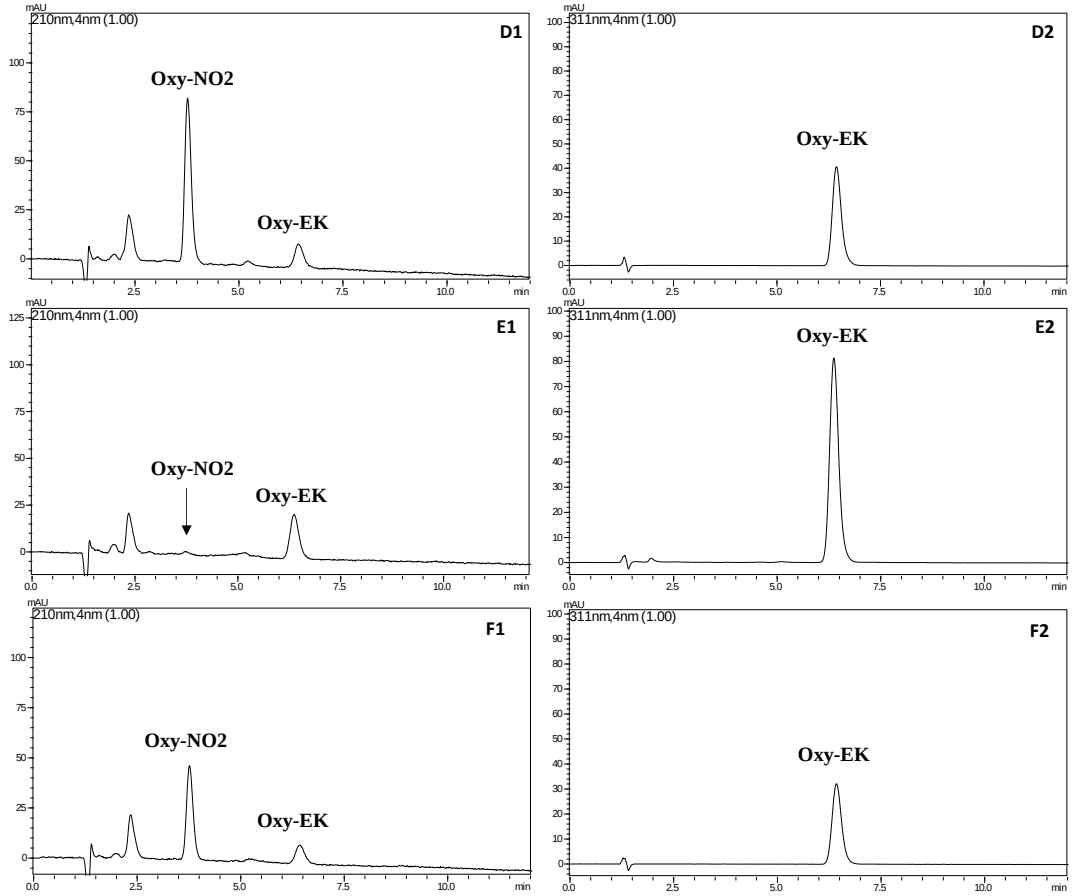

Figure 5. LC-UV chromatogram (λ_a= 210 nm) of a solution of **Oxy-NO2** (t=0 h) **D1**; LC-UV chromatogram (λ_a= 311 nm) of a solution of **Oxy-NO2** (t=0 h) **D2**. LC-UV chromatogram (λ_a= 210 nm) of a solution of **Oxy-NO2** at room temperature (t=24 h) **E1**; LC-UV chromatogram (λ_a= 311 nm) of a solution of **Oxy-NO2** at room temperature (t=24 h) **E2**. LC-UV chromatogram (λ_a= 210 nm) of a solution of **Oxy-NO2** at -20°C (t=48 h) **F1**; LC-UV chromatogram (λ_a= 311nm) of a solution of **Oxy-NO2** at -20°C (t=48 h) **F2**.

The assignment of the structure to **Oxy-EK** was challenging; the observation that **Oxy-EK** arises from the degradation of **Oxy-NO2,** combined with the findings of Szabo and Hermecz (2001) concerning the chemistry of tertiary propargylamine *N*-oxides, suggested that an intramolecular prototropic rearrangement of **Oxy-NO2** occurred with the formation of an enamino ketone moiety. The presence of enaminoketone moiety was in accordance with the chromatographic and spectroscopic properties of **Oxy-EK**: indeed, as expected for an oxygenated degradation product, its retention time was lower than that of **Oxy** (6.6 vs 9.9 min). Moreover, **Oxy-EK** showed an absorption maximum located at 311 nm, an unusually long wavelength, requiring the presence of a chromophore group as the enamino ketone (Figure 6).

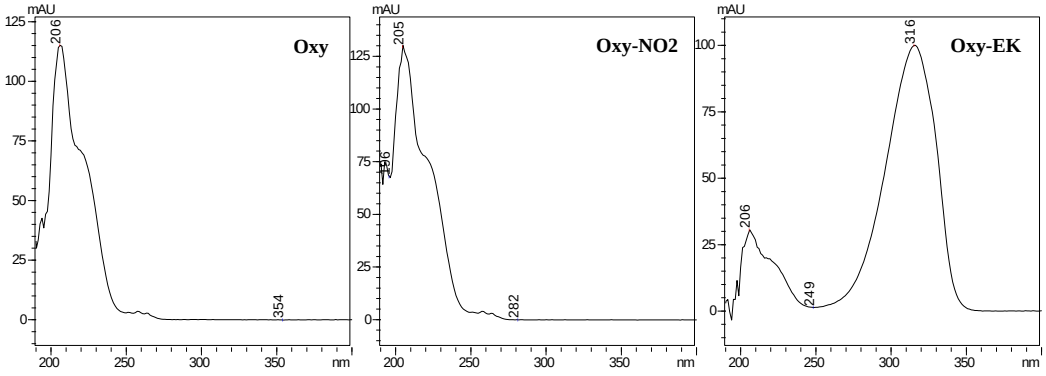

Figure 6. UV spectra of **Oxy**, **Oxy-NO2**, and the **Oxy-EK**. The UV spectra were recorded during the LC-UV analysis (see experimental part)

NMR spectra (Table 1) provided conclusive data for the structure assignment. In the ^{13}C-NMR spectrum the signal at 189.7 ppm indicates the presence of an *α,β*-unsaturated carbonyl group. This was confirmed by the signals at 152.2 and 89.4 ppm attributed to the double bond carbon atoms close to the carbonyl and the *N*,*N*-diethylamino groups respectively; the large difference in chemical shifts may be explained by the different influence of the electron-withdrawing (C=O) and electron-donating ($N(Et)_2$) neighbouring groups. The ^{1}H-NMR spectrum allowed to establish the stereochemistry of double bond (C=C); indeed the observed coupling constant (*J*= 12.6 *Hz*) was similar to that reported for enamino ketone function (Lin et al., 2009; Maingot et al., 2009). Finally, no significant variations in the signal patterns of phenyl, cyclohexyl and hydroxyester moieties were observed in ^{13}C- and ^{1}H-NMR spectra of **Oxy-EK** and **Oxy**. Based on these results, the oxidative degradation scheme of oxybutynin was reported in Figure 7.

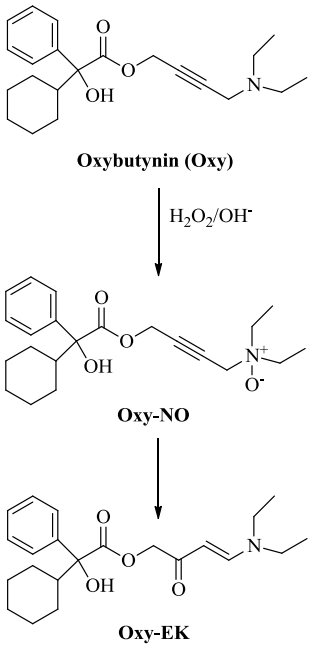

Figure 7. Oxidative degradation scheme of oxybutynin

Taking into account the mechanism of **Oxy-NO2** rearrangement and in particular the cyclic intermediate involved in (Szabò and Hermecz, 2001), it is reasonably that, initially, the *Z*-enaminoketone is formed (Fig. 8); however its stereochemical integrity could be lost through mesomeric phenomena. Indeed the push-pull character of the central double bond would impose a significant presence of a mesomeric and dipolar form that would account also for the unusually high UV-absorption wavelength showed by **Oxy-EK**. Moreover, the mesomeric form could be characterized by a relatively low rotational barrier energy allowing the system to equilibrate to the more stable *E*-isomer: indeed the greater stability of the latter could be due to the lower steric hindrance between the *N*,*N*-diethylamino group and the ketone function.

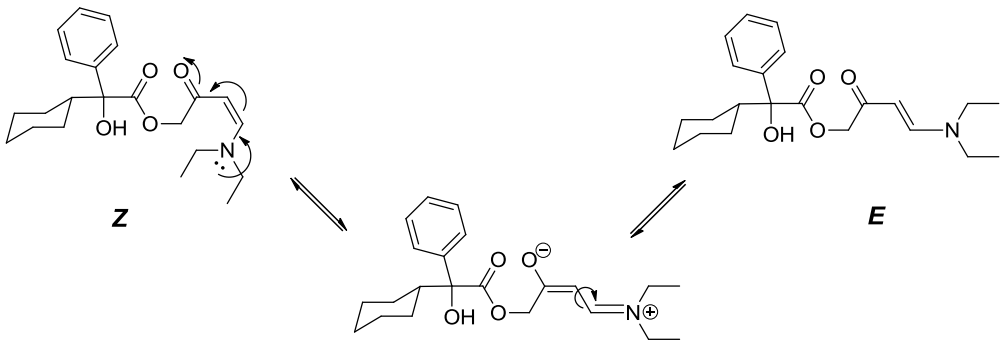

Figure 8. Mechanism of isomerization of **Oxy-EK**.

3.3.3 Synthesis of Oxy-EK

In order to confirm the structure assigned to **Oxy-EK**, its synthesis (Figure 9) was performed in three steps starting from the Weinreb amide **1**, easily obtained by reaction of *N*,*O*-dimethylhydroxylamine hydrochloride with acetoxyacetyl chloride. The known and excellent acylating property of Weinreb amide for organomagnesium reagents, was exploited to obtain the ethynyl ketone derivative **2** through the reaction with ethynylmagnesium bromide. The enamino ketone side chain **3** was eventually obtained through a Michael-type addition of *N*,*N*-diethylamine to hydrogen terminated ethynyl ketone **2**. Finally, **Oxy-EK** was prepared by coupling the enamino ketone side chain with **CHMA** via isobutyl chloroformate. Mass spectral and NMR data of synthetic **Oxy-EK** matched with those of the degradation product isolated from oxidative stress assay. Contrary to **Oxy-NO2**, **Oxy-EK** was a stable compound and this feature, combined with its synthetic accessibility, has allowed its use as the indicator of stability in the stability studies of **Oxy** *free base* containing formulations.

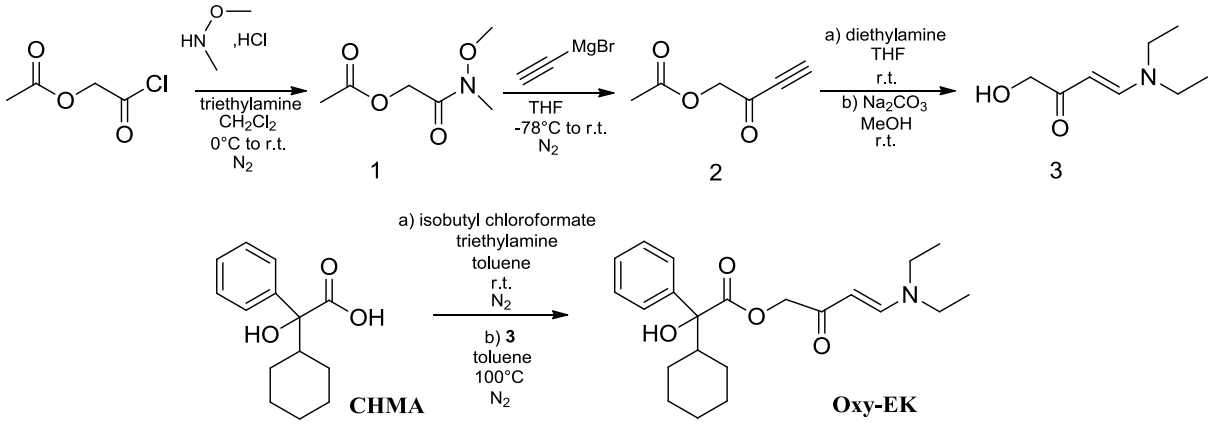

Figure 9. Scheme of **Oxy-EK** synthesis

3.3.4 Analysis of transdermal patches

LC-UV and LC-MS/MS analysis of the sample arising from the extraction of transdermal patches arising from two different lots were reported in figures (10-11).

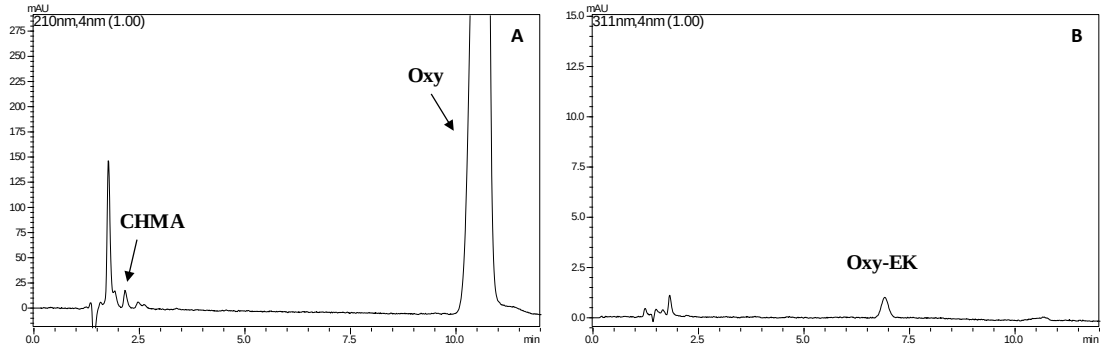

Figure 10. LC-UV chromatogram of the transdermal patch sample solution (lot n° 818002A, t=0 months) monitored at 210 nm (A) and 311 nm (B)

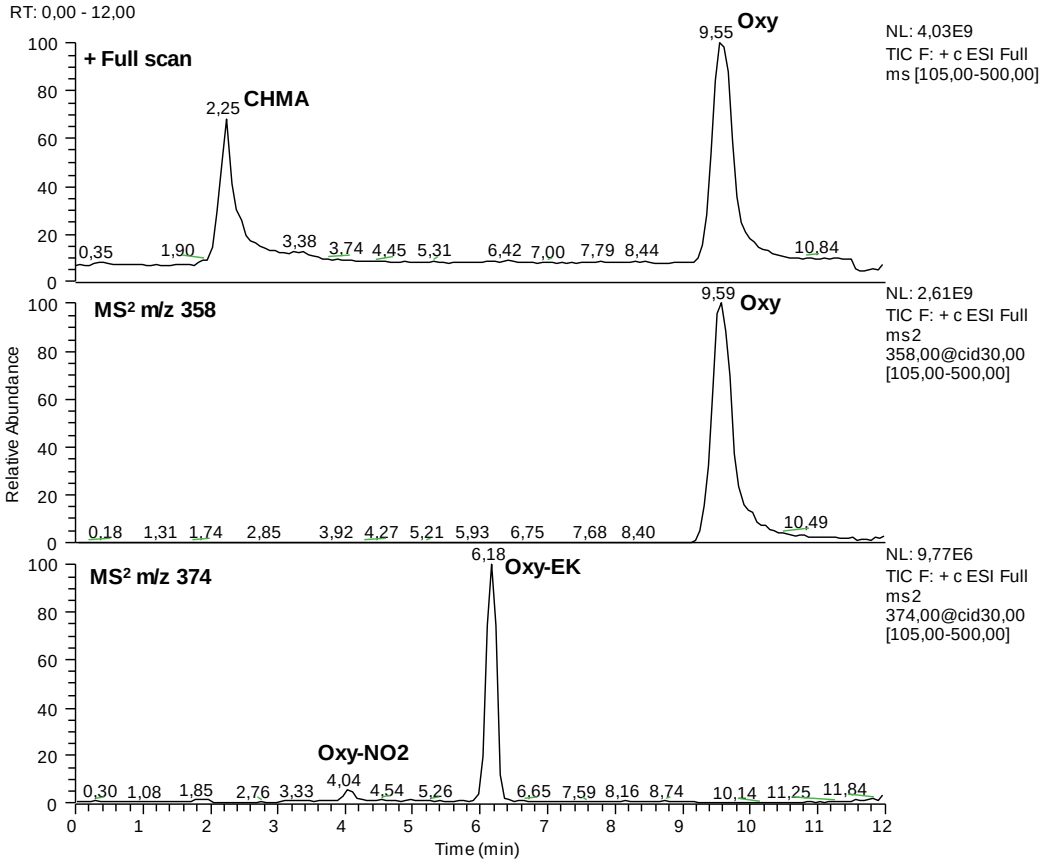

Figure 11. LC-MS^2 chromatogram of the transdermal patch sample solution (lot n° 818002A, t=0 months).

In the LC-UV chromatogram (Fig. 10) the presence of the impurity **Oxy-EK** was observed at 311 nm (peak at t_R= 6.9 min) while at lower wavelenght (210 nm) did not. The same peak, in the LC-MS/MS chromatogram (Fig. 11), was characterized by a protonated molecule at *m/z* 374 being its fragmentation pattern identical to that of **Oxy-EK** synthetic standard. While the intermediate degradation products, **Oxy-NO2** and **Oxy-NO1** were not detected in the LC-UV chromatogram, the presence of **Oxy-NO2** peak was observed in the LC-MS/MS chromatogram (Fig. 11). Moreover, interestingly, the hydrolytic degradation product **CHMA** was also observed both in LC-UV and LC-MS chromatograms (Figure 10, 11) being its protonated molecule at *m/z* 236 (Figure 12): its formation was not further investigated.

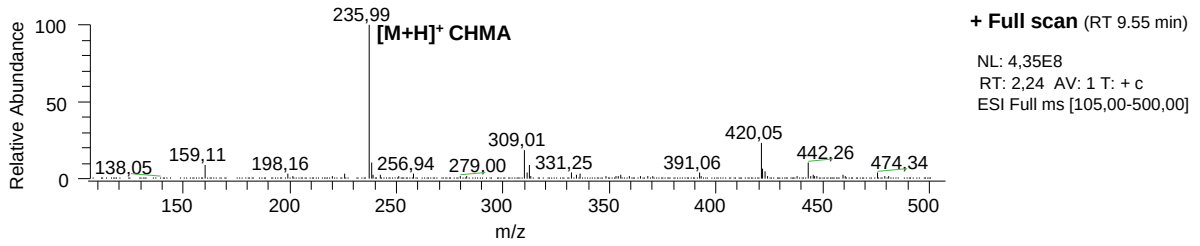

Figure 12. MS spectrum of degradation product **CHMA** found in oxybutynin transdermal patches

To explain the origin of the **Oxy-EK**, an accelerated stability study (40°C, 6 months) on transdermal patches of two different lots was performed: the analysis of the samples, withdrawn at fixed times, showed that the impurity did not increase over a six month period of time Figure 13.

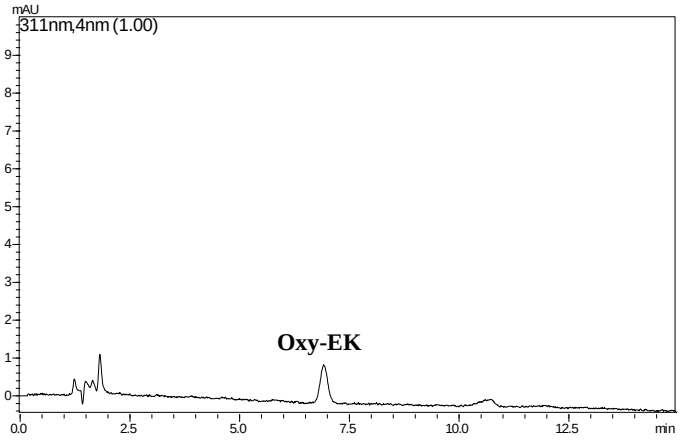

Figure 13. LC-UV chromatogram of the transdermal patch sample solution (lot n° 818002A, t=6 months) monitored at 311 nm

Indeed, the availability of the synthetic standard of **Oxy-EK** allow us to estimate the concentration of **Oxy-EK** obtaining a value of 0.02% that does not change during the stability study. Finally, a sample of oxybutynin *free base* dissolved in triacetin, the main excipient of transdermal patch, and submitted to the same accelerated stability study did not show the formation of **Oxy-EK**. Possibly, these results indicate that the formation of **Oxy-EK** occurred during the preparation of the transdermal patch; alternatively, **Oxy-EK** is already present in oxybutynin *free base* used in the manufacturing process.

3.3.5 Mutagenic activity of Oxy-EK

The structure of **Oxy-EK** contains an *α,β*-unsaturated ketone which could behave as a Michael acceptor reacting with nucleophilic functions of biological macromolecules leading eventually to toxic effects; for this reason, *α,β*-unsaturated carbonyl functions are considered structural alert (Stepan et al., 2011). In the case of **Oxy-EK**, *α,β*-unsaturated ketone function is included in the enamino ketone side chain with, possibly, different electronic properties and reactivity. Nonetheless the mutagenic power of **Oxy-EK**, in term of ability to induce point mutations at gene level, was evaluated *in vitro* by the bacterial reverse mutation assay (Ames test).

Both **Oxy** and **Oxy-EK** produced marked cytotoxic effects starting from the concentration of 100 μg/plate in all the strains tested both in the absence and presence of the S9 metabolic activator (data not shown). Early signs of cytotoxicity, highlighted as a significant reduction in the number of the spontaneous revertant colonies, were observed for both substances at concentration of 50 μg/plate, in all the strains tested in the absence of the S9 metabolic activator (Appendix I). The presence of the metabolic activator seems to reduce the cytotoxicity of the compounds, being not cytotoxic at 50 μg/plate in all strains (Appendix I). At nontoxic concentrations, ranging from 9 to 36 μg/plate, both **Oxy-EK** and **Oxy** did not increase the number of revertant colonies in all strains tested in absence and presence of S9 (Appendix I-II). Conversely, the known mutagens 2NF, SA, 9AA, MMS, and 2AA significantly increased the number of revertant colonies with respect to the vehicle (Appendix I-II), so confirming the ability of the bacteria to detect the DNA-damage. Present data show that **Oxy-EK** and **Oxy** did not induce any kind of point mutations (due to frameshift, base-substitution, cross linking and oxidative mechanisms) so resulting not mutagenic. Further studies allow to better define the genotoxicity profile of the test substances at chromosomal level (including clastogenicity, aneuploidogenicity and DNA strand breaks).

3.4 CONCLUSIONS

In this study the structure of a new and unprecedented degradation product, **Oxy-EK**, found in oxybutynin transdermal patch was elucidated. The mechanism of its formation, through the rearrangement of the oxybutynin *N*-oxide, is linked to the presence of oxybutynin in form of the free base; that form shows more favorable properties in term of lipophylicity and permeability but it results also more prone to oxidation than the corresponding protonated form. Overall, as expected, the oxidative degradation of **Oxy** is dependent on the pH of the assay indicating that there are no concern from this point of view as long as the chloride/hydrochloride salt is used in drug product manufacturing. However **Oxy** *free base* can undergo to oxidation suggesting that this degradation pathway should be taken into account in the course of stability studies. Accordingly, the synthesis of the reference standard of **Oxy-EK** allowed to propose it as the indicator of stability for the oxidative degradation of oxybutynin *free base* both in drug substance and drug product stability studies. Finally, the results of the Ames test highlight a lack of mutagenic effects for both the compounds and suggest the need of further studies in mammal cells in order to exclude their potential genotoxicity.

3.5 REFERENCES

Ames, B.N., Mc Cann, J., Yamasaki, E. (1975). Methods for detecting carcinogens and mutagens with the Salmonella/mammalian-microsome mutagenicity test. *Mutat. Res.*, *31*, 347–64.

Boccardi, G. (2005). Oxidative susceptibility testing, in: Baertschi S.W. (Ed.), *Drugs and the pharmaceutical sciences.: Pharmaceutical stress testing: Predicting drug degradation* (Taylor & Francis, pp. 205–230), New York.

De Schutter, J.A., De Moerloose P. (1988). Determination of oxybutynin chloride in pharmaceuticals by reversed-phase ion-pair liquid chromatography with two counter-ions in the eluent. *J. Chromatogr. A*, *450*, 337–42.

Di Sotto, A., Maffei, F., Hrelia, P., Castelli, F., Sarpietro, M.G., Mazzanti, G. (2013). Genotoxicity assessment of β-caryophyllene oxide. *Regul. Toxicol. Pharmacol.*, *6*, 264–268.

Di Sotto, A., Maffei,, F., Hrelia P., Di Giacomo, S., Pagano, E., Borrelli, F., Mazzanti, G. (2014). Genotoxicity assessment of some cosmetic and food additives. *Regul. Toxicol. Pharmacol.*, *68*, 16–22.

El-Gindy, A. (2005). High performance liquid chromatographic determination of oxeladin citrate and oxybutynin hydrochloride and their degradation products. *Il Farmaco*, *60*, 689–699.

EP 8, (2013) Oxybutynin Hydrochloride. *European Pharmacopoeia, Council of Europe, Strasbourg, France*, pp. 2939–2940.

ICH Harmonized Tripartite Guidelines Q1A (R2) (2003). Stability Testing of New Drug Substances and Products.

Kennelly, M. J. (2010). A Comparative review of oxybutynin chloride formulations: pharmacokinetics and therapeutic efficacy in overactive bladder. *Rev. Urol.*, *12*, 12–19.

Lin, Z.P., Lin, H.C., Wu, H.H., Chou, H.W., Lin, S.K., Sung, K.C., Wong, F. F. (2009). Hydrodeamination of β-enamino ketones to 1,2-dideoxy-D-threo-3-hexulose via palladium. *Tetrahedron Lett.*, *50*, 5120–5122.

Lose, G., J.P. Nérgaard, J. P. (2001). Intravesical oxybutynin for treating incontinence resulting from an overactive detrusor. *BJU International*, *87*, 767–773.

Maingot, L., Vu, N.Q., Collet, S., Guingant, A., Martel, A., Dujardin, G. (2009). [4+2]/HyBRedOx approach to C-naphthyl glycosides: failure in the projuglone series and reinvestigation of the HyBRedOx sequence. *Eur. J. Org. Chem*, *3*, 412–422.

Miyamoto, E., Kawashima, S., Murata, Y., Yamada, Y., Demizu, Y., Kontani, H., Sakai, T.

(1994). Physico-chemical properties of oxybutynin. *Analyst*, *119*, 1489–1492.

Shaw, G.L., Patel, H. R. H. (2007). Transdermal oxybutynin: a review. *Expert Opinion on Drug Metabolism & Toxicology*, *3*(3), 435–439.

Stepan, A.F., Walker, D.P., Bauman, J., Price, D.A., Baillie, T.A., Kalgutkar, A.S., Aleo, M. D. (2011). Structural alert/reactive metabolite concept as applied in medicinal chemistry to mitigate the risk of idiosyncratic drug toxicity: a perspective based on the critical examination of trends in the top 200 drugs marketed in the United States. *Chem. Res. Toxicol*, *24*, 1345–1410.

Szabó, A., & Hermecz, I. (2001). Novel intramolecular rearrangement of tertiary propargylamine *N*-oxides. *Journal of Organic Chemistry*, *66*(21), 7219–7222.

USP 38. (2015). Oxybutynin Hydrochlorid. *United States Pharmacopeial Convention, Inc., Rockville, MD* pp. 4699–4700.

Wagieh, N. E., Hegazy, M. A., Abdelkawy, M., & Abdelaleem, E. A. (2010). Quantitative determination of oxybutynin hydrochloride by spectrophotometry , chemometry and HPTLC in presence of its degradation product and additives in different pharmaceutical dosage forms. *Talanta*, *80*, 2007–2015.

CHAPTER 4. New findings in the *in vitro* metabolism study of oxybutynin

4.1 INTRODUCTION

Antimuscarinics are the mainstay of pharmacological treatment of overactive bladder (OAB), a complex symptom defined by the presence of urinary urgency, usually associated with frequency and nocturia, with or without urgency urinary incontinence. Oxybutynin hydrochloride (4- diethylamino) but-2-ynyl (*RS*)-2-cyclohexyl-2-hydroxy-2-phenyl-acetate hydrochloride, **Oxy**) is a chiral drug administered as a racemic mixture with antimuscarinic agent and widely prescribed to OAB patients with symptoms of urinary urge incontinence. However, its antimuscarinic activity resides predominantly on the (*R*)-enantiomer, which binds selectively muscarinic M1 and M3 receptors, in the detrusor muscle.

Oxy immediate release formulation was the first treatment for OAB approved by the US FDA in 1975 (Arisco et al., 2009). To date, different types of **Oxy** formulations are available on the market: immediate and extended release tablets, oral solutions, syrup and solution for intravesical administration. **Oxy** is well absorbed from the gastrointestinal tract following oral administration, being its absolute bioavailability less than 10% due to extensive presystemic metabolism. The circulating primary metabolite, *N*-desethyloxybutynin (**Oxy-DE**), is present in plasma at concentrations approximately up tenfold those of the parent compound having similar anticholinergic effects to the parent compound. In therapeutic use, **Oxy-DE** appears to contribute greatly to the treatment-limiting anticholinergic side-effects associated with oral administration of **Oxy** (Zobrist et al., 2001 and Staskin et al., 2010). As a consequence, to mitigate the systemic adverse effects, occurring during the therapy, topical formulations, such as adhesive patch, were employed exploiting **Oxy** *free base* as the drug substance (Shaw et al., 2007).

The first observation that **Oxy** undergo an extensive metabolic biotransformation in rat date back as early as 1965 (Lish et al., 1965). In the following decades, the metabolic fate of **Oxy** and its effect on the induction of drug metabolizing enzymes were investigated in rat, dog and human after oral administrations (Shinozaki et al., 1986). These authors reported the formation of a multitude of metabolites in dog and human urine after oral administration and estimated that up to ~ 30% of the administrated dose was excreted as metabolites in urine; they also observed the highest metabolic activity for **Oxy** in rat liver. Four metabolic pathways were identified: *N*-deethylation, hydrolysis of ester, hydroxylation at 3' and 4' positions on cyclohexan ring and the conjugation of the corresponding metabolites. In the

same year Yoshio et al. reported that, after **Oxy** oral administration, cyclohexylmandelic acid is the main metabolite in rat plasma and bile and its glycine conjugate the main one in urine (Yoshio et al, 1986). More recently carboxylesterase 1 (CES1) was identified as the major isozyme responsible for oxybutynin hydrolysis (Sato et al., 2012). In 1998 Yaïch and collaborators (Yaïch et al., 1998) demonstrated that CYP3A4 subfamily is involved in the formation of **Oxy** *N*-desethyl metabolite. Finally, Lindeke et al. (1981) using deuterated substrate and GC-MS analysis firstly reported the *N*-oxidation of the **Oxy** propargylamine moiety in rat liver microsomes. They were not able to reveal directly the presence of the *N*-oxide metabolite (**Oxy-NO**) but its degradation product promoted by high temperature GC-MS analysis.

Indeed, based on their previous studies on pargyline *N*-oxide decomposition, they proposed the formation of propenal and Schiff base derivatives by two consecutive rearrangements of the **Oxy-NO** intermediate.

At the best of our knowledge, over the last thirty years, no further reports addressed the oxidative metabolic fate of **Oxy**. In our previous report (Chapter 3), we elucidated the chemical stability of **Oxy** *free base* in oxidative conditions disclosing the role of the diastereomeric oxybutynin *N*-oxides (**Oxy-NOs**) in the formation of **Oxy-EK**, whose structure and mechanism of formation were elucidated. In the present report, exploiting our recent findings we revisited the *in vitro* oxidative metabolic fate of **Oxy** providing evidence for the metabolic instability of the tertiary propargylamine moiety which underwent enzymatic oxidation followed by chemical rearrangement to generate **Oxy-EK**. Besides, the secondary hydroxylamine **Oxy-HA** was formed by enzymatic oxidation of **Oxy-DE**.

4.2 EXPERIMENTAL

4.2.1 Reagents and chemicals

Methanol (HPLC grade), acrylonitrile, Adenosine 3'-phosphate 5'-phosphosulfate lithium salt hydrate (80%), 1-chloroethyl chloroformate, *m*-chloroperbenzoic acid, trietylamine, were purchased from Sigma-Aldrich (Milano, Italy) or Alfa Aesar (Lancashire, UK). Water (HPLC grade) was obtained from Milli-Q reverse osmosis system (Millipore Co., Billerica MA, USA). Column chromatography was performed on silica gel 60 (230-400 mesh ASTM Merck). TLC was carried out on plates with a layer thickness of 0.25 mm (silica gel 60 F254; Merck); when necessary, they were visualized after spraying with ninhydrin reagent. **Oxy**

(potency: 99.3%), was obtained as gift sample from Pharmafar S.r.l. (Torino, Italy). **Oxy** *free base*, **Oxy-NOs** and **Oxy-EK** were prepared according to the procedures cited in the Chapter 3.

4.2.2 Instrumentation and chromatographic conditions

4.2.2.1 LC-UV analyses

A Shimadzu HPLC system (Shimadzu, Kyoto, Japan), consisting of two LC-10AD Vp module pumps, a SLC-10A Vp system controller, a SIL-10AD Vp autosampler and a DGU-14-A on-line degasser, was used for the analysis. All the chromatographic separations were performed on a Kinetex C18 XB 150 x 4.6 mm (5 μm) core-shell column as a stationary phase protected by a C18-Security Guard™ (Phenomenex, Torrance, CA). The SPD-M10Avp photodiode array detector was used to detect the analyte at 210 and 311 nm. A LC Solution 1.24 software was used to process the chromatograms. Aliquots (20 μl) of supernatants obtained from incubations were injected onto HPLC system. The isocratic mobile phase (flow rate 1.4 ml/min) was composed of eluant A ammonium acetate buffer (20 mM pH=5.7) and eluant B methanol, being the A:B ratio 35:65 (*v/v*) (total run time: 15 min). The eluants were filtered through a 0.45 μm pore size PVDF membrane filter prior to use. All the analyses were carried out at room temperature.

4.2.2.2 LC-MS/MS analyses

A Thermo Finningan LCQ Deca XP plus system equipped with a quaternary pump, a Surveyor AS autosampler, a Surveyor photodiode array detector and a vacuum degasser was used for LC/MS analyses (Thermo Electron Corporation, Waltham, MA). All the chromatographic separations were performed on Kinetex C18 50 x 2.10 mm (2.6 μm) core-shell column as a stationary phase protected by a C18-Security Guard™ (Phenomenex, Torrance, CA) kept at a 35 °C. Aliquots (5 μl) of supernatants obtained from incubations were injected onto the system and eluted with a mobile phase (flow rate 0.2 ml/min) consisting of: A: 10 mM ammonium acetate buffer (pH 5.70), and B: methanol. The following gradient elution was used: 0 to 9.5 min [A=55-20%, B=45-80%], 9.5 to 10 min [A=20-55%, B=80-45%], 10 to 15 min [A=55%, B=45%]. The eluants were filtered through a 0.45-μm pore size polyvinylidene difluoride membrane filter before use. The eluate was injected into the electrospray ion source (ESI) and MS spectra were acquired and processed using Xcalibur® software. The operating conditions on the ion trap mass spectrometer were as follows:

positive mode, spray voltage, 5.00 kV; source current, 80 μA; capillary temperature, 300 °C; capillary voltage, 22.00 V; tube lens offset, 20.00 V; multipole 1 offset, -4.25 V; multipole 2 offset, -8.00 V; sheath gas flow (N_2), 35 Auxiliary Units. *Negative mode*: spray voltage, 3.30 kV; source current, 80 μA; capillary temperature, 300 °C; capillary voltage, -34.00 V; tube lens offset, -35.00 V; multipole 1 offset, 6.25 V; multipole 2 offset, 10.50V; sheath gas flow (N_2), 50 Auxiliary Units. Data was acquired in full-scan and product ion scan modes (MS^n) using mass scan range m/z 105-700. The collision energy was optimized at 28-30%.

4.2.2.3 Spectroscopic analyses

^1H and ^{13}C experiments were performed at 298K on a JEOL Eclipse ECP 300 FT MHz spectrometer (Jeol Ltd. Tokyo, Japan) operating at 7.05T. Chemical shifts are reported in part per million (ppm).

4.2.3 Synthesis of the reference compounds

*4.2.3.1 Benzeneacetic acid, α-cyclohexyl-α-hydroxy-4-(ethylamino)-2-butyn-1-yl ester (**Oxy-DE**)*

Oxybutynin *free base* (1.32 g, 3.70 mmol) was dissolved in freshly prepared anhydrous dichloromethane (30 ml) and 1-chloroethyl chloroformate (2.22 ml, 20.6 mmol) was added dropwise maintaining the reaction at 0°C under magnetic stirring. The reaction was further heated to reflux for 1.5 hours, and after cooling at room temperature, the solvent was evaporated and the crude residue re-dissolved in methanol (30 ml) and heated to reflux for an additional 1.5 hours. Evaporation under reduced pressure of the organic solvent gave a yellow oil which was analyzed by TLC (dichloromethane/methanol 95:5, developed with ninhydrin) obtaining three spots: (unreacted **Oxy**: R_f 0.5 red spot, **Oxy-DE**: R_f 0.2 yellow spot, and unknown product: R_f 0.1 purple spot). The residue was purified by column chromatography using dichloromethane/methanol 95:5 and then 9:1 as eluant to give compound **Oxy-DE** as pale yellow oil (295 mg, 0.90 mmol, 24% yield, HPLC purity at 210 nm 95.8%).

ESI-MS: calculated for $C_{20}H_{27}NO_3$ *M*=329.4; Found *m/z* = 330 $[M+H]^+$

4.2.3.2 Synthesis of benzeneacetic acid, α-cyclohexyl-α-hydroxy-4-(ethylamino)-4-(cyanoethyl)-2-butyn-1-yl ester

Oxy-DE (350 mg, 1.06 mmol) was dissolved in 5 ml of methanol in the presence of a catalytic amount of trietylamine. A small amount of water was then added to the mixture

without leading the solution to be opalescent. Acrylonitrile (105 mg, 2.0 mmol) was added dropwise and the mixture was stirred at room temperature for five hours. The reaction was then evaporated under reduced pressure giving a yellow oil (~300 mg) which was used directly without further purification.

*4.2.3.3 Synthesis of benzeneacetic acid, α-cyclohexyl-α-hydroxy-4-(ethylamino)-4-(hydroxy)-2-butyn-1-yl ester (**Oxy-HA**)*

The crude residue (~300mg, ~0.78mmol) was dissolved in few ml of freshly prepared anhydrous dichloromethane and *m*-CPBA (270 mg, 1.29mmol) dissolved in dichloromethane was added dropwise maintaining the reaction at -78°C under nitrogen for 3 hours. The reaction was further stirred at 0°C for 2 hours. After cooling at room temperature, the reaction was washed with 10% aqueous sodium carbonate solution. The organic layer was dried over anhydrous sodium sulfate, filtered and evaporated under reduced pressure giving a crude oil which was first purified by column chromatography using dichloromethane/methanol 98:2 as eluant and then by a second column using petroleum ether/2-propanol 9:1 as eluant to give compound **Oxy-HA** as a pale yellow oil (85 mg, 0.25 mmol, 32 % yield, 97.3% purity by HPLC assay).

ESI-MS: calculated for $C_{20}H_{27}NO_4$ *M*=345.4; Found *m/z* = 346 $[M+H]^+$

^{1}H-NMR *(300 MHz, $CDCl_3$) δ 7.64-7.30(m, 5H-aromatic), 4.80(d, J=13.4 Hz, O-CH_2-C≡), 4.75(d, J=13.4 Hz, O-CH_2-C≡), 3.59(s, ≡CH_2-N), 2.75(q, J=7.14 Hz, N-CH_2), 2.24-1.09 (m, CH_3 and 11H-cyclohexyl).*

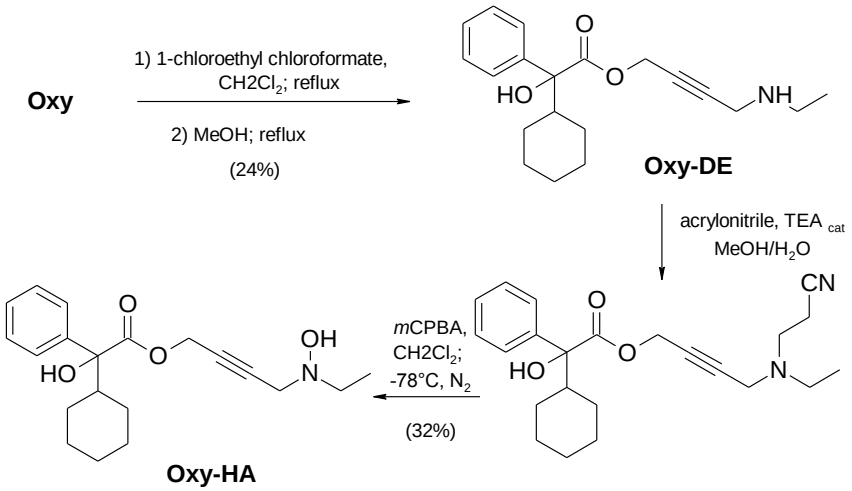

4.2.4 Human and rat Liver Preparations

The human liver microsomes (HLM) (pooled mixed sex, fifty individual donors, protein concentration: 20 mg/ml, total CYP: 360 pmol/mg protein), human liver cytosol (HLC), (pooled mixed sex, fifty individual donors, protein concentration: 20 mg/ml, sulfotransferase: 0.63 nmol/mg protein) and male Wistar rat liver microsomes (RLM), (protein concentration: 25mg/ml, total P450: 0.64 nmol/mg protein) were purchased from BD Gentest™ (Woburn, MA) and used throughout this study.

The incubations were all performed using a horizontal DUBNOFF shaking thermostatic bath (Dese Lab Research, Padova, Italy) and were protected from light.

4.2.5 Phase I incubations with RLM, HLM

The standard incubation mixture (0.5 ml final volume), was carried out in a 50 mM TRIS·HCl buffer (pH 7.4) containing 3.3 mM $MgCl_2$, 1.3 mM $NADPNa_2$, 3.3 mM glucose 6-phosphate, 0.4 Units/ml glucose 6-phosphate dehydrogenase, 5 µl of acetonitrile (1% of total volume), and **Oxy** (200 µM).

After pre-equilibration of the mixture, an appropriate volume of HLM/RLM suspension was added to give a final protein concentration of 1.0 mg/ml. The mixture was shaken for 60 minutes at 37°C. Control incubations were carried out both without the presence of NADPH-regenerating system or microsomes. Each incubation was stopped by addition of 0.5 ml ice-cold acetonitrile, vortexed and centrifuged at 12,500 rpm for 10 min. The supernatants were analyzed by LC-UV and LC-ESI-MS. Alternatively, when the chemical reactivity of the metabolites was studied, GSH (3mM) was added to the incubation mixture.

When compounds **Oxy-DE**, Oxy-**HA** and **Oxy-EK** were studied as substrates, they were incubated following the same procedure reported above.

4.2.6 Phase II incubation with HLC fraction

4.2.6.1 Glucuronide

The standard incubation mixture, constituted by 2 mM UDPGA cofactor, in a 50 mM TRIS·HCl buffer, pH 7.4, containing 5 µL of acetonitrile (1% of total volume), Oxy or Oxy-HA (200 µM) brought to a final volume of 0.250 mL. After preequilibration of the mixture at 37 °C, an appropriate volume of HLM suspension, previously activated by Brij 58 surfactant (0.5 mg/mg protein) in ice for 15 min, was added to give a final protein concentration of 1.0

mg/mL; the incubation mixture was shaken for 60 minutes at 37°C. Control incubation was carried out both in the absence of HLM or UDPGA cofactor. Incubation were stopped by addition of 0.250 mL ice-cold acetonitrile, vortexed and centrifuged at 11,000 r.p.m. for 5 min prior to LC-ESI-MS analyses of the supernatants.

4.2.6.2 Sulphate

The standard incubation mixture, constituted by 0.1 mM PAPS cofactor, in a 50 mM TRIS·HCl buffer, pH 7.4, containing 5 µl of acetonitrile (1% of total volume), and compound **Oxy-HA**, brought to a final volume of 0.5 ml. After pre-equilibration of the mixture at 37 °C, an appropriate volume of HLC suspension was added to give a final protein concentration of 1.5 mg/ml; the incubation mixture was shaken for 60 minutes at 37°C. Control incubation was carried out in the absence of PAPS. Each incubation was stopped by addition of 0.5 ml ice-cold acetonitrile, vortexed and centrifuged at 12,500 rpm for 5 min. The supernatants were analyzed by LC-ESI-MS.

4.3 RESULTS

The *in vitro* metabolic stability of **Oxy** was assessed through its incubation in rat and human liver subcellular preparations in the presence or absence of a NADPH-regenerating system and of the appropriate cofactors. The incubation samples were analysed by LC-UV and LC-ESI-MS to obtain data on the metabolic stability and the structures of the metabolites respectively.

When the microsomal mixed-function oxidase system was activated by the presence of NADPH, **Oxy** underwent a relevant oxidative transformation with the residual substrate ranging from 10% (RLM) to 56% (HLM). Similar values were obtained in incubations supplied with 3mM GSH ranging the residual substrate from 15% (RLM) to 62% (HLM). Structural characterization of **Oxy** metabolites was achieved by tandem mass spectrometry analysis. All the metabolites were characterized based on their predicted mass shift from the **Oxy** protonated molecule ($[M+H]^+$= 358), and the interpretation of their MS^n spectra. The characterization of **Oxy** metabolites was performed using the incubations obtained with human liver microsomes. No further tests were carried out to assess the metabolic pattern of **Oxy** arising from RLM incubations.

Human liver microsomal **Oxy** incubation samples were analyzed by LC-ESI-MS in both positive full scan and product ion scan modes revealing the phase I metabolites reported in the chromatograms in Figure 1. As a matter of fact, incubation analyses revealed the presence of ten metabolite-related ions as shown in Figure 1 whose MS^2 spectra and the proposed fragmentation pathways are depicted in Figures 2a and 2b.

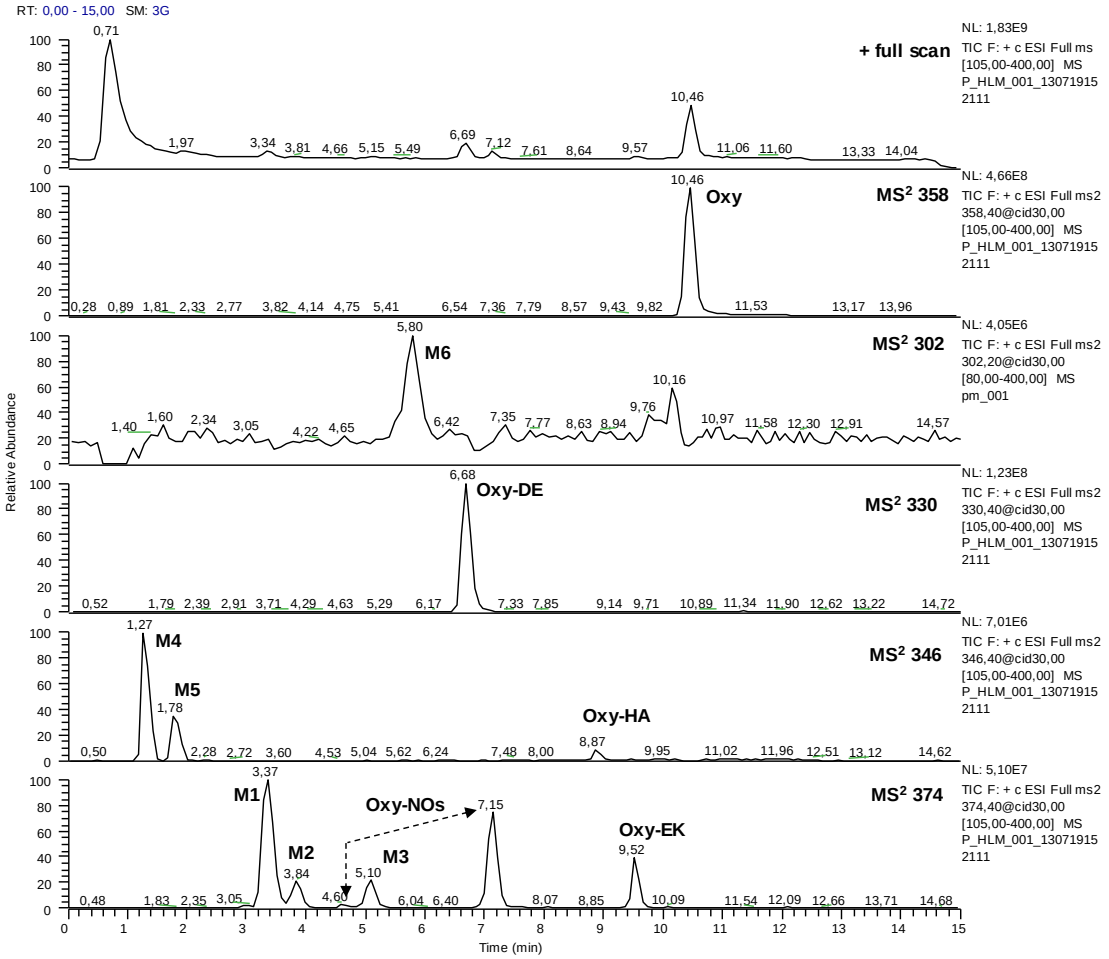

Figure 1. LC-MS chromatograms of **Oxy** incubations (HLM, 200µM) performed in positive full mass and product ion scan mode (MS^2)

Monitoring the ion at *m/z* 374, the LC-MS^2 chromatogram revealed the presence of six peaks corresponding to the following metabolites: **Oxy-NOs** (*N*-oxide diastereoisomers) eluting at 4.40 and 7.15 min, **Oxy-EK** (9.52 min), and three additional metabolites (**M1**-**M3**) eluting at 3.87, 3.84, and 5.10 min respectively (Figure 1). **Oxy-NOs** product ion spectra (*m/z* 374) (Figure 2b) gave two diagnostic fragment ions at *m/z* 189, and 171 corresponding to the same ions observed in **Oxy** MS^2 spectrum (Figure 2a). Moreover the presence of the fragment ions at *m/z* 356 (loss of water), and 158 (ester cleavage), both shifted of 16 Da with respect to the

same ions in **Oxy** spectrum, clearly demonstrated that the enzymatic oxidation occurred on the propargylamine moiety leading to the formation of *N*-oxide metabolites. The structures of **Oxy-NOs** were further confirmed by comparison their mass spectral data with those arising from *N*-oxide synthetic standards (data not shown).

Oxy-EK protonated molecule (*m/z* 374) generated a two-fragment MS^2 spectrum (Figure 2a). The most abundant ion (*m/z* 356) was due to the neutral loss of water whereas the ion at *m/z* 158 (generated from the ester cleavage) corresponded to the **Oxy** fragment ion at *m/z* 142 shifted of 16 Da. Considered together, these data indicated that the structure and the mechanism of formation of **Oxy-EK** are identical to those described for the degradation product previously highlighted in the chemical stability study of **Oxy** (Chapter 3). Even if the structure of **Oxy-EK** presents an *α,β*-unsaturated ketone function, its formation was not affected by the presence of GSH in the incubation, indicating the whole stability of the enaminoketone moiety.

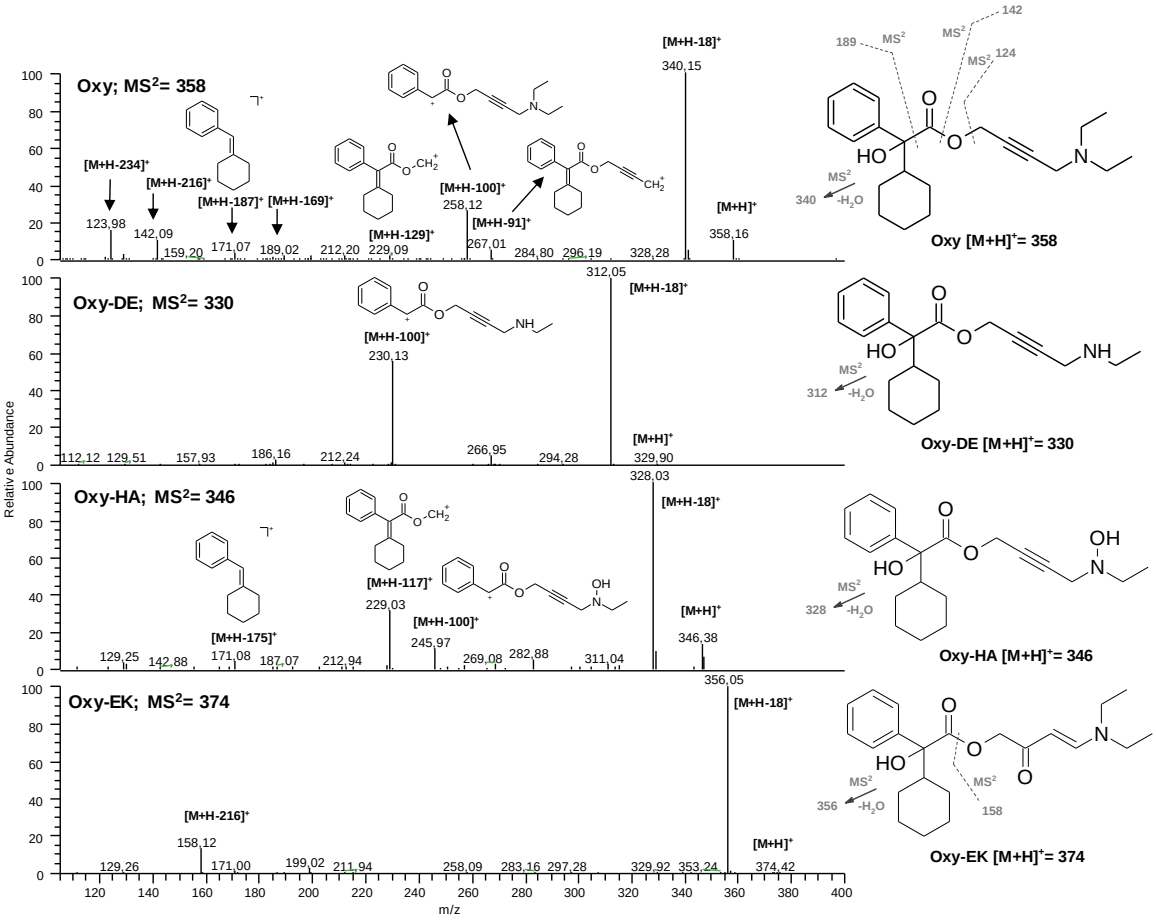

Figure 2a. LC-MS^2 spectra of **Oxy** and the metabolites **Oxy-DE**, **Oxy-HA**, **Oxy-EK** formed in HLM incubations of Oxy (200µM)

Metabolites **M1**, **M2**, and **M3** showed identical product ion spectra: among them, the MS^2 spectrum of **M1** is reported in figure 2b. For these metabolites, the protonated molecule at *m/z* 374 gave rise to a fragmentation pathway similar to that observed for **Oxy**. Indeed the fragment ions at *m/z* 124, 142, and 258 are the same observed in the **Oxy** spectrum, whereas the fragment at *m/z* 187, 283 and 356 presented a shift of 16 Da with respect to the same ions found in **Oxy** spectrum. Overall, this set of data suggested that **M1**, **M2**, and **M3** metabolites arose from the enzymatic oxidation on the cyclohexan ring.

As previously reported in the literature, **Oxy-DE,** arising from oxidative *N*-deethylation was the main metabolite; it was characterized by a protonated molecule at *m/z* 330 whose fragmentation generated the ions at *m/z* 312 (loss of water) and a at *m/z* 230 (100 Da neutral fragment loss) which corresponded to the ion at *m/z* 258 observed in **Oxy** spectrum. In human liver microsomes **Oxy-DE** underwent further oxidative *N*-deethylation generating the primary propargylamine metabolite **M6**. The structure assignment was based on the presence of the protonated molecule at *m/z* 302, whose fragmentation generated the ions at *m/z* 284 (loss of water) and at *m/z* 202 (100 Da neutral fragment) which corresponded to the ion at *m/z* 230 observed in **Oxy-DE** spectrum. Moreover, **Oxy-DE** underwent both *N*-oxidation, generating the hydroxylamine **Oxy-HA**, and the aliphatic hydroxylation of the cyclohexan ring (metabolites **M4** and **M5**). In particular, metabolites **M4** and **M5** gave identical MS^2 spectra featured by the presence of the diagnostic ions at *m/z* 187, 215, and 283 (the same ions were found in **M1** spectrum), and the ion at *m/z* 230, resulting by the neutral loss of a 116 Da fragment. This fragmentation pattern indicated that the metabolites **M4** and **M5** arose from the aliphatic hydroxylation on the cyclohexan ring. Metabolite **Oxy-HA** gave a protonated molecule at *m/z* 346; the presence of the fragment ions at *m/z* 171, 229 and 246 (loss of a 100 Da neutral fragment) indicated that oxidation on the propargyl amine moiety occurred for this metabolite. The structure of **Oxy-HA** was unequivocally confirmed by comparison of its retention time and MS spectrum with those of the synthetic standard.

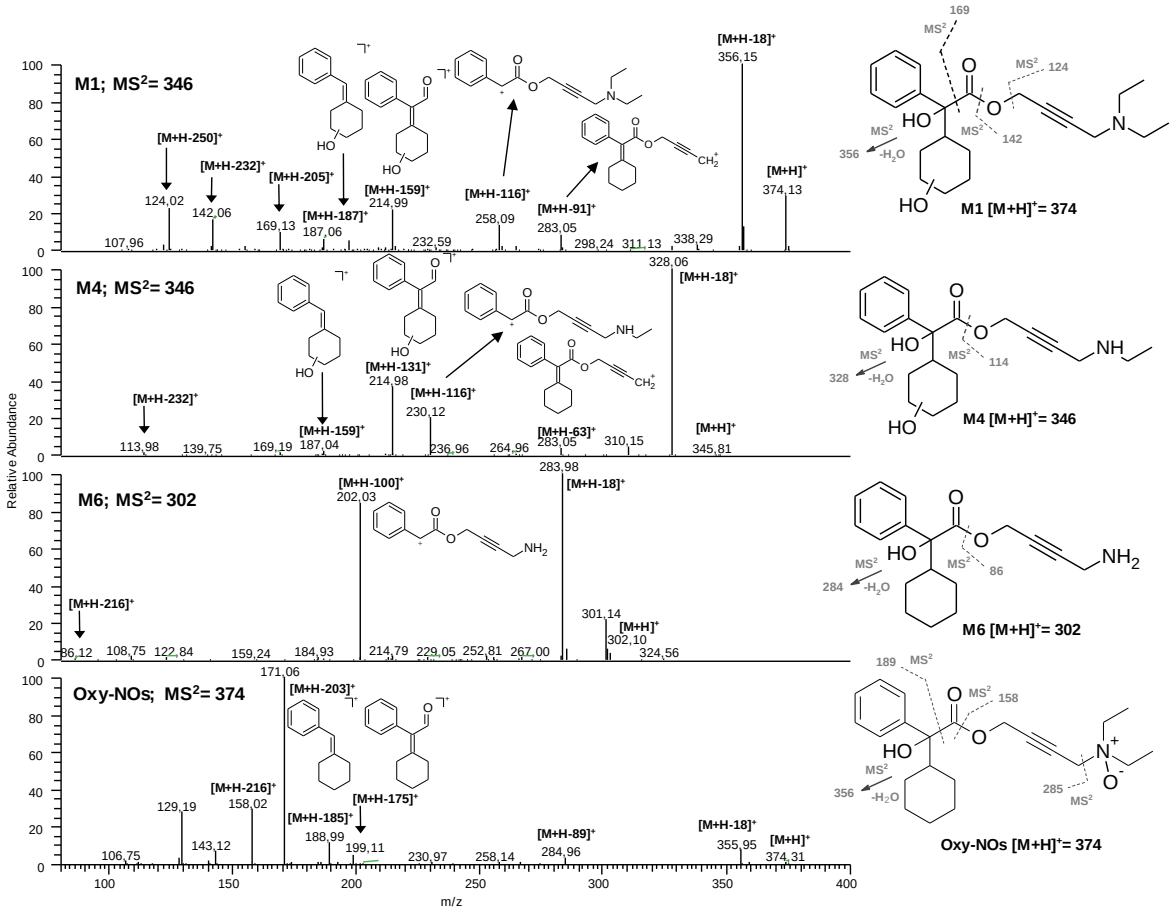

Figure 2b. LC-MS^2 spectra of the metabolites **M1, M4, M6** and **Oxy-NOs** formed in HLM incubations of **Oxy** (200µM)

Finally, contrary to the results of Sato et al. (2012), the formation of cyclohexylmandelic acid arising from the ester function hydrolysis, was never observed throughout the study.

4.3.1 Phase II incubation with human liver subcellular fractions

Glucuronidation and sulfation

In order to assess the formation of **Oxy** and **Oxy-HA** glucuronides, HLM incubations were carried out in the presence of UDPGA cofactor whereas the formation of sulfates was assessed by incubating **Oxy** and **Oxy-HA** in the presence of human liver cytosol (HLC), with PAPS cofactor. All the incubations were analyzed by LC-ESI-MS in negative ionization mode.

As shown in figure 3, the formation of a metabolite eluting at 4.04 min was observed in the **Oxy-HA** incubation in the presence of UDPGA, while the same peak is absent in control incubations. The metabolite generated a deprotonated molecule at *m/z* 520, corresponding to

the addition of 175 Da with respect to the parent compound, suggesting the formation of the oxybutynin hydroxylamine glucuronide. This attribution was further supported by the presence of the diagnostic fragment ion at 344 *m/z* (neutral loss of glucuronic acid) as well as the presence of additional fragments at *m/z* 502, 304 and 233 *m/z* whose structures were depicted in figure 4. On the contrary, the formation of **Oxy** glucuronide was ruled out due to the lack of peaks in the LC-ESI-MS (negative ionization mode) monitoring the ion at *m/z* 532 (data not shown). The absence of **Oxy** glucuronide indicated that the glucuronidation of **Oxy** tertiary alcohol did not occur, confirming the glucuronidation of hydroxylamine function. Finally the absence of peaks in LC-ESI-MS/MS chromatograms (negative ion at *m/z* 424) of **Oxy-HA** incubations performed in HLC fraction and in the presence of PAPS indicated that the sulfate metabolite was not formed (data not shown).

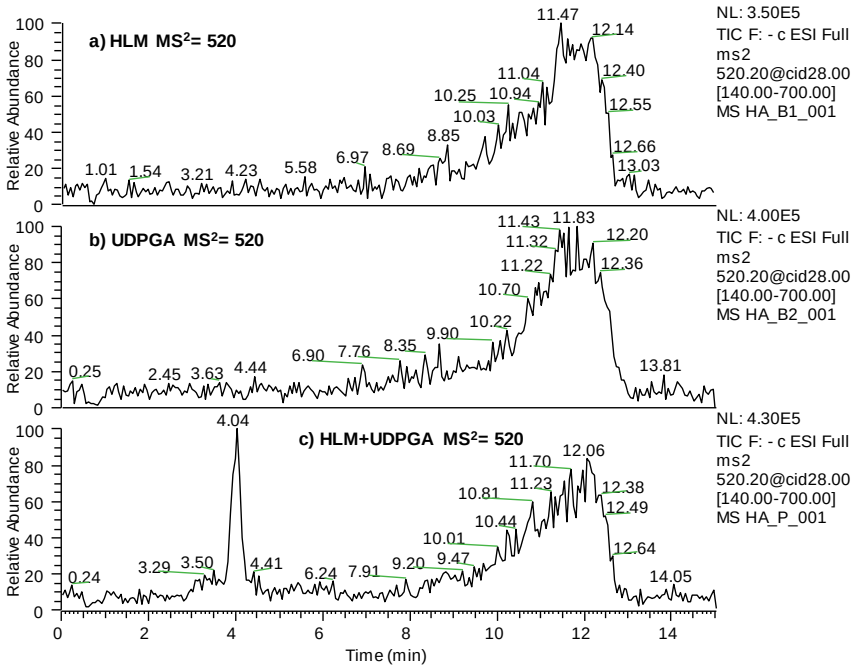

Figure 3. Negative LC-ESI-MS chromatogram of HLM/UDPGA incubations of **Oxy-HA** a) control incubation with HLM; b) control incubation with UDPGA and c) with both UDPGA and HLM

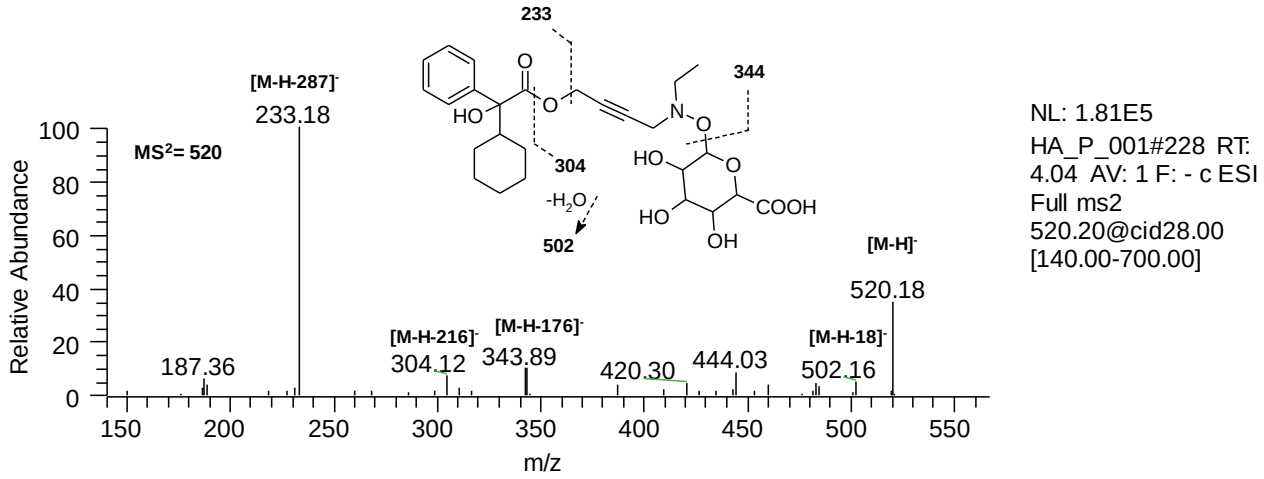

Figure 4. Negative ESI-MS-MS spectrum (*m/z* 520) of peak at t_R= 4.04 minutes.

4.4 DISCUSSION

In this work, the oxidative transformation of oxybutynin has been studied in the presence of human liver subcellular preparations and a metabolic scheme for *in vitro* metabolic fate of **Oxy** was proposed and reported in the figure 5. The metabolism showed a good degree of regioselectivity being oxidized the cyclohexyl and the tertiary amine moieties only. As a consequence, two distinct metabolic pathways were observed: the aliphatic hydroxylation and *N*-oxidation. In particular, as from literature data, **Oxy** is extensively metabolized and *N*-desethyloxybutynin (**Oxy-DE**), arising from oxidative *N*-dealkylation is the main metabolite.

Interestingly the formation of hydroxylated metabolites on cyclohexyl ring both on **Oxy (M1-M3)** and **Oxy-DE (M4-M5)** was also observed for the first time; however no further characterization of their structures was attempted.

The *N*-oxidation of **Oxy** to generate the diastereomeric **Oxy-NOs** has been previously proposed by Lindeke et al. (1981); however, due to the intrinsic chemical instability of **Oxy-NOs**, they were not able to detect them using GC-MS analysis generally performed at high temperature. In this study the presence of **Oxy-NOs** in human liver microsomes incubations was detected by means of LC-MS/MS analysis. Besides, the presence of the unprecedented metabolite **Oxy-EK** was observed: its formation, through the prototropic rearrangement of **Oxy-NOs,** previously described in the Chapter 3, was proposed. Interestingly, differently from **Oxy-NOs**, **Oxy-EK** was a chemically and metabolically stable metabolite, which did not seem undergo to further oxidative and hydrolytic transformation (data not shown).

Moreover, despite the presence of an *α,β*-unsaturated function, no reactivity between **Oxy-EK** and GSH was observed.

Besides, the primary metabolite **Oxy-DE** underwent to *N*-oxidation, generating the hydroxylamine **Oxy-HA** and *N*-deethylation to give the primary propargylamine metabolite, **M6**. The presence of **Oxy-HA** was confirmed by glucuronidation of hydroxylamine function and by means of its synthesis. It is worth of mention that the identification of **Oxy-HA** has not been reported so far. Contrary to what one might expect the formation of the metabolite **CHMA** was not detected even if the formation of this metabolite has been reported in the literature: this is worth of further investigation.

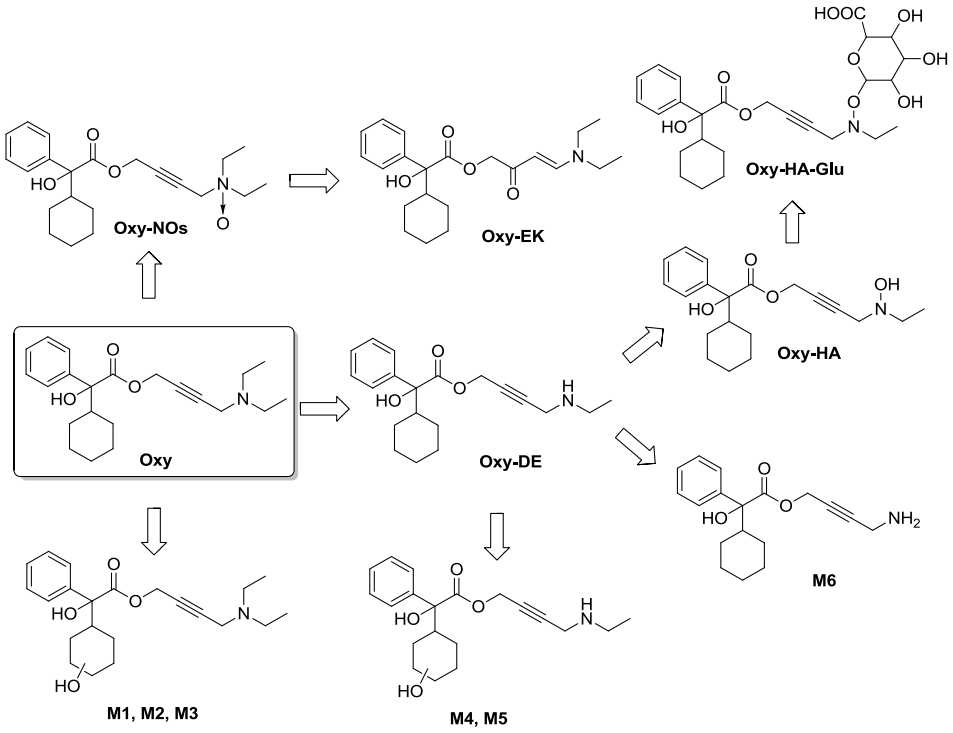

Figure 5. *In vitro* metabolic scheme of oxybutynin

4.5 REFERENCES

Arisco, A. M., Brantly, E. K., Kraus, S. R. (2009). Oxybutynin extended release for the management of overactive bladder: a clinical review. *Drug Design, Development and Therapy*, *3*, 151–61.

Lindeke, B., Hallström, G., Johansson, C., Ericsson, O., Olsson L.I., Stromberg S. (1981). Metabolism of Oxybutynin: establishment of desethyloxybutynin and oxybutynin N-oxide formation in rat liver preparation using deuterium substitution and gas chromatographic mass spectrometric analysis. *Biomed Mass Spectrom.*, *8*(10), 506–513.

Lish, P.M., Labudde J.A., Peters E.L., Robbins, S. (1965). Oxybutynin a musculotropic antispasmodic drug with moderate anticholinergic action. *Arch Int Pharmacodyn Ther.*, *156*(2), 467–88.

Sato, Y., Miyashita, A., Iwatsubo, T., Usui, T. (2012). Conclusive identification of the oxybutynin-hydrolyzing enzyme in human liver. *Drug Metabolism and Disposition*, *40*(5), 902–906.

Shaw, G.L., Patel, H. R. . (2007). Transdermal oxybutynin: a review. *Expert Opinion on Drug Metabolism & Toxicology*, *3*(3), 435–439.

Shinozaki, Y., Monden, R., Manaka, A., Hisa, H., Naito, S., Igarashi T., (1986). Studies on metabolic fate of oxybutynin hydrochloride. Metabolism in human and dog and the site of biotransfornation and the effect on enzymes induction in the rats. *Drug Metabolism and Pharmacokinetics*, *1*(4), 341–352.

Staskin, D.R., Salvatore, S. (2010). Oxybutynin topical and transdermal formulations: an update. *Drugs of Today*, *46*(6), 417–25.

Yaïch, M., Popon, M., Medard, Y., Aigrain, E.J. (1998). *In-vitro* cytochrome P450 dependent metabolism of oxybutynin to *N*-deethyloxybutynin in humans. *Pharmacogenetics*, *8*(5), 449–451.

Yoshio, A., Hideko, K., Yutaka, S., Goro U. (1986). Studies on the metabolic fate of oxybutynin hydrochloride. *Iyakuhin Kenkyu*, *17*(5), 1070–7.

Zobrist, R. H., Schmid, B., Feick, A., Quan, D., Sanders, S. W. (2001). Pharmacokinetics of the R- and S-enantiomers of oxybutynin and *N*-desethyloxybutynin following oral and transdermal administration of the racemate in healthy volunteers. *Pharmaceutical Research*, *18*(7), 1029–34.

CHAPTER 5. Forced degradation study of selegiline

5.1 INTRODUCTION

Selegiline hydrochloride (**SG**) is an optically active compound and in its levorotatory optical isomer (L-deprenyl) is an irreversible inhibitor of MAO-B enzyme. Selegiline is used alone or in combination with levodopa in the treatment of Parkinson's disease. Moreover clinical studies evaluated the use of **SG** as a beneficial solution to smoking addition and it may also have positive effects in the treatment of Alzheimer's disease, attention deficit hyperactivity disorder (ADHD) and several types of depression (Riederer et al., 2004; Youdim et al., 2006). Selegiline, administered orally, undergoes considerably higher first pass metabolism, resulting in formation of amphetamine derivatives. To avoid or mitigate first pass metabolism, new formulations have been developed exploiting the favourable phisico-chemical properties of selegiline (e.g. low molecular weight (187.3) and good lipohilicity, logP: 3.4) (Chen et al. 2011). The transdermal patches (Emsam®), that enable absorption through the skin, and the orally disintegrating tablets (Zelapar®), that are absorbed primarily through the buccal mucosa, pass directly into the bloodstream, thereby reducing the first pass metabolism. Moreover a thermogel was used for controlled release transdermal delivery of selegiline (Kalász et al., 2014). Recently Fowler et al. (2015) reported that new formulations of selegiline (transdermal patches and orally disintegrating tablets) also have an antidepressant activity at high doses, suggesting that when plasma levels of selegiline are elevated, brain MAO-A might also be inhibited. In fact, selegiline transdermal system (Emsam®) was approved for treating major depressive disorders.

Two main analytical techniques have been applied to the analysis of **SG** in various matrices. HPLC-UV methods were mainly used for pharmaceutical applications (Tzanavaras et al., 2008) and LC–MS bioanalytical assays were used for analysis of biological matrices such as human hair (Nishida et al., 2006) and human plasma (Slawson et al., 2002)

In particular, to fulfil the requirements of the international guidelines (ICH, 2003), the analytical methods used in the field of pharmaceutical analysis should be stability-indicating. This aspect involves the knowledge of the intrinsic chemical stability of the drug substance and, as a consequence, the knowledge of the structures of degradation products and the corresponding degradative pathways. Moreover, in the case of selegiline the chemical

stability should be determined both on the *free base* and salt form; indeed both forms are used in drug product manufacturing.

However, at the best of our knowledge, a comprehensive chemical stability study of selegiline was not reported so far. Hence, in the present work we have established for the first time the intrinsic chemical stability of **SG** through a forced degradation study based on LC-UV and LC-ESI-MS/MS analysis. In oxidative conditions, the formation of diastereomeric *N*-oxides (**SG-NOs**) and a novel degradation product indicator of stability, arising from rearrangement of tertiary propargylamine *N*-oxides, were identified.

Based on these data a stability-indicating LC-UV method for simultaneous estimation of **SG** and its main degradation product was developed. The validation of the proposed method will be carried out and its applicability will be evaluated analyzing the commercially available forms.

5.2 EXPERIMENTAL

5.2.1 Reagents and chemicals

Methanol (HPLC grade), ammonium acetate, concentrated acetic acid, sodium hydroxide (pellets), concentrated hydrochloric acid (37%), iron (III) trichloride hexahydrate, copper sulphate pentahydrate, 30% *w/w* hydrogen peroxide solution, 4,4′-azobis-(4-cyanovaleric acid) (**ACVA**), sodium hydrogen carbonate, sodium phosphate dibasic, concentrated phosphoric acid, anhydrous sodium sulphate, dichloromethane, ninhydrin, selegiline hydrochloride ($\geq$ 99%) were purchased from Sigma-Aldrich (Milano; Italy). Water (HPLC grade) was obtained from Milli-Q reverse osmosis system. Propiolaldehyde diethyl acetal (97%) was purchased from Alfa Aesar. (+) Methamphetamine hydrochloride was purchased by Sigma-Aldrich (St. Louis MO; USA). Since methamphetamine is a DEA controlled item the purchase and the laboratory use were authorized by Ministero della Salute (Ministerial authorization n° UCS/SP/155).

Column chromatography was performed on silica gel 60 (230-400 mesh ASTM Merck). TLC was carried out on plates with a layer thickness of 0.25 mm (silica gel 60 F254; Merck); when necessary, they were visualized after spraying with ninhydrin reagent.

5.2.2 Instrumentation and chromatographic conditions

5.2.2.1 LC-UV analyses

A Shimadzu HPLC system, consisting in two LC-10AD Vp module pumps and a DGU-14-A on-line vacuum degasser, was used. The analyses were carried out on a Luna C18(2) (150 x 4.6 mm I.D., 5μm dp; Phenomenex, Torrance, CA, USA) column as a stationary phase. The isocratic mobile phase (flow rate 1.2 ml/min) was composed of eluant A ammonium acetate buffer (20 mM pH=5.0) and eluant B methanol, the A:B ratio being 40:60 (*v/v*).

The eluants A and B were filtered through a 0.45 μm PVDF membrane filter prior the use. A SIL-10AD Vp autosampler was used for the injection of samples (20μL). The SPD-M10A Vp photodiode array detector was used to detect **SG** and the degradation products at 210 nm and degradation product **SG-EA** at 290 nm. A LC solution 1.24 software was used to process the chromatograms. All the analysis were carried out at room temperature.

5.2.2.2 LC-MS/MS analyses

A Thermo Finningan LCQ Deca XP Plus system equipped with a quaternary pump, a Surveyor AS autosampler, a Surveyor PDA detector and a vacuum degasser was used for LC-MS analysis (Thermo Electron Corporation, Waltham, MA, USA). The analysis were performed on a Luna C18(2) (100 x 4.6 mm I.D., 5μm d_p; (Phenomenex, Torrance, CA, USA) column as a stationary phase maintained at 35°C and protected by a Security Guard C18. The sample injection volume was 3 μL. The mobile phase was composed of eluant A: ammonium acetate buffer (pH 5.0; 10 mM) and eluant B: methanol, using a gradient mode, the ratio A:B was set 60:40 The following gradient, at a constant flow rate of 0.2 mL/min, was used: from 0 to 8 min, the composition was increased from 40.0 to 60.0% B. From 8 to 12 min the percentage of eluant B was increased again to 80.0% and then maintained 2 min. From 14 to 14.50 the percentage of eluant B was decreased to 40.0% and then maintained 3.5 min for column equilibration. The eluate was injected into the electrospray ion source (ESI) and the MS and MS/MS spectra were acquired and processed using the Xcalibur® software (Thermo Electron Corporation, Waltham, MA, USA).

The operating conditions on the ion trap mass spectrometer in positive ion mode were as follows: spray voltage, 5.0 kV; source current, 80.0 μA; capillary temperature, 350.0 °C; capillary voltage, 26.0 V; tube lens offset, -5.0 V; multipole 1 offset, -8.25 V; multipole 2 offset, -9.50 V; sheath gas flow (N_2), 60.0 Auxiliary Units; sweep gas flow (N_2): 5.0

Auxiliary Units. Data were acquired both full scan and MS/MS product ion scan modes using mass scan range *m/z* 50 to 200 and *m/z* 80 to 600, optimizing the collision energy at 18-30%.

5.2.2.3 Spectroscopic analyses

^{1}H and ^{13}C experiments were performed at 298K on a JEOL Eclipse ECP 300 FT MHz spectrometer (Jeol Ltd. Tokyo, Japan) operating at 7.05T. Chemical shifts are reported in part per million (ppm).

5.2.3 Forced degradation conditions

Degradation studies in solution were done at a selegiline-HCl at concentration of 1 mg/mL. For acidic degradation study, **SG** was dissolved in 0.5 N HCl and the solution was left protected from light at 50°C for 24 h.

The degradation in alkaline conditions was done in 0.5 N NaOH in presence of methanol/water 50/50 and the solution was left protected from light at 50°C for 24 hours.

The oxidative degradation pathway was studied using four different protocols:

a) The degradation was done in a 3% H_2O_2 solution (pH=5 acetate buffer); the mixture was left in the dark at room temperature for 24h.
b) The degradation was done in a 1% H_2O_2 solution (50/50 methanol/water) in the presence of sodium hydrogen carbonate; the mixture was left in the dark, at room temperature, for 1h.
c) To evaluate the influence of transition metals, **SG** solution was treated with 1.5 mM Cu^{2+} or Fe^{3+} at ambient temperature for 4h.
d) To a solution of **SG** in 50/50 methanol/water, the radical iniziator **ACVA**, previously dissolved in water (1mg/ml) was added in the presence of sodium hydrogen carbonate. The mixture of reaction (**ACVA**: 1mM final concentration) was stored at 60° for 24h.

For thermal degradation, a sample of **SG** was placed in a hot air oven maintained at 60°C for 18 h. Photodegradation studies were carried out, at room temperature, by exposing a thin layer (10 mg) of **SG** to daylight and UV-light (365 nm) for 18 days and 4 hours respectively. For both thermal and photodegradation tests, **SG** was assayed as powder.

5.2.4 Isolation and purification of SG-EA

To a solution of **SG** (250 mg, 1.12 mmol) in 5 ml of water, 120 mg of sodium hydrogen carbonate 5 ml of methanol and 1 ml of 30% *w/w* hydrogen peroxide were added. The mixture was reacted, under stirring at r.t., for 16h monitoring by TLC analysis (eluant: CH_2Cl_2/MeOH 9:1). At the end of the reaction, methanol was evaporated under reduced pressure. The aqueous residue was extracted (3x15 ml) with CH_2Cl_2. The pooled organic layers were washed with brine, dried over anhydrous sodium sulphate, filtered and evaporated in vacuo to dryness. The pale-yellow oily residue was left overnight at r.t. and then purified by column chromatography using dichloromethane/methanol 98/2 as eluant to give pure **SG-EA** (55 mg, 24% yield; 98% purity by HPLC assay at 290 nm).

5.2.5 Synthesis of degradation product

*5.2.5.1 3-[methyl(1-methyl-2-phenylethyl)amino]- 2-Propenal (**SG-EA**)*

To a solution of propiolaldehyde, arising from propiolaldehyde diethyl acetal (90 mg, 0.7 mmol) hydrolysis (0.2 N HCl solution, 5 mL) at 40 °C for 0.5 h, (+)-methamphetamine hydrochloride as free base (100 mg, 0.7 mmol) dissolved in EtOH (5 mL) was added dropwise. After being stirred for 2 h at 50 °C, the reaction mixture was diluted with H_2O (20 mL), and EtOH was distilled off. The pH of the aqueous phase was adjusted to 12 with 1 N NaOH solution, and the reaction mixture was extracted with Et_2O. The ethereal solution was washed with H_2O. The evaporation of the dried organic phase gave an oil that was purified by column chromatography dichloromethane/MeOH 90/10 to afford **SG-EA** (60 mg, 41%).

ESI-MS: calculated for $C_{13}H_{17}NO$ *M*= 203.28; Found *m/z* = 204 $[M+H]^+$

^{1}H-NMR *(300 MHz, $CDCl_3$) δ (ppm): 8.9 (d, J= 8.1 Hz, 1H), 7.26-7.19 (m, 3H), 7.07 (d, J= 6.8 Hz; 2H), 6.86 (d, J=12.0 Hz; broad 1H), 5.03 (dd, J= 8.2 Hz, J=12.3 Hz; 1H), 3.61-3.56 (m; 1H), 2.79(d, J=8.5 Hz; 2H), 2.69 (s, 3H), 1.29 (d, J=6.5 Hz; 3H)*

^{13}C-NMR *(300 MHz, $CDCl_3$) δ (ppm):189.4 (CO) 158.8(C=C), 137.5 (C) 128.8 (2CH), 128.7 (2CH), 126.9(CH); 101.2 (C=C); 64.2 (CH), 41.4(CH_2); 32.1(NCH_3); 19.07(CH_3)*

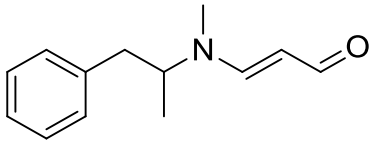

SG-EA

5.3 RESULTS AND DISCUSSION

5.3.1 Forced degradation study and structural characterization of degradation products

The chemical stability of **SG** was investigated following the requirements of international guidelines (ICH, 2003). In the Table 1 the stress conditions used in this work are summarized.

Stressor	Temperature (°C)	Time of the analysis
HCl 0.5N	50	4, 24 h
NaOH 0.5N	50	4, 24 h
3% H_2O_2 pH=5	RT	4, 24 h
1% H_2O_2 pH≈8	RT	1 h
Transition metals	RT	4, 24 h
Radical initiator	60	1, 4, 24 h
UV light	RT	4 h
Sunlight	RT	18 days
Thermal	60	18 h

Table 1. Stress conditions applied in the forced degradation study of selegiline hydrochloride

5.3.1.1 Degradation in acidic and basic conditions

As expected, selegiline hydrochloride was found to be stable in acidic and alkaline conditions. In the presence of 0.5N NaOH and 0.5N HCl at 50°C for 24h no degradation occurred as showed in Figure 1a and 1b. The chromatographic peak at retention time 10.5 min is attributable to selegiline, no other peak corresponding to the formation of degradation products was observed.

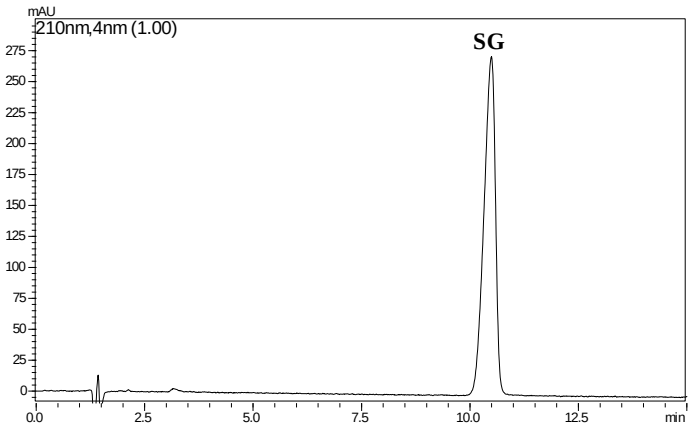

Figure 1a. LC-UV chromatogram (λ_a=210 nm) of **SG** in 0.5N NaOH solution (t= 24h at 50°C)

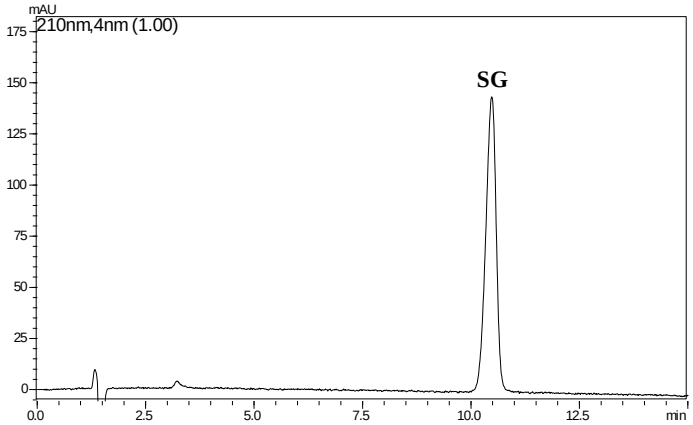

Figure 1b. LC-UV chromatogram (λ_a=210 nm) of **SG** in 0.5N HCl solution (t= 24h at 50°C)

5.3.1.2 Thermal degradation and photodegradation

For photodegradation studies, **SG** was exposed to daylight and 365 nm UV-light for eighteen days and 4h respectively; in these conditions no degradation occurred (data not shown). Similarly, the thermal stress test on **SG** was conducted without observing the formation of degradation product.

5.3.1.3 Degradation in oxidative conditions

The presence in selegiline of a tertiary amine aliphatic function, suggests that it could be oxidized to the corresponding *N*-oxide; in particular, since selegiline is more prone to oxidation in its *free base* form, the oxidative degradation was investigated at acidic and alkaline pH. Furthermore, the degradation in oxidative conditions was studied using three different oxidants: hydrogen peroxide, radical chain initiators and transition metal ions.

LC-UV chromatograms reported in Figures 2-5 clearly showed the pH effect on *N*-oxide formation. In acidic pH no degradation occurred; the peak of selegiline was detected at t_R=10.0 min, whereas the peaks appearing at t_R=1.3 and 3.1 min are attributable to H_2O_2 and the solvent respectively, as evidenced by the LC-UV chromatogram of the control degradation (Figure 3). On the contrary, at alkaline pH, a degradation product was observed at t_R= 2.6 min after 1h, having an absorption maximum at 210 nm (Figure 4). Moreover the formation of another peak at t_R= 3.6 min was observed at higher wavelength (λ_a= 290 nm) (Fig.5), suggesting the presence of a new chromophore group in its structure.

It is worth mentioning that increasing the time of degradation and/or the concentration of hydrogen peroxide, the intensity of the peak at 3.6 min corresponding to **SG-EA** increased. Besides, the analysis of the stress test performed at lower concentration of oxidant and/or with

shorter reaction time highlighted the formation of **SG-NOs** as the first degradation product followed by **SG-EA**.

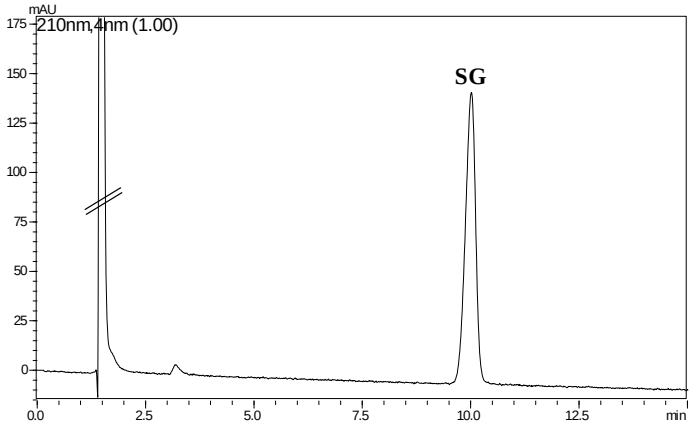

Figure 2. LC-UV chromatogram of **SG** degradation in hydrogen peroxide (pH=5, t= 4h).

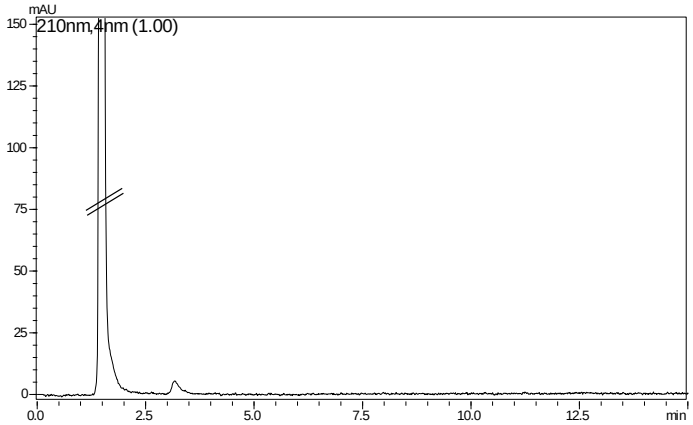

Figure 3. LC-UV chromatogram of control degradation in hydrogen peroxide (pH=5, t=6 h).

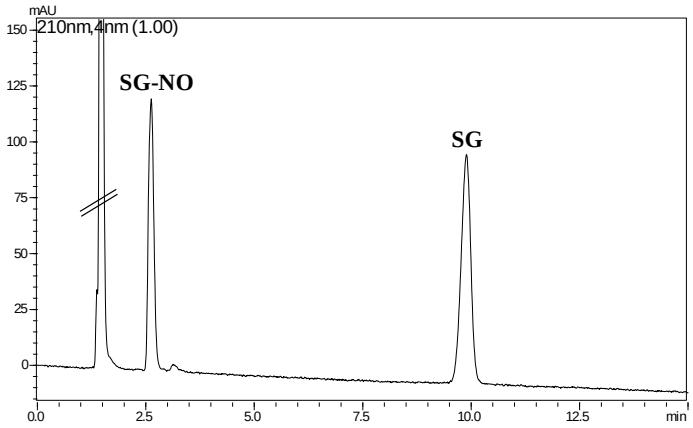

Figure 4. LC-UV chromatogram (λ_a=210 nm) of SG in 1% H_2O_2 (alkaline solution, t= 1h)

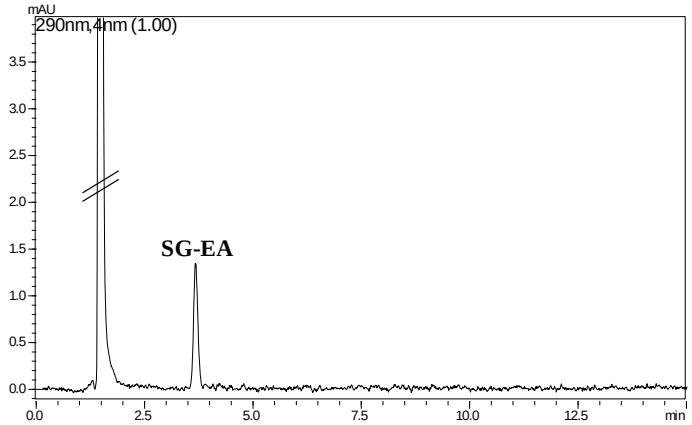

Figure 5. LC-UV chromatogram (λ_a=290 nm) of **SG** in 1% H_2O_2 (alkaline solution, t= 1h)

The oxidative degradation of selegiline was evaluated also in the presence of the radical initiator **ACVA** in slightly alkaline conditions. In the chromatogram reported in Figure 6, the peak at t_R= 10.5 min is attributable to selegiline, whereas the formation of the peak of **SG-NO** was not detected. On the contrary, when the LC-UV analysis was performed at higher wavelength (λ_a= 290nm) the presence of a degradation product (Figure 7a) was observed, being its chromatographic properties identical to those of the peak **SG-EA** observed in Figure 5. The presence of **SG-EA** was confirmed by the analysis of the synthetical standard (Figure 7b). As previously reported regarding the chemical stability of oxybutynin hydrochloride, the use of radical initiator allowed a better representation of the degradation in oxidative conditions.

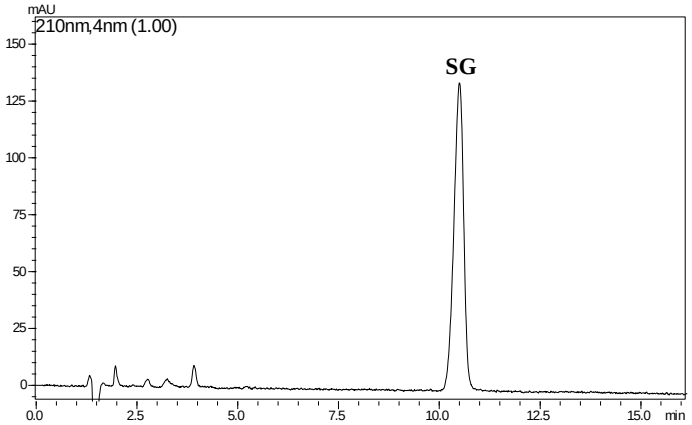

Figure 6. LC-UV chromatogram (λ_a=210 nm) of **SG** in presence of radical initiator (t= 24h)

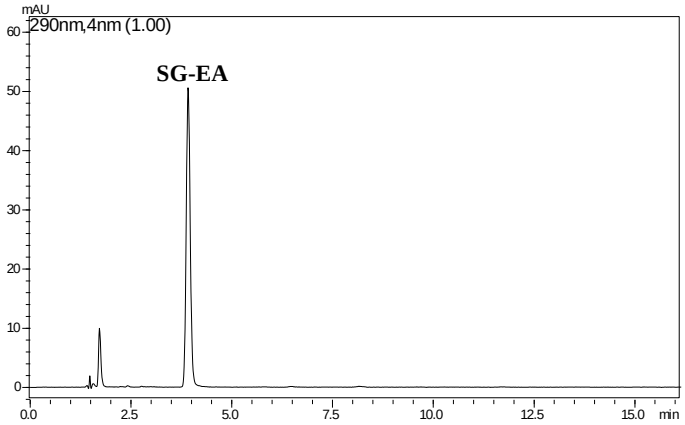

Figure 7a. LC-UV chromatogram (λ_a=290 nm) of **SG** in presence of radical initiator (t= 24h)

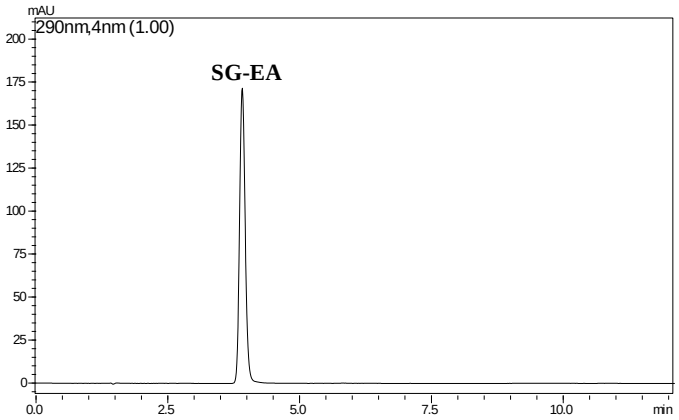

Figure 7b. LC-UV chromatogram (λ_a=290 nm) of **SG-EA** synthetic standard

Finally, in the stress test done in the presence of the transition metals Fe^{3+} and Cu^{2+}, **SG** did not undergo degradation as showed in the LC-UV chromatograms reported in the Figure 8a and 8b. Possibly the lack of oxidative degradation in the presence of transition metal ions could be due to the acidic conditions used in the test promoting the presence of the protonated form of selegiline.

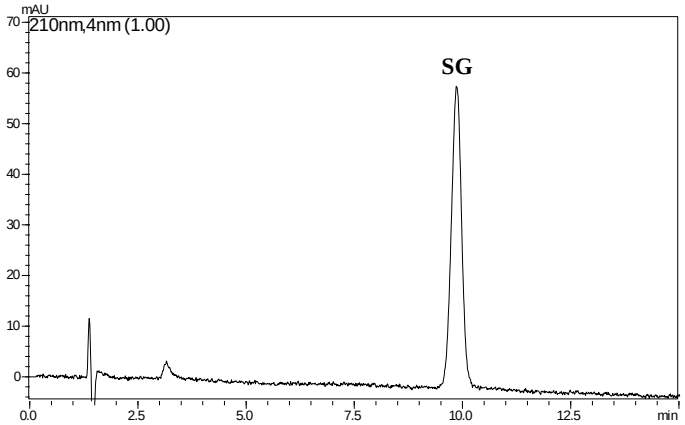

Figure 8a. LC-UV chromatogram of **SG** degradation in the presence of Fe^{3+}

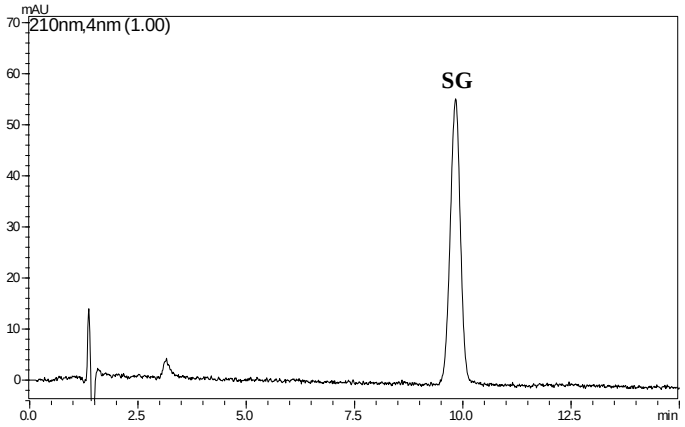

Figure 8b. LC-UV chromatogram of **SG** degradation in the presence of Cu^{2+}

5.3.2 Structural characterization of selegiline degradation products by LC-ESI-MS/MS analysis

In order to obtain information on the structures of the degradation products formed in oxidative conditions, the degradation test samples were analyzed by **LC-ESI-MS/MS**.

The **LC-ESI-MS** analysis of the $H_2O_2/NaHCO_3$ sample, showed the formation of two degradation products (**SG-NOs)** in the full mass chromatogram (Figure 9, top), having the same protonated ion at *m/z* 204, and corresponding to the insertion of an oxygen atom in the structure of selegiline *free base* ($[M+H]^+ = 188$). The presence of the tertiary amine function and the same fragment ion pattern in their MS/MS spectra (Fig. 10) suggested that they are the diastereomeric *N*-oxides of selegiline. Since selegiline *N*-oxides were the first degradation products detected in the stress test done in the presence of low concentration of hydrogen peroxide, they could represent the first step in the oxidative degradation of selegiline.

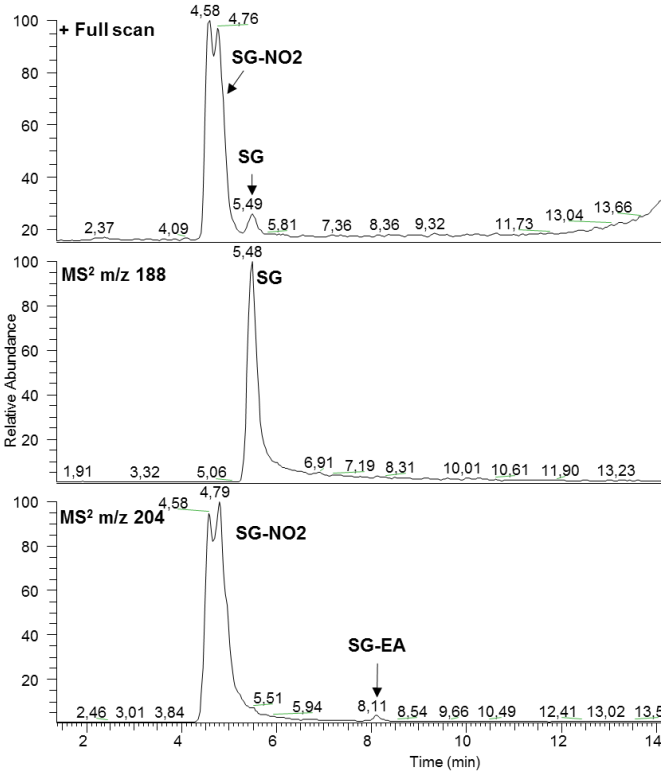

Figure 9. LC-MS chromatogram of **SG** in 1% H_2O_2 (alkaline solution, t= 1h)

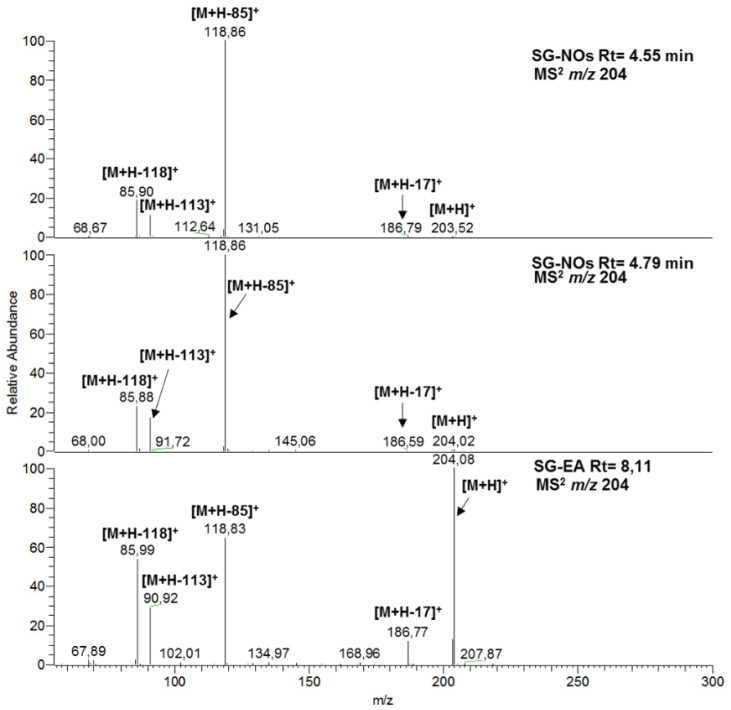

Figure 10. LC-MS^2 fragmentation patterns of **SG-NOs** and **SG-EA**

Selegiline *N*-oxides appeared rather unstable, forming, over the time, a secondary degradation product, **SG-EA,** showing a similar but not identical MS^2 spectrum (Figure 10). In particular, the peak of **SG-EA** protonated molecule is far more intense than those of **SG-NOs** indicating the high stability of the secondary degradation product.

The assignment of the structure to **SG-EA** was based on the findings of Szabó and Hermecz (2001), concerning the chemistry of tertiary propargylamine *N*-oxides, and our results about the chemical stability of oxybutynin hydrochloride (Chapter 3): these data suggested the synthesis of selegiline enaminoaldehyde through the reaction of methamphetamine with the in situ generated propiolaldehyde to give **SG-EA** standard whose mass spectral data and chromatographic characteristics are identical to those of the degradation product (Figure 11).

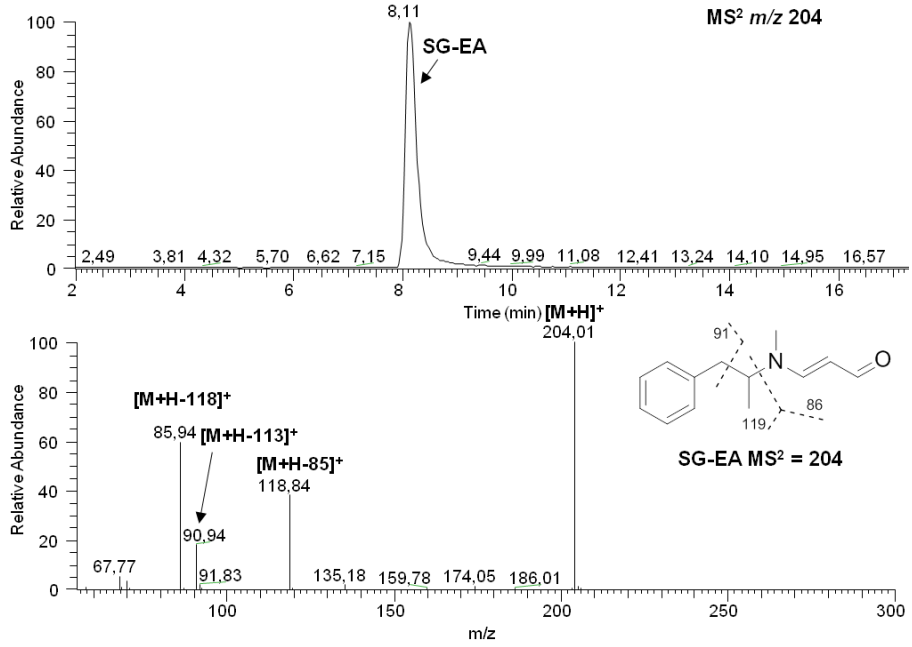

Figure 11. LC-MS chromatogram and MS^2 spectrum of **SG-EA** synthetic standard

Interestingly, the spectroscopic properties (Figure 12) of **SG-EA** were in accordance with the presence of enaminoaldehyde moiety in its structure; indeed the absorption maximum at 290 nm is due to the enamino-aldehyde chromophore which was not found in selegiline and selegiline *N*-oxides whose UV-Vis spectra showed an absorption maximum at about 210 nm.

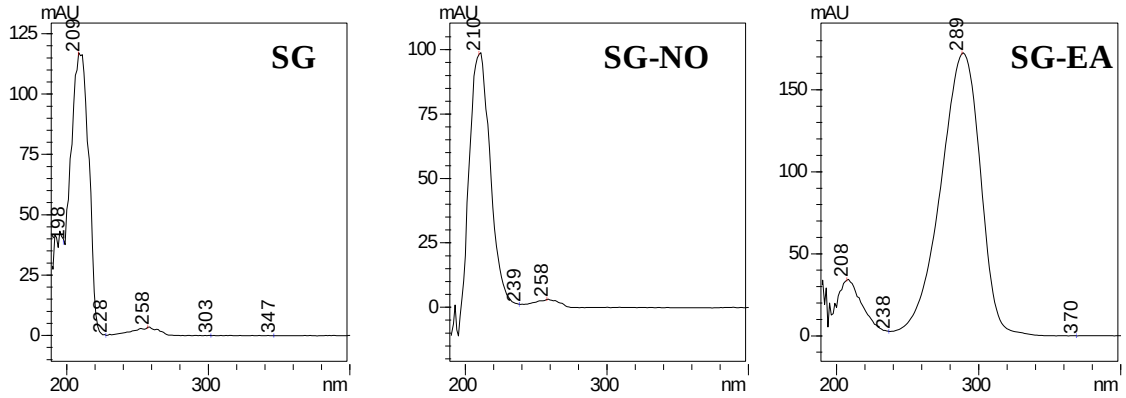

Figure 12. UV spectra of **SG**, **SG-NO**, and the **SG-EA**. The UV spectra were recorded during the LC-UV analysis (see experimental part)

A plausible mechanism of formation of **SG-EA** could be proposed on the basis of literature data (Szabó and Hermecz 2001; Szabó et al., 2004): this involves the formation of isoxazolinium intermediate, generated by addition of the selegiline *N*-oxide oxygen to the carbon-carbon triple bond and subsequent proton transfer from a protic solvent. Subsequently after deprotonation of isoxazolinium the enamino-aldehyde is formed (Figure 13).

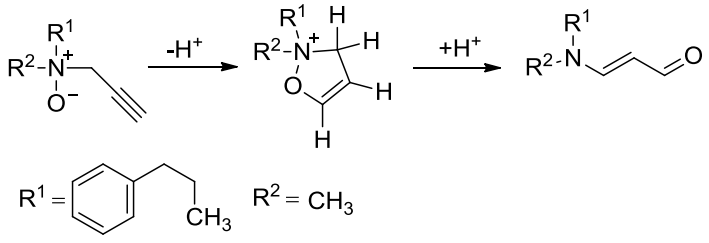

Figure 13. Proposed mechanism of the rearrangement of selegiline *N*-oxides

5.4 CONCLUSIONS

In the present work the instrinsic chemical stability of **SG** was evaluated by a forced degradation study using LC-UV and LC-MS/MS analysis. In oxidative condition the formation of a new and unprecedented degradation product **SG-EA** was identified and the degradation scheme for selegiline was proposed and reported in the figure 14.

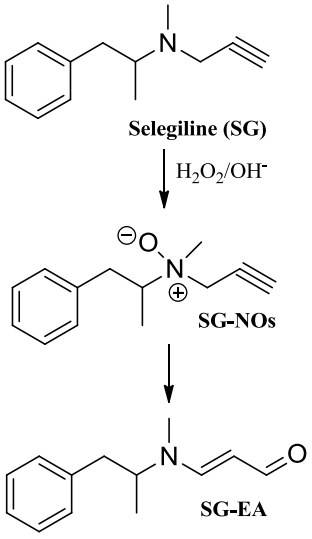

Figure 14. Oxidative degradation pathways of selegiline

The formation of **SG-EA** take place through the rearrangement of the primary degradation products selegiline *N*-oxides. As expected, the oxidative degradation is dependent on the pH and selegiline in the protonated form did not undergo *N*-oxidation and the subsequent rearrangement to **SG-EA**. This feature indicate that are no concern for drug products in which selegiline is used as hydrochloride salt. However since **SG** *free base* results more prone to oxidation, the oxidative degradation should be taken into account in the course of stability study of the drug products (e.g. transdermal system) containing selegiline *free base* as a drug substance. Though selegiline *N*-oxides were the primary degradation products, their instability prevented their use as the indicators of stability in the development of stability-indicating analytical methods for the determination of selegiline and its impurities. On the contrary **SG-EA** was stable and synthetically accessible in pure form and it could be advantageously employed as the indicator of stability for oxidative stresses and included in the development of stability-indicating analytical methods for selegiline. Moreover the presence in the **SG-EA** structure of a α,β-unsaturated aldehydo group which could behave as a Michael acceptor

reacting with nucleophilic functions of biological macromolecules, suggest to test this compound for its potential toxicity/genotoxicity.

5.5 REFERENCES

Chen, C. C., Fang, C.L., Al-Suwayeh, S. A., Leu, Y.L., and Fang, J.Y. (2011). Transdermal delivery of selegiline from alginate-Pluronic composite thermogels. *International Journal of Pharmaceutics*, *415*(1-2), 119–28.

Fowler, J. S., Logan, J., Volkow, N. D., Shumay, E., McCall-Perez, F., Jayne, M., et al. (2015). Evidence that Formulations of the Selective MAO-B Inhibitor, Selegiline, which Bypass First-Pass Metabolism, also Inhibit MAO-A in the Human Brain. *Neuropsychopharmacology*, *40*(3), 650–7.

ICH Harmonized Tripartite Guidelines Q1A(R2) (2003). Stability Testing of New Drug Substances and Products.

Kalász, H., Magyar, K., Szőke, É., Adeghate, E., Adem, A., Hasan, M.Y., Nurulain, S.M., Tekes, K. (2014). Metabolism of Selegiline [(-)-Deprenyl]. *Current Medicinal Chemistry*, *21*, 1522–1530.

Nishida, K., Itoh, S., Inoue, N., Kudo, K., & Ikeda, N. (2006). High-Performance Liquid Chromatographic- Mass Spectrometric Determination of Methamphetamine and Amphetamine Enantiomers , Desmethylselegiline and Selegiline , in Hair Samples of Long-Term Methamphetamine Abusers or Selegiline Users. *Journal of Analytical Toxicology*, *30*, 232–237.

Riederer P., Lachenmayer L., Laux G. (2004). Clinical applications of MAO-inhibitors. *Current Medicinal Chemistry*, *11*, 2033–2043.

Slawson, M. H., Taccogno, J. L., Foltz, R. L., and Moody, D. E. (2002). Quantitative Analysis of Selegiline and Three Metabolites (N -Desmethylselegiline , Methamphetamine , and Amphetamine) in Human Plasma by High-Performance Liquid Chromatography – Atmospheric Pressure Chemical Ionization-Tandem Mass Spectrometry. *Journal of Analytical Toxicology*, *26*, 19–23.

Szabó, A., Galambos-Faragó, Á., Mucsi, Z., Timári, G., Vasvári-Debreczy, L., and Hermecz, I. (2004). Solvent-Dependent Competitive Rearrangements of Cyclic Tertiary Propargylamine N-Oxides. *European Journal of Organic Chemistry*, (4), 687–694.

Szabó, A., Hermecz, I. (2001). Novel intramolecular rearrangement of tertiary propargylamine *N*-oxides. *Journal of Organic Chemistry*, *66*(21), 7219–22.

Tzanavaras, P. D., Themelis, D. G., Zotou, A., Stratis, J., & Karlberg, B. (2008). Optimization and validation of a dissolution test for selegiline hydrochloride tablets by a novel rapid HPLC assay using a monolithic stationary phase. *Journal of Pharmaceutical and Biomedical Analysis*, *46*(4), 670–675.

Youdim M. B. H., Bakhle Y. S. (2006). Br. J. Pharmacol. *Monoamine Oxidase: Isoforms and Inhibitors in Parkinson's Disease and Depressive Illness*, *147*, S287–S296.

CHAPTER 6. New findings in the *in vitro* metabolism of selegiline

6.1 INTRODUCTION

Selegiline hydrochloride (**SG**) or L-deprenyl is a potent, irreversible and selective inhibitor of monoamine oxidase B (MAO-B) and is used in the treatment of Parkinson's disease.

Selegiline is quickly absorbed after oral administration and undergoes considerably higher first pass metabolism. The metabolism of selegiline has been extensively studied in literature in the past fifty years and it is well known that **SG** is predominantly metabolized into methamphetamine, amphetamine and *N*-desmethylselegiline. In addition more than 40 minor metabolites of selegiline have also been either detected or proposed as recently reviewed by Kalász et at., 2014. Among these, the formation of selegiline *N*-oxide as a metabolite of selegiline has been suggested by Wu and Ichikawa (1995) and was also identified in human urine (Katagi et al., 2001; Katagi et al, 2002).

Lévai et al. (2004) described the formation of selegiline *N*-oxides (**SG-NOs**) *in vitro* from selegiline in liver microsomal preparations from different species, reporting that the extent of formation is species-dependent. They reported that the formation of **SG-NOs** was more intensive in dog and hamster microsomal preparations, whilst less **SG-NOs** were formed in the mouse, guinea pig and rabbit ones, and very little selegiline was metabolized to **SG-NOs** in the human preparation. Moreover they reported the synthesis of selegiline *N*-oxides hydrochloride salt (as a 1:1 mixture of the diastereomers), whose structure was confirmed by MS and NMR data.

The chromatographic separation of the R,R-selegiline-NO and R,S-selegiline-NO was achieved by means of a HPLC method, which also allows to determine the diastereomeric form of selegiline-*N*-oxide that is preferentially originated in the different animal species. In particular the R,S-diastereomer is preferentially formed in the liver microsomal preparations of dog, rat, rabbit, mouse, guinea pig and human, whilst the R,R-selegiline-NO is the preferred form in the hamster microsomes. Moreover the authors suggested that the formation of selegiline-NOs might be catalyzed, at least partly, by the isoforms CYP2D6 and CYP3A4. No further metabolites were detected after incubation of the mixture of selegiline-NOs with rat liver microsomes.

Interestingly, although the formation of **SG-NOs** has been examined in deep by Levai et al. (2014) and the formation of rearrangement product from tertiary propargylamine *N*-oxides

has been described in literature (Szabó and Hermecz, 2001), no rearrangement product from **SG-NOs** was reported in their study.

The aim of this work is to achieve more insights in the metabolic fate of selegiline, focusing our attention on the potential formation of the rearrangement product arising from selegiline *N*-oxide. This hypothesis was suggested by the results of the chemical stability study of selegiline reported in chapter 5 and on the basis of the results obtained in the *in vitro* metabolism study of oxybutynin.

6.2 EXPERIMENTAL

6.2.1 Reagents and chemicals

Methanol (HPLC grade), ammonium acetate, concentrated acetic acid, selegiline hydrochloride (≥ 99%), 2-mercaptoethanol were purchased from Sigma-Aldrich (Milano; Italy). Water (HPLC grade) was obtained from Milli-Q reverse osmosis system.

6.2.2 Instrumentation and chromatographic conditions

6.2.2.1 LC-MS/MS analyses

A Thermo Finningan LCQ Deca XP Plus system equipped with a quaternary pump, a Surveyor AS autosampler, a Surveyor PDA detector and a vacuum degasser was used for LC-MS analysis (Thermo Electron Corporation, Waltham, MA, USA). The analysis were performed on a Luna C18(2) (100 x 4.6 mm I.D., 5μm d_p; (Phenomenex, Torrance, CA, USA) column as a stationary phase maintained at 35°C and protected by a Security Guard C18. The sample injection volume was 3 μL. The mobile phase was composed of eluant A: ammonium acetate buffer (pH 5.0; 10 mM) and eluant B: methanol, using a gradient mode, the ratio A:B was set 60:40 The following gradient, at a constant flow rate of 0.2 mL/min, was used: from 0 to 8 min, the composition was increased from 40.0 to 60.0% B. From 8 to 12 min the percentage of eluant B was increased again to 80.0% and then maintained 2 min. From 14 to 14.50 the percentage of eluant B was decreased to 40.0% and then maintained 3.5 min for column equilibration. The eluate was injected into the electrospray ion source (ESI) and the MS and MS/MS spectra were acquired and processed using the Xcalibur® software (Thermo Electron Corporation, Waltham, MA, USA). The operating conditions on the ion trap mass spectrometer in positive ion mode were as follows: spray voltage, 5.0 kV; source current, 80.0

µA; capillary temperature, 350.0 °C; capillary voltage, 26.0 V; tube lens offset, -5.0 V; multipole 1 offset, -8.25 V; multipole 2 offset, -9.50 V; sheath gas flow (N_2), 60.0 Auxiliary Units; sweep gas flow (N_2): 5.0 Auxiliary Units. Data were acquired both full scan and MS/MS product ion scan modes using mass scan range *m/z* 50 to 200 and *m/z* 80 to 600, optimizing the collision energy at 18-30%.

6.2.3 Rat and Human liver microsomes

Male Wistar rat liver microsomes (RLM), (protein concentration: 25mg/ml, total P450: 0.64 nmol/mg protein) and the cryopreserved pooled human liver microsomes (HLM), (pooled mixed sex, ten individual donors, protein concentration: 20 mg/ml, total P450: 0.36 nmol/mg) were purchased from BD Gentest™ (Woburn, MA) and used throughout this study. The incubations were all carried out using a horizontal DUBNOFF shaking thermostatic bath (Dese Lab Research, Padova, Italy) and were protected from light.

6.2.4 *In vitro* RLM and HLM incubations of selegiline

The standard incubation mixture (500 µl final volume), in 1.5 ml Eppendorf tubes, was carried out in a 50 mM TRIS buffer (pH 7.4) containing 3.3 mM $MgCl_2$, 1.3 mM $NADPNa_2$, 3.3 mM glucose 6-phosphate, 0.4 Units/ml glucose 6-phosphate dehydrogenase and 100 µM **SG**. After pre-equilibration of the mixture, an appropriate volume of microsomal suspension was added to give a final protein concentration of 1 mg/ml. The mixture was shaken for 60 min at 37°C, and the reaction was quenched by diluting the samples with 500 µl of ice-cold acetonitrile. The samples were then centrifuged at 13,000 rpm for 5 min, and the supernatant was directly injected onto the column for analysis. Control incubations without the presence of substrate, NADP(H)-regenerating system, or microsomes were also carried out.

6.2.5 *In vitro* RLM incubation of SG-EA

The standard incubation mixture (500 µl final volume), in 1.5 ml Eppendorf tubes, was carried out in a 50 mM TRIS buffer (pH 7.4) containing 3.3 mM $MgCl_2$, 1.3 mM $NADPNa_2$, 3.3 mM glucose 6-phosphate, 0.4 Units/ml glucose 6-phosphate dehydrogenase and 100 µM **SG-EA**. After pre-equilibration of the mixture, an appropriate volume of microsomal suspension was added to give a final protein concentration of 1 mg/ml. The incubation, the

sample preparation and the analysis of supernatants were performed following the same procedure described before.

6.2.6 Incubation of selegiline in the presence of nucleophilic trapping agents

The formation of electrophilic species in **SG** incubations was studied by adding 2-mercaptoethanol (final concentration: 3mM) to the incubation mixture. The incubations were performed using the same conditions reported in the paragraph 6.2.4. The sample were then centrifuged to remove the insoluble matter and an aliquot (3µl) was analyzed by LC-ESI-MS.

6.3 RESULTS AND DISCUSSION

The oxidative metabolism of selegiline was assessed through an *in vitro* study performed in rat and human liver microsomes.

The LC-ESI-MS analyses of the RLM and HLM incubations are reported in figures 1a and 1b and showed the formation of three metabolites having the same protonated molecule at *m/z* 204, and corresponding to the insertion of an oxygen atom in the structure of selegiline *free base* ($[M+H]^+ = 188$). It is worth of mention that in the present study no attempt to separate the peaks of **SG-NOs** was undertaken. Nonetheless, the formation of two *N*-oxides may be inferred from the presence of a shoulder on the peak at 4.80 min; the intensity of the peak at 4.80 min is higher in RLM than in HLM incubations, as previously highlighted in literature (Lévai et al., 2004). The identity of the metabolites **SG-NOs**, formed in RLM and HLM incubations, was assigned comparing the retention time and the fragmentations patterns (Figure 2) with those of **SG-NOs** synthetic standard (Figure 3) that was freshly prepared from the reaction of selegiline with hydrogen peroxide, as previously reported in the Chapter 5.

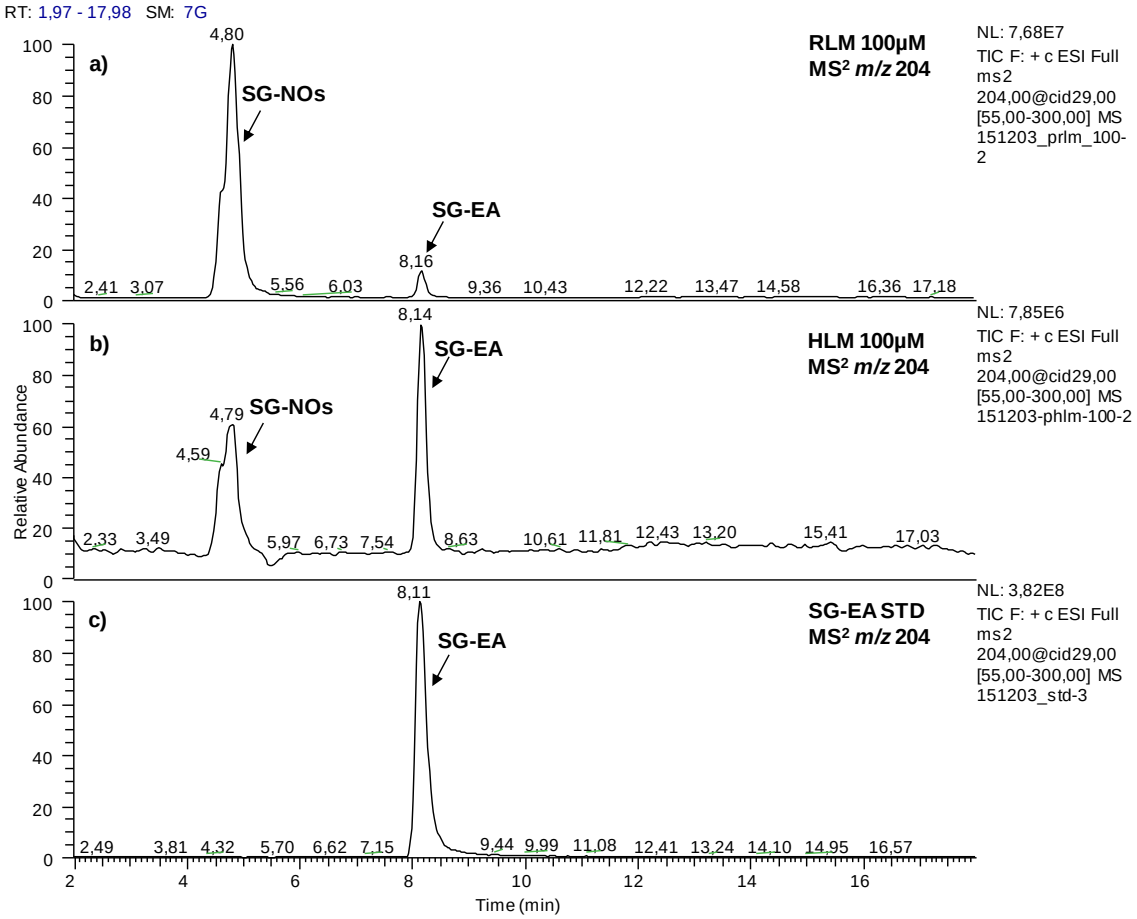

Figure 1. LC-MS/MS chromatograms of rat and human microsomal incubations of **SG** (100µM) (a,b). and of the synthetic standard of **SG-EA** (c)

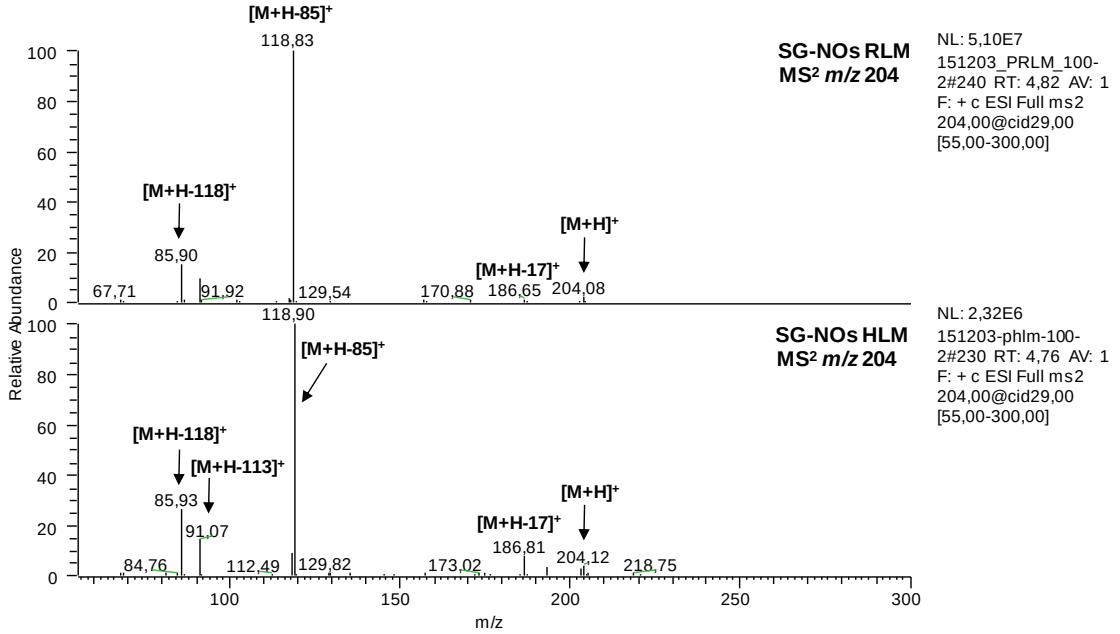

Figure 2. LC-MS^2 spectra of **SG-NOs** formed in rat and human microsomal incubations of **SG** (100µM).

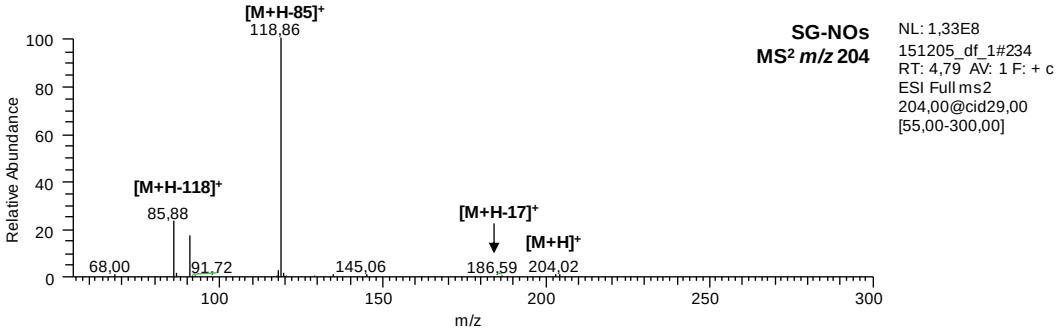

Figure 3. LC-MS^2 spectrum of a freshly prepared sample of **SG-NOs** using hydrogen peroxide

Besides the formation of **SG-NOs**, a new and more lipophilic metabolite (**SG-EA**) was observed in the chromatograms reported in figures 1a and 1b. The assignment of its structure was achieved by comparing its retention time with that of the authentic reference compound (figura 1c), whose synthesis has been reported in the Chapter 5. Moreover the evaluation of the fragmentation pattern in the LC-MS^2 spectrum confirmed that the structure of the new metabolite **SG-EA**, formed in RLM and in HLM incubations, matched with that of the synthetic standard (figure 4).

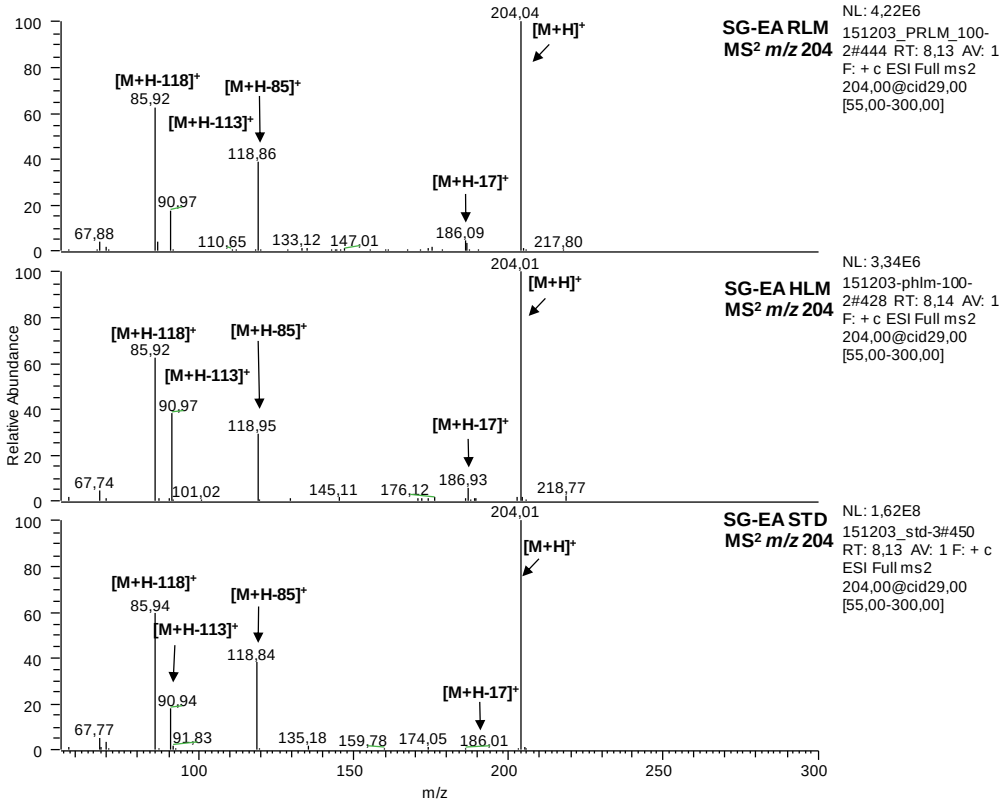

Figura 4. LC-MS^2 spectra of **SG-EA** formed in RLM and HLM incubations and LC-MS^2 spectra of the synthetic **SG-EA** standard (**SG-EA STD**)

According to the results obtained during the chemical stability study of selegiline hydrochloride, as well as on the data of Szabò and Hermecz (2001), it is possible to hypothesize that **SG-EA** was formed through the chemical rearrangement of **SG-NOs**, as reported in the figure 5.

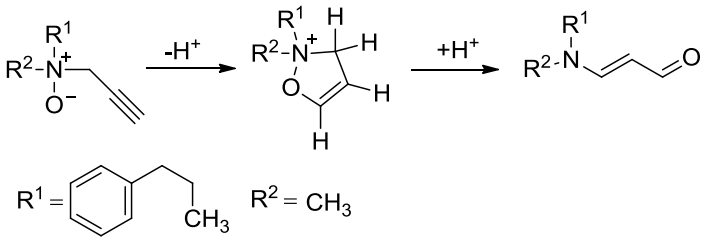

Figure 5. Proposed mechanism of the rearrangement of selegiline *N*-oxides

Another hypothesis to explain the metabolic formation of **SG-EA** arises from the known reactivity of propiolaldehyde with amine derivatives to form enaminoaldehyde. Indeed, since propioladehyde and methamphetamine were metabolites, formed during the enzymatic *N*-dealkylation of **SG**, they might react together giving **SG-EA**.

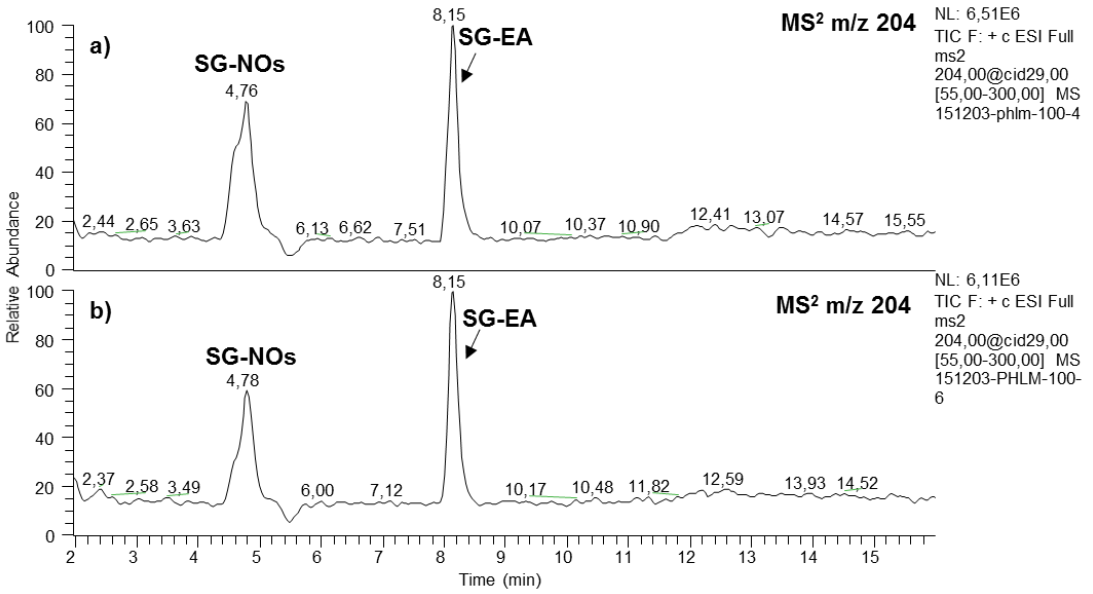

Figure 5. LC-MS/MS chromatograms of HLM incubation (**SG**: 100µM) monitoring the ion at *m/z* 204: a) without 2-mercaptoethanol, b) with 2-mercaptoethanol (3mM)

However, this hypothesis was ruled out since the formation of **SG-EA** was observed, in the incubations carried out in the presence of 2-mercaptoethanol used as nucleophilic trapping agent (figure 5). This fact showed that the reaction between the propioladehyde and 2-mercaptoethanol does not interfere with the formation of **SG-EA** which depends on oxidation of propargylamine moiety.

Finally to evaluate the formation of other potential metabolites from further transformation of **SG-EA**, the incubation of the synthetic standard in RLM microsomes was performed: no metabolite could be detected by LC-ESI-MS/MS confirming the relevant stability of **SG-EA** (data not shown).

6.4 CONCLUSION

The metabolic fate of selegiline was extensively described in literature and several metabolites were proposed and identified so far. In this work the oxidative metabolism of selegiline was re-investigated focusing the attention on the potential formation of **SG-EA** through the rearrangement of **SG-NOs**. As expected, the presence of **SG-EA** was detected in the incubations with rat and human liver microsomes and its formation might not appear to be catalyzed by enzymes, but due to the prototropic rearrangement of **SG-NOs**. Interestingly, differently from **SG-NOs**, **SG-EA** was a stable metabolite which did not seem undergo to further oxidative and hydrolytic transformation.

6.5 REFERENCES

Lévai F., Fejér,E., Szeleczky,G., Szabó,A., Takácsy,T.E., Hajdu, F., Szebeni,G., Szatmári, I. H. (2004). *In vitro* formation of selegiline-*N*-oxide as a metabolite of selegiline in human, hamster, mouse, rat, guinea-pig, rabbit and dog. *European Journal of Drug Metabolism and Pharmacokinetics*, *29*(3), 169–178.

Kalász, H., Magyar, K., Szőke, É., Adeghate, E., Adem, A., Hasan, M.Y., Nurulain, S.M., Tekes, K. (2014). Metabolism of Selegiline [(-)-Deprenyl]. *Current Medicinal Chemistry*, *21*, 1522–1530.

Katagi, M., Tatsuno, M., Tsutsumi, H., Miki, A., Kamata, T., Nishioka, H., Nakajima, K., Nishikawa, M., Tsuchihashi H. (2002). Urinary excretion of selegiline *N*-oxide, a new indicator for selegiline administration in man. *Xenobiotica*, *32*, 823–831.

Katagi, M., Tatsuno, M., Miki, A., Nishikawa, M., Nakajima, K., and Tsuchihashi, H. (2001). Simultaneous determination of selegiline-*N*-oxide, a new indicator for selegiline administration, and other metabolites in urine by high-performance liquid chromatography-electrospray ionization mass spectrometry. *Journal of Chromatography B, 759*(1), 125–33.

Szabó, A., and Hermecz, I. (2001). Novel intramolecular rearrangement of tertiary propargylamine N-oxides. *Journal of Organic Chemistry*, *66*(21), 7219–22.

Wu, R. F., Ichikawa Y. (1995). Inhibition of 1-methyl-4-phenyl-1,2,3,6-tetrahydropyridine metabolic activity of porcine FAD-containing monooxygenase by selective monoamine oxidase-B inhibitors. *FEBS Letters*, *358*, 145–148.

CHAPTER 7. Forced degradation study of rasagiline: identification and characterization of degradation products based on LC-UV and LC-ESI-MS/MS analysis

7.1 INTRODUCTION

Rasagiline mesylate ((1R)-2,3-Dihydro-*N*-2-propynyl-1*H*-inden-1-amine methanesulfonate, **RG**) is a selective and irreversible inhibitor of monoamine oxidase type B (MAO-B) enzyme. Rasagiline has been used for the treatment of idiopathic Parkinson's disease (PD) both as monotherapy and as adjunctive therapy for levopoda in advanced disease. The recommended oral dosage for initial monotherapy is 1 mg once daily. When rasagiline is used as adjunctive therapy with levopoda, the recommended initial dose is 0.5 mg/day and may be increased to 1mg/day if the desired clinical effect is not achieved. In patients with advanced PD and motor fluctuations, the maximum daily dosage could be increased to 5 mg. Rasagiline is well tolerated and is not associated with "cheese effect". The "cheese effect" is the risk of a tyramine pressor response after ingestion of foods rich in tyramine, which normally is metabolized by MAO type A in the gastrointestinal tract (Lin et al., 2013).

Tablets of rasagiline mesylate (Azilect®) are available on the market while transdermal patches are under development; the free base form of rasagiline is a promising candidate for delivery via the transdermal delivery system due to its relatively low-molecular weight, high potency and lipid solubility (Lin et al., 2013)

A literature survey showed that several stability-indicating methods were developed for the determination of rasagiline in tablet dosage forms (Lakshmi et al., 2010; Narendra Kumar et al., 2010; Venkatesh et al., 2012) and in some papers the stability of rasagiline under different stress conditions was evaluated (Kathirvel et al., 2012; Shelke et al., 2014)

The formation of a degradation product in presence of hydrogen peroxide was reported by Balaji et al. (2013), revealing that rasagiline is sensitive to peroxide compared to other conditions, but the characterization of the unknown product was not attempted.

In the publication of Reddy et al. (2012) a forced degradation study was performed identifying the impurities from synthesis, whereas not further information is available on the structure of the unknown product arising from stress tests.

Overall, these data showed that the structure(s) of the degradation product(s) of rasagiline and the corresponding degradation pathways were not elucidated so far.

In this work we investigated the chemical stability of rasagiline in all the stress conditions required by the international guidelines. In oxidative conditions we identified two new degradation products **RG-NOH** and **RG-EA** whose structure and mechanism of formation were discussed.

7.2 EXPERIMENTAL

7.2.1 Reagents and chemicals

Methanol (HPLC grade), ammonium acetate, concentrated acetic acid, sodium hydroxide (pellets), concentrated hydrochloric acid (37%), iron (III) trichloride hexahydrate, copper sulphate pentahydrate, 30% *w/w* hydrogen peroxide solution, 4,4′-azobis-(4-cyanovaleric acid) (**ACVA**), acrylonitrile, *m*-chloroperbenzoic acid (*m*-CPBA), sodium hydrogen carbonate, sodium phosphate dibasic, concentrated phosphoric acid, anhydrous sodium sulphate, dichloromethane and ninhydrin were purchased from Sigma-Aldrich (Milano; Italy). Propiolaldehyde diethyl acetal (97%) was purchased from Alfa Aesar. Water (HPLC grade) was obtained from Milli-Q reverse osmosis system. Column chromatography was performed on silica gel 60 (230-400 mesh ASTM Merck). TLC was carried out on plates with a layer thickness of 0.25 mm (silica gel 60 F254; Merck); when necessary, they were visualized after spraying with ninhydrin reagent.

Rasagiline mesylate (potency ≥ 99%), was purchased from Biovision Inc. (California, USA)

7.2.2 Instrumentation and chromatographic conditions

7.2.2.1 LC-UV analyses

A Shimadzu HPLC system, consisting in two LC-10AD *Vp* module pumps and a DGU-14-A on-line vacuum degasser, was used. The analyses were carried out on a Luna C18(2) (150 x 4.6 mm I.D., 5μm d_p; Phenomenex, Torrance, CA, USA) column as a stationary phase, protected by a Security Guard C18. The isocratic mobile phase (flow rate 1.0 ml/min) was composed of eluant A ammonium acetate buffer (20 mM pH=5.0) and eluant B methanol, being the A:B ratio 42:58 (*v/v*). The eluants A and B were filtered through a 0.45 μm PVDF *membrane* filter prior the use. A SIL-10AD *Vp* autosampler was used for the injection of

samples (20µL). The SPD-M10A *Vp* photodiode array detector was used to detect **RG** and the degradation product (**RG-NOH)** at 210 nm whereas the degradation product **RG-EA** was monitored at 285 nm. A LC solution 1.24 software was used to process the chromatograms. All the analysis were carried out at room temperature.

7.2.2.2 LC-MS/MS analyses

A Thermo Finningan LCQ Deca XP Plus system equipped with a quaternary pump, a Surveyor AS autosampler, a Surveyor PDA detector and a vacuum degasser was used for LC-MS analysis (Thermo Electron Corporation, Waltham, MA, USA). The analysis were performed on a Luna C18(2) (100 x 4.6 mm I.D., 5µm d_p; Phenomenex, Torrance, CA, USA) column as a stationary phase maintained at 35°C and protected by a Security Guard C18. The sample injection volume was 3 µL. The mobile phase was composed of eluant A: ammonium acetate buffer (pH 4.7; 10 mM) and eluant B: acetonitrile, using a gradient elution, the ratio A:B was set 95:5. The following gradient, at a constant flow rate of 0.2 ml/min, was used: from 0 to 7 min, the composition was increased from 5.0 to 17.0% B. From 7 to 16 min the percentage of eluant B was increased again to 80.0% and then maintained 2 min. From 18 to 18.50 min the percentage of eluant B was decreased to 5.0% and then maintained 4 min for column equilibration. When appropriate, the eluate was injected into the Surveyor PDA detector and the LC-UV chromatograms were acquired and processed using the Xcalibur® software (Thermo Electron Corporation, Waltham, MA, USA).

The eluate was injected into the electrospray ion source (ESI) and the MS and MS/MS spectra were acquired and processed using the Xcalibur® software (Thermo Electron Corporation, Waltham, MA, USA).

The operating conditions of the ion trap mass spectrometer in positive ion mode were as follows: spray voltage, 5.0 kV; source current, 80.0 µA; capillary temperature, 275.0 °C; capillary voltage, 4.0 V; tube lens offset, -40.0 V; multipole 1 offset, -2.0 V; multipole 2 offset, -7.0 V; sheath gas flow (N_2), 60.0 Auxiliary Units; sweep gas flow (N_2): 6.0 Auxiliary Units. Data were acquired both full scan and MS/MS product ion scan modes using mass scan range *m/z* 50 to 200 and *m/z* 80 to 600, optimizing the collision energy at 18-30%.

7.2.2.3 Spectroscopic analyses

^{1}H and ^{13}C experiments were performed at 298K on a JEOL Eclipse ECP 300 FT MHz spectrometer (Jeol Ltd. Tokyo, Japan) operating at 7.05T. Chemical shifts are reported in part per million (ppm).

7.2.3 Forced degradation conditions

Degradation studies in solution were done at a **RG** concentration of 1 mg/mL. For the acidic degradation study, **RG** was dissolved in 0.5 N HCl and the solution was left protected from light at 50°C for 48 h.

The degradation in alkaline conditions was done in 1 N NaOH in presence of methanol/water 50/50 and the solution was left protected from light at 50°C for 48h.

The oxidative degradation pathway was studied using four different protocols:

a) The degradation was done in a 3% H_2O_2 solution (pH=5.0 acetate buffer); the mixture was left in the dark at room temperature for 24h.
b) The degradation was prepared in a 3% H_2O_2 solution (50/50 methanol/water) in presence of sodium hydrogen carbonate and it was left in the dark at room temperature for 6h.
c) To evaluate the influence of transition metals, **RG** solution was treated with 1.5 mM Cu^{2+} or Fe^{3+} at ambient temperature for 4 h.
d) To a solution of **RG** in 50/50 methanol/water, the radical initiator **ACVA**, previously dissolved in water (1 mg/mL) was added in presence of sodium hydrogen carbonate. The mixture of reaction (**ACVA**: 1 mM final concentration) was stored at 60° for 24h.

For thermal degradation, a sample of **RG** was placed in a hot air oven maintained at 60°C for 18 h. Photodegradation studies were carried out, at room temperature, by exposing a thin layer (10 mg) of **RG** to daylight and UV-light (365 nm) for 15 days and 4 hours respectively.

For both the thermal and photodegradation tests, **RG** was assayed as powder.

7.2.4 Sample preparation

Before LC-UV and LC-MS/MS analyses, acidic and alkaline samples were first neutralized by addition of a suitable amount of sodium phosphate dibasic and diluted phosphoric acid (8.5% *w/v*) respectively, and then diluted with mobile phase. The other stressed samples were dissolved or tenfold diluted in mobile phase only; finally, solid samples were dissolved in

mobile phase to attain ~0.1 mg/ml concentration. For comparison purposes a freshly prepared aqueous solution of **RG** (~1 mg/ml) was diluted and analyzed as above

7.2.5 Synthesis of degradation product

*7.2.5.1 Rasagiline free base (**RG** free base)*

1.0 g of racemic 1-aminoindan (7.50 mmol) and 1.04 g of K_2CO_3 (7.52 mmol) were added to 7.5 mL of acetonitrile. The resulting suspension was heated to 60°C and 450 mg of propargyl chloride (6.04 mmol) were added dropwise. The mixture was stirred at 60°C overnight, after which most of the volatiles were removed under vacuum. The residue was partitioned between 2.5N aqueous sodium hydroxide and dichloromethane. The pooled organic layers were dried over anhydrous sodium sulphate, filtered and evaporated in vacuo to dryness. The pale-yellow oily residue was purified by column chromatography eluting with ethyl acetate/ petroleum ether 20/80 to give pure **RG** *free base* (730 mg, 57% yield; 99% purity by HPLC assay).

***ESI-MS*:** calculated for $C_{12}H_{13}N$ *M* = 171.24; Found *m/z* = 172 $[M+H]^+$

*7.2.5.2 Rasagiline hydroxylamine (**RG-NOH**) [2,3-Dihydro-N- hydroxy-N-2-propynyl-1H-inden-1-amine]*

Acrylonitrile (500 mg, 9.41 mmol) was added under stirring to a solution of **RG** *free base* (300 mg, 1.75 mmol) in methanol (5 mL). The reaction mixture was stirred at room temperature for 1 month and the methanol was added during this period to compensate for evaporation. The reaction was constantly monitored by TLC and, at the end, the methanol was evaporated under reduced pressure. The resultant yellow oil was purified by flash chromatography on silica gel eluting with dichloromethane, yielding 0.35 g (90%) of *N*-cyanoethyl intermediate as a thick liquid.

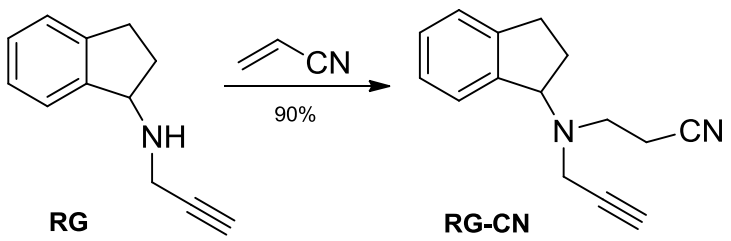

ESI-MS: calculated for $C_{15}H_{16}N_2$ *M*= 224.30; Found *m/z* = 225 $[M+H]^+$

^{1}H-NMR *(300 MHz, $CDCl_3$) δ (ppm): 7.43 (m; 1H), 7.25-7.21 (m, 3H), 4.54 (t, J= 7,3; 1H), 3.49 (m; 2H), 2.93-2.79 (m; 4H), 2.52 (t, J= 7,0; 2H), 2.25-2.21 (m; 2H), 2.20-2.05 (m; 1H)*

A stirred solution of *N*-cyanoethylrasagiline (0.300g, 1.34 mmol) in dry CH_2Cl_2 (10 mL) was cooled to –78°C and *m*-CPBA (77%, 0.110 g, 0.49 mmol) was added.

The reaction mixture was stirred under nitrogen atmosphere at –78°C for 3 hours, and then washed with ice-cold aqueous 10% K_2CO_3 solution (3 x 10 mL), water (3 x 10 mL), saturated NaCl solution (3 x 10 mL), and dried over anhydrous sodium sulfate. Evaporation of the solvent gave the crude product, which was purified by silica gel flash column chromatography eluting with ethyl acetate/petroleum ether 20/80 affording 0.185g (74% yield) of rasagiline hydroxylamine as a thick liquid.

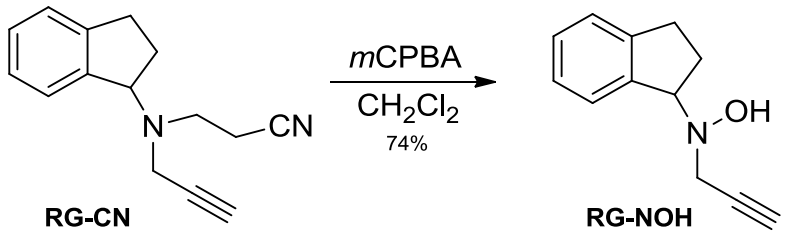

ESI-MS: calculated for $C_{12}H_{13}NO$ *M*= 187.24; Found *m/z* = 188 $[M+H]^+$

^{1}H-NMR *(300 MHz, $CDCl_3$) δ (ppm): 7.49 (d, J=6.9; 1H), 7.25-7.16 (m, 3H) 6.56 (broad 1H), 4.51(dd, J=7.1; J=3.3; 1H), 3.56 (m; 2H), 3.08-3.03 (m; 1H), 2.83-2.80 (m; 1H), 2.33-2.04 (m; 3H).*

*7.2.5.3 3-[2,3-dihydro-1H-inden-1-yl(prop-2-yn-1-yl)amino]prop-2-enal (**RG-EA**)*

To a solution of propiolaldehyde, arising from propiolaldehyde diethyl acetal (230 mg, 1.8 mmol) hydrolysis (0.2N HCl solution, 5 mL) at 40 °C for 0.5 h, **RG** *free base* (307 mg, 1.8 mmol) dissolved in EtOH (5 mL) was added dropwise.

After being stirred for 2 h at 50 °C, the reaction mixture was diluted with H_2O (20 mL), and EtOH was distilled off. The pH of the aqueous phase was adjusted to 12 with 1N NaOH solution, and the reaction mixture was extracted with Et_2O (15 mL). The pooled organic layers (phases) were washed with H_2O. The evaporation of the solvent gave a yellow powder that was purified by column chromatography (ethyl acetate/ petroleum ether 20/80) to afford **RG-EA** (121 mg, 30%).

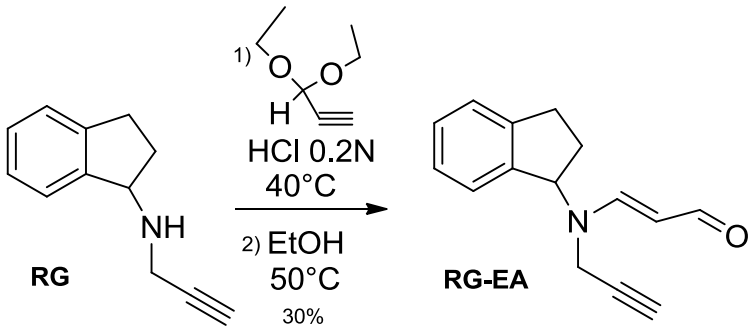

ESI-MS: calculated for $C_{15}H_{15}NO$ *M*= 225.29; Found *m/z* = 226 $[M+H]^+$

^{1}H-NMR *(300 MHz, $CDCl_3$) δ (ppm): 9.12 (d, J=7.9; 1H), 7.28-7.19 (m, 5H) 5.44 (dd, J=8.2; J=13.1; 1H), 5.06 (s, 1H), 3.79-3.77 (m; 2H), 3.03-2.87 (m; 2H), 2.54-2.51 (m; 1H), 2.28-2.15 (m; 2H).*

7.3 RESULTS AND DISCUSSION

7.3.1 Forced degradation study and structural characterization of degradation products

Forced degradation studies of **RG** were previously reported in literature, however the identification of the related degradation products formed under a variety of stress conditions was not achieved. In the present work all the stress conditions required by ICH guidelines were included in order to identify the degradation products arising from stress testing and to establish the corresponding degradation pathways. Moreover in order to avoid unrealistic degradation pathways, the conditions were adjusted to obtain a 10–25% degradation of the parent compound.

The structure characterization of degradation products was achieved by in LC-UV and LC–ESI-MS/MS analysis and by means of synthesis of authentic standards. The degradation conditions employed in this study are summarized in the Table 1.

Stressor	Temperature (°C)	Time of the analysis
HCl 0.5N	50	48 h
NaOH 1N	50	48 h
3% H_2O_2 pH=5	RT	6, 24 h
3% H_2O_2 pH≈8	RT	6, 24 h
Transition metals	RT	4, 24 h
Radical initiator	60	4, 24 h
UV light	RT	4 h
Sunlight	RT	15 days
Thermal	60	18 h

Table 1. Stress conditions applied in the forced degradation study of rasagiline mesylate

7.3.1.1 Degradation in acidic and basic conditions

Rasagiline was found to be stable in acidic and alkaline conditions. In presence of 1N NaOH and 5N HCl at 50°C for 48 h no degradation occurred as showed in Figure 1a and 1b. The chromatographic peak at retention time 2.9 min is attributable to rasagiline; no other peak corresponding to the formation of degradation products was observed.

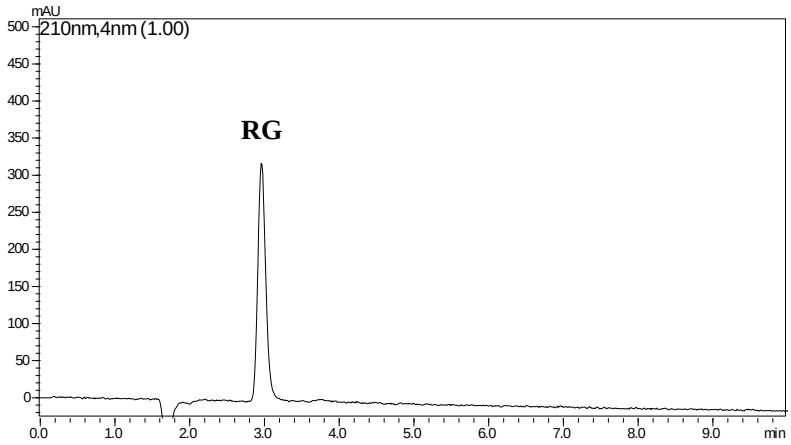

Figure 1a. LC-UV chromatogram (λ_a=210 nm) of **RG** in 0.5N HCl solution (t= 48h at 50°C).

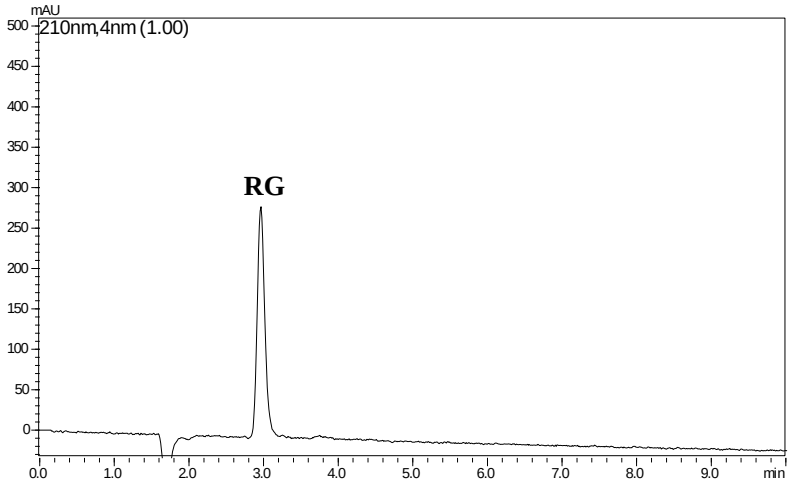

Figure 1b. LC-UV chromatogram (λ_a=210 nm) of **RG** in 1N NaOH solution (t= 48h at 50°C)

7.3.1.2 Photodegradation and thermal degradation

For photodegradation studies, **RG** was exposed to daylight and 365 nm UV-light for two weeks and 4h respectively, in these conditions no degradation occurred (data not shown). Similarly, the thermal stress test of **RG** was conducted without observing the formation of degradation product.

7.3.1.3 Degradation in oxidative conditions

The degradation in oxidative conditions was studied using three different protocols, in presence of hydrogen peroxide reagent, radical chain initiators and with transition metal ions (Fe^{3+} and Cu^{2+}). Rasagiline is characterized by the presence of a secondary amine susceptible to oxidation to its corresponding hydroxylamine; in particular, since rasagiline is more prone to oxidation in its *free base* form, the oxidative degradation was investigated both in acidic and alkaline pH.

LC-UV chromatograms reported in Figures 2-4 clearly showed the pH effect on the *N*-oxidation of the secondary amine. At acidic pH no degradation occurred (Fig. 2); the peak at t_R=2.94 min is attributable to rasagiline and the peak at t_R=1.73 min is due to the hydrogen peroxide reagent as highlighted in the LC-UV chromatogram of the control degradation (Fig 3). Conversely, in hydrogen peroxide at alkaline pH, the presence of a degradation product (**RG-NOH**) was observed at t_R=7.48 min, having an absorption maximum at 210 nm (Figure 4).

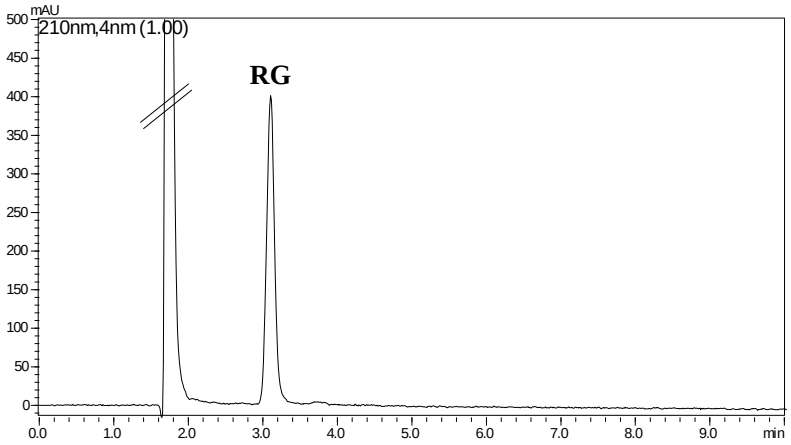

Figure 2. LC-UV chromatogram of **RG** degradation in hydrogen peroxide (pH=5, t=6 h).

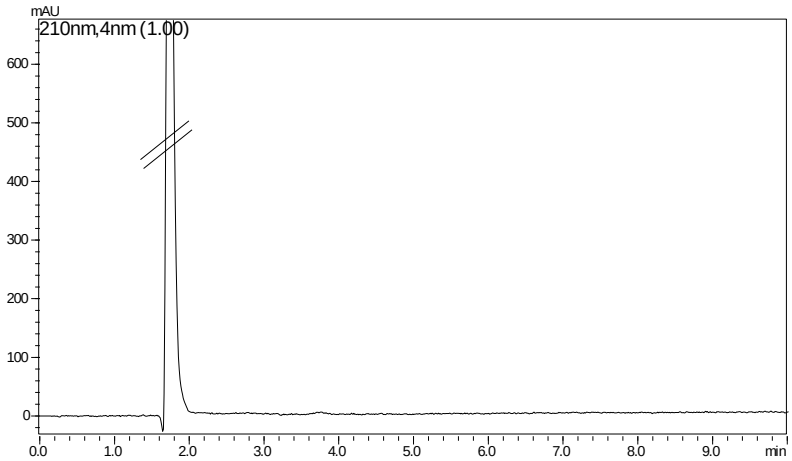

Figure 3. LC-UV chromatogram of control degradation in hydrogen peroxide (pH=5, t=6 h).

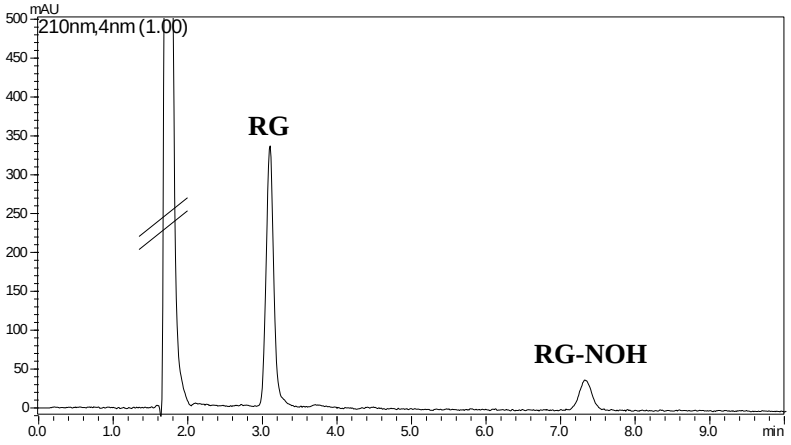

Figure 4. LC-UV chromatogram (λ_a=210 nm) of **RG** in 3% H_2O_2 alkaline solution (t= 6h)

The oxidative degradation of **RG** was evaluated also in the presence of the radical initiator **ACVA**; in this condition the formation of the peak of **RG-NOH** was not detected (Fig. 5) whereas the presence of a degradation product at t_R=5.40 min, having an absorption maximum at 285 nm was pointed out (Figure 6).

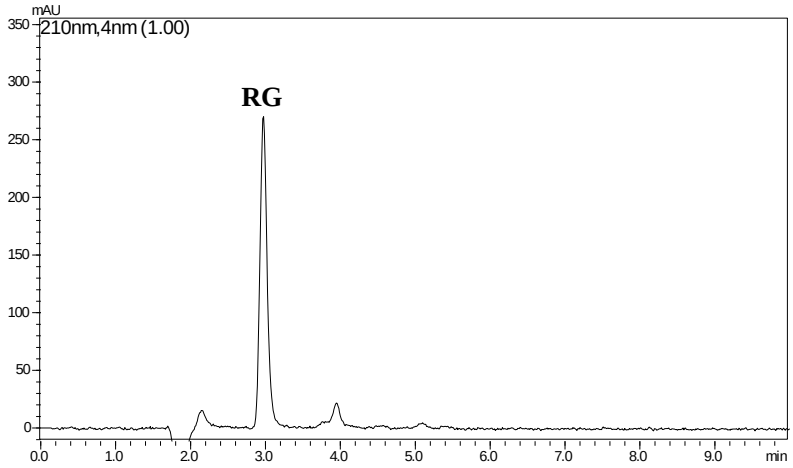

Figure 5. LC-UV chromatogram (λ_a=210 nm) of **RG** in the presence of radical initiator (t= 24h)

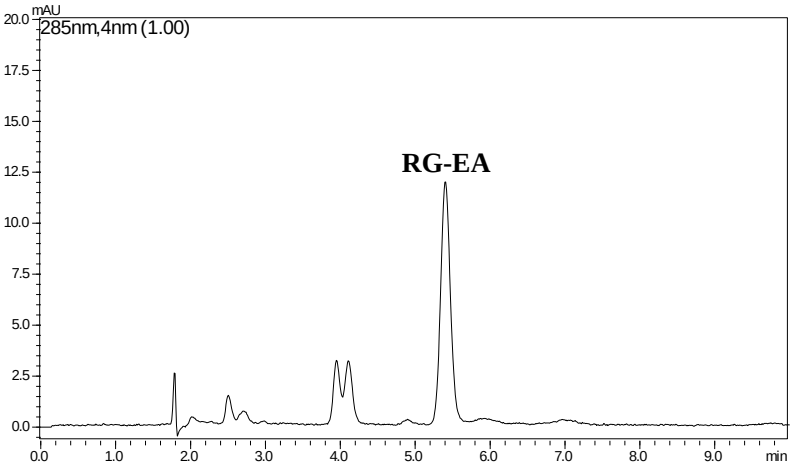

Figure 6. LC-UV chromatogram (λ_a=285 nm) of **RG** in the presence of radical initiator (t= 24h)

Finally, in presence of the transition metals Fe^{3+} and Cu^{2+}, **RG** did not undergo degradation as showed in the LC-UV chromatograms reported in the Figure 7 and 8.

Once again the lack of oxidative degradation in the presence of transition metal ions could be due to the acidic conditions used in the test.

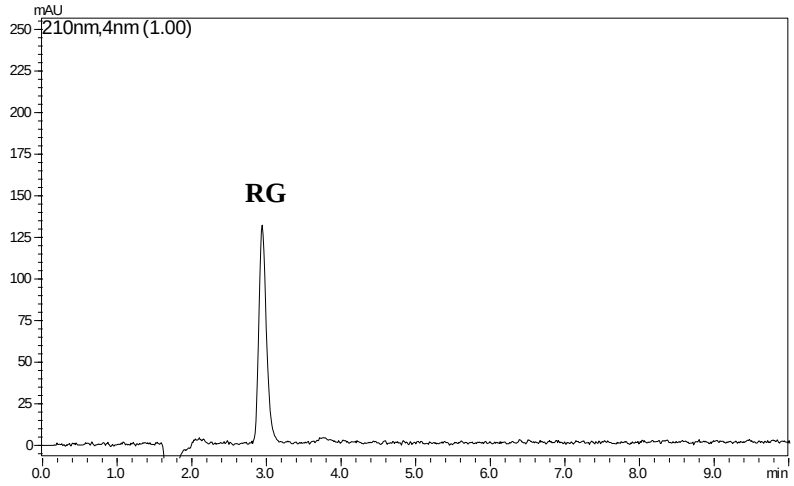

Figure 7. LC-UV chromatogram of **RG** degradation in the presence of Fe^{3+}

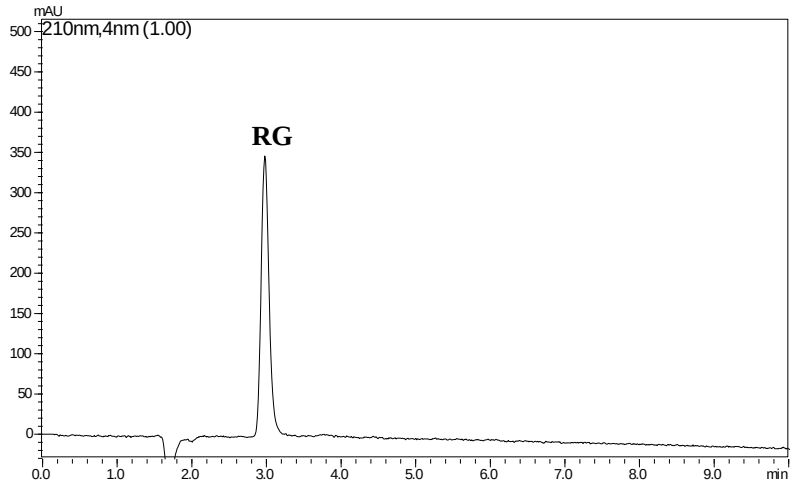

Figure 8. LC-UV chromatogram of **RG** degradation in the presence of Cu^{2+}

7.3.2 Structural characterization of rasagiline degradation products by LC-ESI-MS/MS analysis

In order to obtain information on the structures of the degradation products formed in oxidative conditions, the degradation test samples were analyzed by LC-ESI-MS/MS.

The LC-ESI-MS/MS analysis of the H_2O_2/$NaHCO_3$ sample, showed the formation of the degradation product **RG-NOH** at *m/z* 188 (Figure 9), corresponding to the insertion of an oxygen atom in the structure of rasagiline *free base*. The MS^2 spectrum of **RG-NOH** (Fig. 9) showed the presence of two fragment ions at *m/z* 117 and *m/z* 72: unfortunately, they are not sufficiently diagnostic for the attribution of the structure of **RG-NOH**.

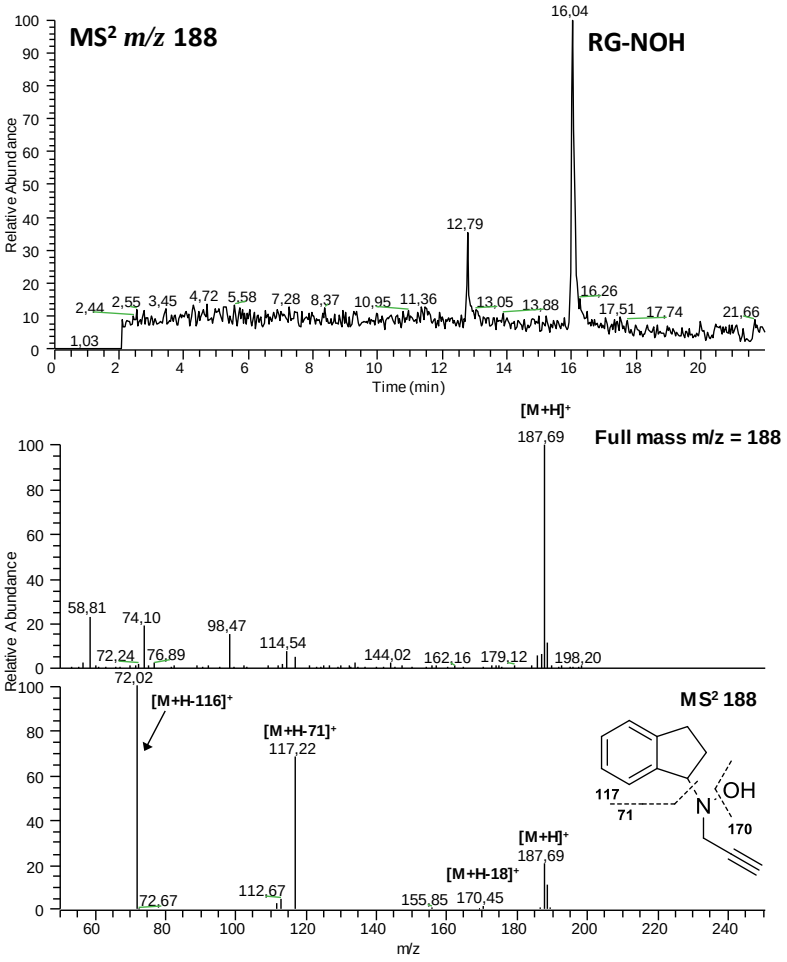

Figura 9. LC-MS chromatogram of **RG** in 3% H_2O_2 alkaline solution (t= 6h) monitoring the ion at *m/z* 188 and LC-MS^2 fragmentation pattern of **RG-NOH**

The presence in the **RG** structure of a secondary amine function, susceptible to oxidation, suggested the formation of the rasagiline hydroxylamine, whose synthesis starting from rasagiline, was performed following the procedure reported by Hanson et al. (2010); the procedure involved the *N*-alkylation of the secondary amine with acrylonitrile, followed by *N*-oxidation with *m*-CPBA and Cope elimination of the protecting group.

The LC-ESI-MS/MS analysis of the standard obtained by synthesis showed the presence of a pseudomolecular ion at 188 *m/z* which has the same retention time and MS^2 spectrum of the degradation product **RG-NOH** observed in the presence of hydrogen peroxide (Figura 10, 11).

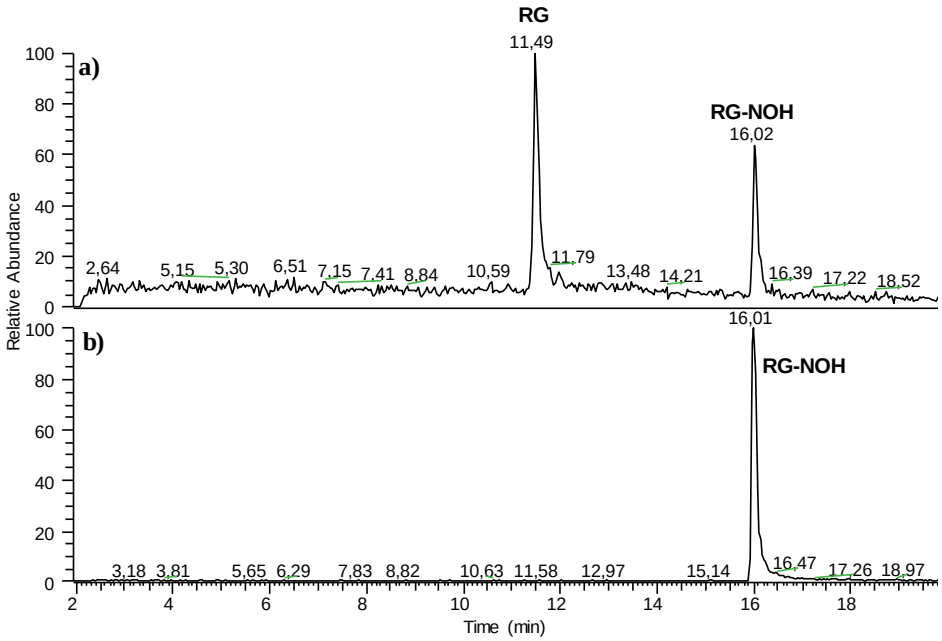

Figura 10. LC-MS chromatogram of **RG** in 3% H_2O_2 alkaline solution (t= 6h) monitoring the ion at *m/z* 172 and *m/z* 188 **(a)**; LC-MS chromatogram of **RG-NOH** synthetic standard monitoring the ion at *m/z* 172 and *m/z* 188 **(b)**

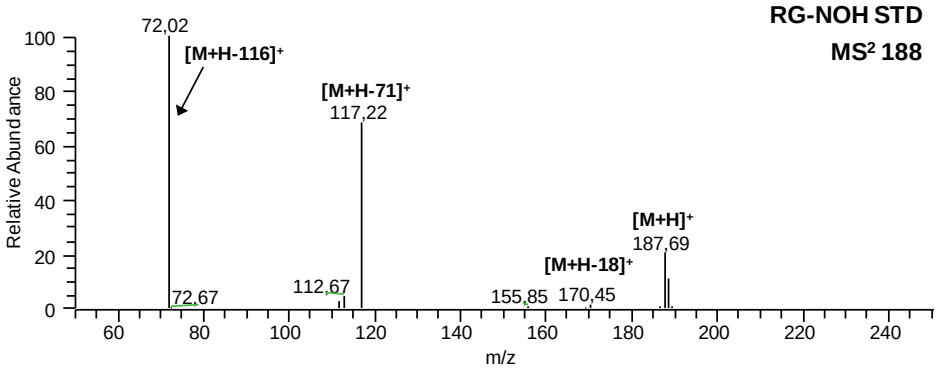

Figura 11. MS^2 spectrum of **RG-NOH** synthetic standard

In general, secondary hydroxylamines are not usually very stable and hence difficult to isolate. On the contrary what one might expect this compound was stable and was isolated and completely characterized.

The chemical stability of **RG** was also evaluated in presence of the radical initiator **ACVA**. As shown in LC-UV analysis (Fig. 6), the presence of a degradation product having a higher retention time than **RG** (2.9 vs 5.4) and an absorption maximum at 285 nm was observed.
To obtain further information regarding the structure of the degradation product a LC-MS analysis was performed showing the presence of a peak at t_R= 16.11 min (Fig. 12), having a protonated molecule at *m/z* 226 (+54 Da more than RG). The LC-MS/MS spectrum of peak at *m/z* 226 showed a main fragment ion at *m/z* 109 (loss of indane scaffold) as reported in the figure 13. The product obtained showed the same mass spectral data and chromatographic characteristics of the metabolite **RG-EA** observed during the *in vitro* metabolism study of rasagiline (Chapter 8). The formation of **RG-EA** in presence of radical initiator could be explained exploiting the property of rasagiline to form radical species through the activation of propargylamine moiety rather than the addiction of propiolaldehyde to the structure of **RG**; however, this hypothesis was not confirmed and further investigation is required to assess the mechanism of formation of this degradation product.

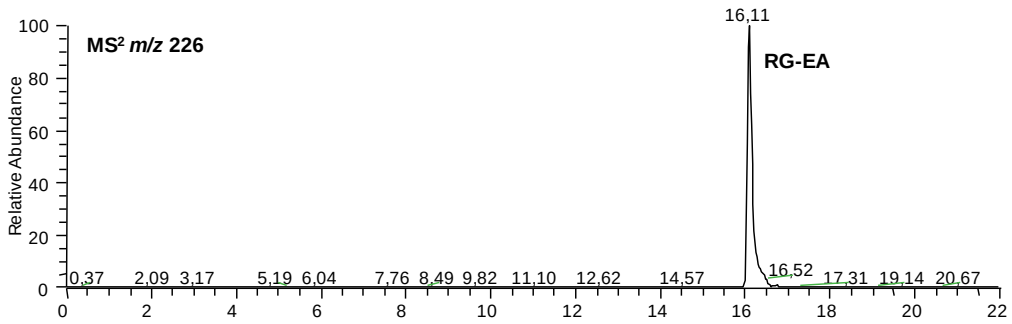

Figura 12. LC-MS^2 chromatogram of **RG** presence of radical initiator

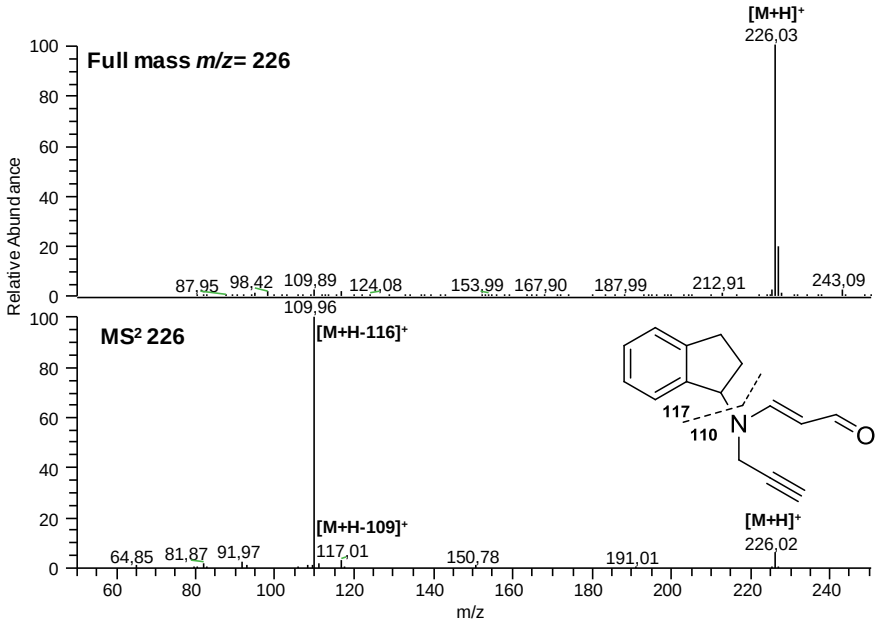

Figura 13. LC-MS^2 fragmentation pattern of **RG-EA**

7.4 CONCLUSION

In the present work the intrinsic chemical stability of rasagiline was investigated by a forced degradation study using LC-UV and LC-MS/MS analysis. In oxidative conditions the formation of two different degradation products **RG-NOH** and **RG-EA** was observed and the degradation scheme for rasagiline was proposed in the figure 14.

As expected, the oxidative degradation is dependent on the pH and **RG** *free base* results more prone to oxidation; this should be taken into account in the course of stability study of the drug products (e.g. transdermal system) containing **RG** *free base* as a drug substance. The identification and the synthesis of two degradation products allowed the development of a stability-indicating HPLC-UV method for the determination of **RG** in the active ingredient and its pharmaceutical formulations.

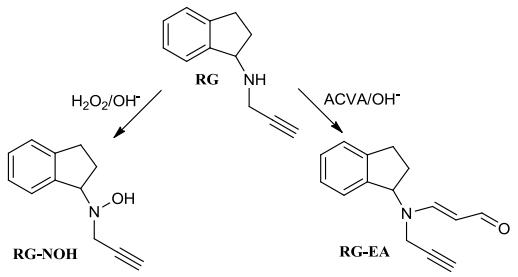

Figure 14. Oxidative degradation pathways of rasagiline

7.5 REFERENCES

Balaji N.; Sivaraman V. R. Neeraja P. (2013). Development and Validation of a Stability-Indicating RP-UPLC Method for the Quantitative Analysis of antiparkinson drug and its related impurities. *IOSR Journal of Applied Chemistry (IOSR-JAC)*, *3*(3), 14–21.

Hanson, K. L., Vandenbrink, B. M., Babu, K. N., Allen, K. E., Nelson, W. L., and Kunze, K. L. (2010). Sequential Metabolism of Secondary Alkyl Amines to Metabolic-Intermediate Complexes : Opposing Roles for the Secondary Hydroxylamine and Primary Amine Metabolites of Desipramine, (S)-Fluoxetine, and N- Desmethyldiltiazem. *Drug Metabolism and Disposition*, *38*, 963–972.

ICH Harmonized Tripartite Guidelines Q1A(R2) (2003). Stability Testing of New Drug Substances and Products.

Kathirvel, S., Satyanarayana, S. V., Devalarao, G. (2012). Development and Validation of a Stability-Indicating HPTLC Method for Analysis of Rasagiline Mesylate in the Bulk Drug and Tablet Dosage Form. *Chromatography Research International*, *2012*, 1–6.

Lakshmi, M. V., Seshagiri Rao, J.V.L.N., Lakshmana Rao, A. (2010). Development and validation of RP-HPLC method for the simultaneous estimation of rasagiline tablet dosage forms. *Rasayan J. Chem.*, *4*, 621–624.

Lin, Y., Zou Y., Lin, J., Zhang, T., Deng, J. (2013). Comparative single-dose pharmacokinetics of rasagiline in minipigs after oral dosing or transdermal administration via a newly developed patch. *Xenobiotica*, *43*(8), 705–710.

Narendra Kumar, Nageswara Rao G., Naidu P. Y. (2010). Stability indicating RP-LC method for determination of rasagiline mesylate in bulk and pharmaceutical dosage forms. *International Journal of Applied Biology and Pharmaceutical Technology*, (2), 247–259.

Reddy S.P., Sudhakar, B. K. and Kumar N. (2012). Development and Validation of a Stability-Indicating RP-HPLC Method for the Simultaneous Estimation of Process Related Impurities and Degradation Products of Rasagiline Mesylate in Pharmaceutical Formulation P. *Journal of Chromatographic Science*, 1–8.

Shelke, P.G., Chandewar, A.V. (2014). Study of stress degradation behavior of rasagiline mesylate under hydrolytic conditions by high performance liquid chromatography. *Drug Research*, *64*(4), 182–185.

Venkatesh, D., Pavani, V., Vasanth P.M., Ramesh, M. (2012). A stability indicating analytical method for the estimation of rasagiline in solid dosage forms by RP- HPLC. *International Journal of Biological & Pharmaceutical Research*, *3*(6), 822–825.

CHAPTER 8. *In vitro* metabolism study of Rasagiline

8.1 INTRODUCTION

L-Monoamino oxidases (MAO) (EC 1.4.3.4) are a family of a flavin-containing enzymes responsible for the oxidative deamination of a wide range of biogenic amines (e.g., dopamine and noradrenaline) and which is widely distributed in most tissue of mammals (Gong et al., 2006). Moreover, MAO are membrane-bound enzymes mainly located in mithocondria and two isoforms owing different selectivities for substrates and inhibitors, known as monoamine oxidase type A (MAO-A) and type B (MAO-B), have been characterized so far. In particular, MAO-B is involved in the neurodegenerative events leading to Parkinson's disease and the inhibition of this enzyme system has been proposed to have a protective effect against the degeneration of dopaminergic neurons. Propargylamines are a class of amine compounds that potently and selectively inhibit MAO-A (e.g chlorgiline) or MAO-B (e.g. pargiline, selegiline and rasagiline), through an irreversible site-directed inhibition, forming a covalent bond with the N5 nitrogen of flavin, a component of the enzyme active site.

Accordingly, rasagiline mesylate (*N*-propargyl-1(*R*)-aminoindan mesilate, **RG**), a selective and irreversible MAO-B inhibitor, has been developed for the treatment of idiopathic PD that is characterized by a deficiency of dopamine in nigrostriatal nerve terminals (Tabakman et al., 2004). Rasagiline has been used both as monotherapy and as adjunctive therapy for levodopa in advanced disease. The recommended initial dose is 0.5 mg administered once daily. If a sufficient clinical response is not achieved, the dose may be increased to 1 mg administered once daily (Azilect® package insert). Upon oral administration, **RG** is rapidly absorbed and widely distributed into body tissues and cross the blood-brain-barrier. Maximum plasma concentration of rasagiline is reached approximately at 5h after an oral dose of 2 mg, and the elimination half-life is about 0.6-2h. The absolute bioavailability is ~36%, indicating that rasagiline undergoes a significant first-pass metabolism, but inversely to what occurs with selegiline no amphetamine metabolites are formed. Indeed, selegiline, whose structure is based on a methamphetamine scaffold, is extensively metabolized to neurotoxic L-methamphetamine and L-amphetamine.

On the contrary, 1-(*R*)-aminoindan (**AI**) is the major metabolite of rasagiline. In literature, the data regarding the pharmacological activity of 1-(*R*)-aminoindan (**AI**), are conflicting. Some

authors suggested that **AI** is not pharmacologically active (Chen et al., 2007), whereas the neuroprotective properties of **AI** were proposed by others (Bar-Am et al., 2010).

More in general, the metabolic fate of rasagiline has been previously highlighted in the literature by several authors. Lecht et al. (2007) stated that the main metabolic pathway is via *N*-dealkylation to form **AI** and by hydroxylation to form 3-hydroxy-*N*-propargyl-1-aminoindan (**3OH-RG**). Other authors (Youdim et al., 2001; Finberg, 2010; Chen et al., 2005) claimed that **AI** was the main metabolite without mentioning the hydroxylation pathway. Interestingly, all these statements were entirely or partially based on data found in the Azilect® package insert in which is reported that the metabolism of rasagiline proceeds through two main pathways: *N*-dealkylation and/or hydroxylation to yield: **AI**, **3OH-RG** and 3-hydroxy-1-aminoindan (**3OH-AI**); moreover the glucuronidation of rasagiline and its metabolites, with subsequent urinary excretion, was also reported.
As expected, these data were also found in the Azilect® product information available from EMA (EMA, Azilect, Product Information, 2009); however, in the corresponding scientific discussion, (EMA, Azilect, Scientific Discussion 2005) while the formation of **AI** and **3OH-RG** was reported, the formation of metabolite **3OH-AI** did not. Moreover, it was also stated that the sulphation or glucuronidation acid occurred during the metabolism of rasagiline.
Overall these data appear to agree with the formation of **AI** as the primary metabolite but at the same time they do not on the formation of other metabolites. For example, although the presence of the metabolite **3OH-AI** is mentioned in the monograph of Azilect® no further references are available (could be found) supporting its formation.
Finally, to the best of our knowledge no experimental data were reported in literature about *in vitro/in vivo* metabolism of rasagiline. Taken together these considerations prompted us to investigate the *in vitro* metabolism of **RG** in the presence of both rat and human microsomes. Beside the well-known **AI** and **3OH-RG**, new metabolites arising from oxidative metabolism were identified by means of LC-MS and LC-UV analyses and synthesis, while their biological activities will be studied.

8.2 EXPERIMENTAL

8.2.1 Reagents and chemicals

Methanol (HPLC grade), acetonitrile (HPLC grade), ammonium acetate, concentrated acetic acid, sodium hydrogen carbonate, semicarbazide hydrochloride, polyoxyethylene 20 cetyl ether (Brij 58), acrylonitrile, *m*-chloroperbenzoic acid (*m*-CPBA) were purchased from Sigma-Aldrich (Milano; Italy). Propiolaldehyde diethyl acetal (97%) was purchased from Alfa Aesar. Water (HPLC grade) was obtained from Milli-Q reverse osmosis system (Millipore Co., Billerica MA, USA). (±)-Aminoindan (99%), propiolaldehyde diethyl acetal (97%) were purchased from Alfa Aesar. Column chromatography was performed on silica gel 60 (230-400 mesh ASTM Merck). TLC was carried out on plates with a layer thickness of 0.25 mm (silica gel 60 F254; Merck); when necessary, they were visualized after spraying with ninhydrin reagent. **RG** (potency ≥ 99%) was purchased from Biovision Inc.(California, USA). The following compounds were synthetized according to literature procedures: **3OH-AI** and **3OH-RG** (Luan et al., 2013); **7OH-AI** and **7OH-RG** (Sterling et al., 2002).; **4OH-AI**, **4OH-RG**, **6OH-AI** and **6OH-RG** (Herzig et al., 2005).

8.2.2 Instrumentation and chromatographic conditions

8.2.2.1 LC-UV analyses

A Shimadzu HPLC system, consisting in two LC-10AD *Vp* module pumps and a DGU-14-A on-line vacuum degasser, was used. The analyses were carried out on a Luna C18(2) (150 x 4.6 mm I.D., 5µm d_p; Phenomenex, Torrance, CA, USA) column as a stationary phase, protected by a Security Guard C18. The mobile phase (flow rate 1.2 ml/min) was composed of eluant A, ammonium acetate buffer (20 mM pH=5), and eluant B, methanol, while the initial ratio A:B was set at 60:40. The elution was done using the following gradient: from 0 to 12 min, the composition was increased from 40.0 to 90.0% B and then maintained 5 min. From 18 min, the percentage of eluant B was decreased to 40.0% and then maintained for column equilibration. The eluants A and B were filtered through a 0.45 µm PVDF membrane filter prior the use. A SIL-10AD *Vp* autosampler was used for the injection of samples (20µL). The SPD-M10A *Vp* photodiode array detector was used to detect **RG** and the metabolite (**RG-NOH)** at 210 nm whereas the metabolites **RG-EA** and **AI-EA** were monitored at 285 nm. A LC solution 1.24 software was used to process the chromatograms. All the analysis were carried out at room temperature.

8.2.2.2 LC-MS/MS analyses

A Thermo Finningan LCQ Deca XP Plus system equipped with a quaternary pump, a Surveyor AS autosampler, a Surveyor PDA detector and a vacuum degasser was used for LC-MS analysis (Thermo Electron Corporation, Waltham, MA, USA). The analysis were performed on a Luna C18(2) (100 x 4.6 mm I.D., 5μm d_p; Phenomenex, Torrance, CA, USA) column as a stationary phase maintained at 35°C and protected by a Security Guard C18. The sample injection volume was 3 μL. The mobile phase was composed of eluant A: ammonium acetate buffer (pH 4.7; 10 mM) and eluant B: acetonitrile, using a gradient elution, the ratio A:B was set 95:5. The following gradient, at a constant flow rate of 0.2 mL/min, was used: from 0 to 7 min, the composition was increased from 5.0 to 17.0% B. From 7 to 16 min the percentage of eluant B was increased again to 80.0% and then maintained 2 min. From 18 to 18.50 min the percentage of eluant B was decreased to 5.0% and then maintained 4 min for column equilibration. When appropriate, the eluate was injected into the Surveyor PDA detector and the LC-UV chromatograms were acquired and processed using the Xcalibur® software (Thermo Electron Corporation, Waltham, MA, USA).

The eluate was injected into the electrospray ion source (ESI) and the MS and MS/MS spectra were acquired and processed using the Xcalibur® software (Thermo Electron Corporation, Waltham, MA, USA).

The operating conditions of the ion trap mass spectrometer were as follows: *positive modes* spray voltage, 5.0 kV; source current, 80.0 μA; capillary temperature, 275.0 °C; capillary voltage, 4.0 V; tube lens offset, -40.0 V; multipole 1 offset, -2.0 V; multipole 2 offset, -7.0 V; sheath gas flow (N_2), 60.0 Auxiliary Units; sweep gas flow (N_2): 6.0 Auxiliary Units. *Negative mode:* spray voltage, 3.4 kV; source current, 80.0 μA; capillary temperature, 275.0 °C; capillary voltage, -15.0 V; tube lens offset, -30.0 V; multipole 1 offset, 5.0 V; multipole 2 offset, 7.0 V; sheath gas flow (N_2), 60.0 Auxiliary Units; sweep gas flow (N_2): 6.0 Auxiliary Units. Data were acquired both full scan and MS/MS product ion scan modes using mass scan range *m/z* 50 to 200 and *m/z* 80 to 600, optimizing the collision energy at 18-30%.

8.2.2.3 Spectroscopic analyses

^{1}H and ^{13}C experiments were performed at 298K on a JEOL Eclipse ECP 300 FT MHz spectrometer (Jeol Ltd. Tokyo, Japan) operating at 7.05T. Chemical shifts are reported in part per million (ppm).

8.2.3 Human intestinal and liver microsomes

The cryopreserved Pooled Human Intestinal Microsomes (HIM), (pooled mixed sex, protein concentration: 10 mg/ml, total P450: 0.26 nmol/mg) and Pooled Human Liver Microsomes (HLM), (pooled mixed sex, ten individual donors, protein concentration: 20 mg/ml, total P450: 0.36 nmol/mg) were purchased from BD Gentest™ (Woburn, MA) and used throughout this study.

8.2.4 Rat liver cytosol and microsomes

Male Sprague-Dawley rat liver cytosol (RLC), (protein concentration: 20 mg/ml, sulfotransferase: 0.64 nmol/mg protein) and male Wistar rat liver microsomes (RLM), (protein concentration: 25mg/ml, total P450: 0.64 nmol/mg protein) were purchased from BD Gentest™ (Woburn, MA) and used throughout this study.

The incubations were all carried out using a horizontal DUBNOFF shaking thermostatic bath (Dese Lab Research, Padova, Italy) and were protected from light.

8.2.5 *In vitro* RLM, HLM and HIM incubations of rasagiline

The standard incubation mixture (500-µl final volume), in 1.5-ml Eppendorf tubes, was carried out in a 50-mM TRIS buffer (pH 7.4) containing 3.3-mM $MgCl_2$, 1.3-mM $NADPNa_2$, 3.3-mM glucose 6-phosphate, 0.4-Units/ml glucose 6-phosphate dehydrogenase and 100µM or 500µM **RG**. After pre-equilibration of the mixture, an appropriate volume of microsomal suspension was added to give a final protein concentration of 1 mg/ml. The mixture was shaken for 60 min at 37°C, and the reaction was quenched by diluting the samples with 500 µl of ice-cold acetonitrile. The samples were then centrifuged at 13,000 rpm for 5 min, and the supernatant was directly injected onto the column for analysis. Control incubations without the presence of substrate, NADP(H)-regenerating system, or microsomes were also carried out.

8.2.6 Chemical stability of RG-NOH

The chemical stability of the freshly prepared **RG-NOH** synthetic standard was evaluated at two different temperatures protecting the samples from light. An aliquot of **RG-NOH** (~10 mg) was stored as is at room temperature for 96h. A second aliquot of **RG-NOH** (~10 mg) was dissolved in a 50 mM TRIS·HCl buffer (pH 7.4) to give a concentration of 1 mg/ml, in

presence of acetonitrile (1% of total volume) and left in a shaking thermostatic bath at 37°C for 96h. The LC-UV and LC-MS analyses were carried out at 0, 4, 8, 24, 48, 72, 96h by weighing and dissolving, in 50/50 (*v/v*) methanol/water, an appropriate amount of **RG-NOH** control sample and diluting the sample to attain ≈ 0.1 mg/ml concentration.

8.2.7 Phase I metabolic stability of RG-NOH

The standard incubation mixture (500µl final volume), in 1.5-ml Eppendorf tube, was carried out in a 50 mM TRIS buffer (pH 7.4) containing 3.3-mM $MgCl_2$, 1.3-mM $NADPNa_2$, 3.3-mM glucose 6-phosphate, 0.4-Units/ml glucose 6-phosphate dehydrogenase and 500µM **RG-NOH**. After pre-equilibration of the mixture, an appropriate volume of microsomal suspension (RLM) was added to give a final protein concentration of 1 mg/ml. The incubation, protein precipitation and analysis of supernatants were performed following the same procedure described in the paragraph 8.2.5.

8.2.8 Incubation of rasagiline in the presence of nucleophilic trapping agents

The formation of electrophilic species in **RG** incubations was studied by adding 2-mercaptoethanol or semicarbazide hydrochloride (final concentration: 3mM) to the incubation mixture. The incubations were performed using the same conditions reported in the paragraph 8.2.5. The samples were then centrifuged to remove the insoluble matter and an aliquot (3µl) was analysed by LC-UV and/or LC-ESI-MS.

8.2.9 Phase II incubations

8.2.9.1 RLM glucuronidation

The standard incubation mixture (500-µl final volume), in 1.5-ml Eppendorf tube, was carried out in a 50 mM TRIS·HCl buffer (pH 7.4) containing 5 µL of acetonitrile (1% of total volume), 2.0 mM UDPGA and 500µM **RG-NOH**.

After pre-incubation of the mixture, an appropriate volume of microsomal suspension, previously activated in Brij 58 surfactant (0.5 mg/mg protein) for 15 min at 0°C, was added to give a final protein concentration of 1 mg/ml.

The mixture was shaken for 60 min at 37°C, and the reaction was quenched by diluting the samples with 500 µl of ice-cold acetonitrile. Control incubations were done without the

presence of UDPGA. The samples were then centrifuged at 13,000 rpm for 5 min, and the supernatants were analysed by LC-UV and LC-ESI-MS.

8.2.9.2 Cytosol sulfation

The standard incubation mixture, in Eppendorf tube, was carried out in a 50 mM TRIS·HCl buffer (pH 7.4) containing 5 µL of acetonitrile (1% of total volume), 0.2 mM PAPS and 500µM **RG-NOH**. After pre-equilibration of the mixture, an appropriate volume of cytosol suspension, was added to give a final protein concentration of 2 mg/ml; the mixture was shaken for 60 min at 37°C and the reaction was quenched by diluting the samples with 500 µl of ice-cold acetonitrile. Control incubations were done without the presence of PAPS. The samples were centrifuged and analysed as reported for glucuronidation assay.

8.2.10 Synthesis of reference standards

*8.2.10.1 Rasagiline free base (**RG** free base)*

1.0 g of racemic 1-aminoindan (7.50 mmol) and 1.04 g of K_2CO_3 (7.52 mmol) were added to 7.5 mL of acetonitrile. The resulting suspension was heated to 60°C and 450 mg of propargyl chloride (6.04 mmol) were added dropwise. The mixture was stirred at 60°C overnight, after which most of the volatiles were removed under vacuum. The residue was partitioned between 2.5N aqueous sodium hydroxide and dichloromethane. The pooled organic layers were dried over anhydrous sodium sulphate, filtered and evaporated in vacuo to dryness. The pale-yellow oily residue was purified by column chromatography eluting with ethyl acetate/ petroleum ether 20/80 to give pure **RG** *free base* (730 mg, 57% yield; 99% purity by HPLC assay).

***ESI-MS*:** calculated for $C_{12}H_{13}N$ *M* = 171.24; Found *m/z* = 172 $[M+H]^+$

*8.2.10.2 Rasagiline hydroxylamine (**RG-NOH**) [2,3-Dihydro-N- hydroxy-N-2-propynyl-1H-inden-1-amine]*

Acrylonitrile (500 mg, 9.41 mmol) was added under stirring to a solution of **RG** *free base* (300 mg, 1.75 mmol) in methanol (5 mL). The reaction mixture was stirred at room temperature for 1 month and the methanol was added during this period to compensate for evaporation. The reaction was constantly monitored by TLC and, at the end, the methanol was evaporated under reduced pressure. The resultant yellow oil was purified by flash

chromatography on silica gel eluting with dichloromethane, yielding 0.35 g (90%) of *N*-cyanoethyl intermediate as a thick liquid.

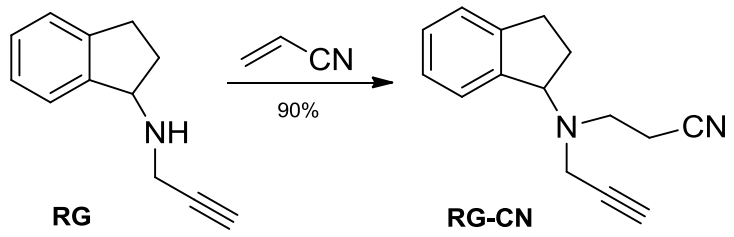

ESI-MS: calculated for $C_{15}H_{16}N_2$ *M*= 224.30; Found *m/z* = 225 $[M+H]^+$

^{1}H-NMR *(300 MHz, $CDCl_3$) δ (ppm): 7.43 (m; 1H), 7.25-7.21 (m, 3H), 4.54 (t, J= 7,3; 1H), 3.49 (m; 2H), 2.93-2.79 (m; 4H), 2.52 (t, J= 7,0; 2H), 2.25-2.21 (m; 2H), 2.20-2.05 (m; 1H)*

A stirred solution of *N*-cyanoethylrasagiline (0.300g, 1.34 mmol) in dry CH_2Cl_2 (10 mL) was cooled to –78°C and *m*-CPBA (77%, 0.110 g, 0.49 mmol) was added.

The reaction mixture was stirred under nitrogen atmosphere at –78°C for 3 hours, and then washed with ice-cold aqueous 10% K_2CO_3 solution (3 x 10 mL), water (3 x 10 mL), saturated NaCl solution (3 x 10 mL), and dried over anhydrous sodium sulfate. Evaporation of the solvent gave the crude product, which was purified by silica gel flash column chromatography eluting with ethyl acetate/petroleum ether 20/80 affording 0.185g (74% yield) of rasagiline hydroxylamine as a thick liquid.

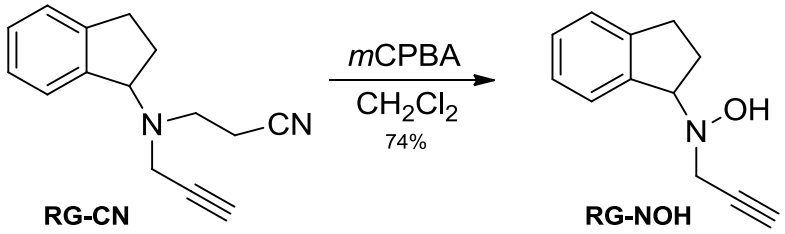

ESI-MS: calculated for $C_{12}H_{13}NO$ *M*= 187.24; Found *m/z* = 188 $[M+H]^+$

^{1}H-NMR *(300 MHz, $CDCl_3$) δ (ppm): 7.49 (d, J=6.9; 1H), 7.25-7.16 (m, 3H) 6.56 (broad 1H), 4.51(dd, J=7.1; J=3.3; 1H), 3.56 (m; 2H), 3.08-3.03 (m; 1H), 2.83-2.80 (m; 1H), 2.33-2.04 (m; 3H).*

*8.2.10.3 3-(2,3-dihydro-1H-inden-1-ylamino)prop-2-enal (**AI-EA**)*

To a solution of propiolaldehyde, arising from propiolaldehyde diethyl acetal (230 mg, 1.8 mmol) hydrolysis (0.2N HCl solution, 5 mL) at 40 °C for 0.5 h, 1-aminoindan (240 mg, 1.8 mmol), dissolved in EtOH (5 mL), was added dropwise.

After being stirred for 2 h at 50 °C, the reaction mixture was diluted with H_2O (20 mL), and EtOH was distilled off. The reaction mixture was extracted with Et_2O. The evaporation of the organic phase gave an oil that was purified by column chromatography eluting with dichloromethane/MeOH 95/5, to afford **AI-EA** (50 mg, 9% yield).

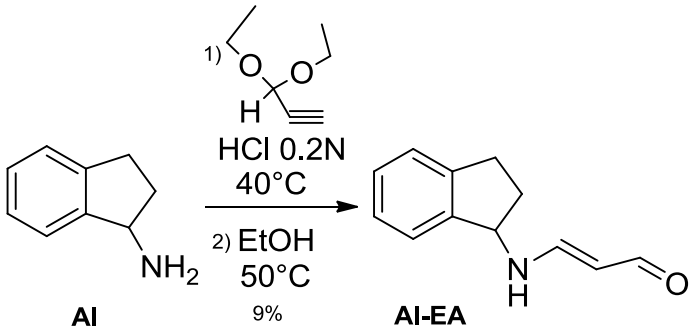

ESI-MS: calculated for $C_{12}H_{13}NO$ *M*= 187.24; Found *m/z* = 188 $[M+H]^+$

^{1}H-NMR *(300 MHz, CD_3OD) δ (ppm): 8.91-8.79 (m; 1H) 7.62-7.44 (m; 1H), 7.25 (m; 4H), 5.52-5.37 (m; 1H), 5.00-4.81 (m; 1H), 3.01-2.90 (m; 2H), 2.58-2.54 (m; 1H), 1.95-1.91 (m; 1H).*

*8.2.10.4 **RG-EA** 3-[2,3-dihydro-1H-inden-1-yl(prop-2-yn-1-yl)amino]prop-2-enal*

To a solution of propiolaldehyde, arising from propiolaldehyde diethyl acetal (230 mg, 1.8 mmol) hydrolysis (0.2N HCl solution, 5 mL) at 40 °C for 0.5 h, **RG** *free base* (307 mg, 1.8 mmol) dissolved in EtOH (5 mL) was added dropwise.

After being stirred for 2 h at 50 °C, the reaction mixture was diluted with H_2O (20 mL), and EtOH was distilled off. The pH of the aqueous phase was adjusted to 12 with 1N NaOH solution, and the reaction mixture was extracted with Et_2O (15 mL). The pooled organic layers (phases) were washed with H_2O. The evaporation of the solvent gave a yellow powder that was purified by column chromatography (ethyl acetate/ petroleum ether 20/80) to afford **RG-EA** (121 mg, 30%).

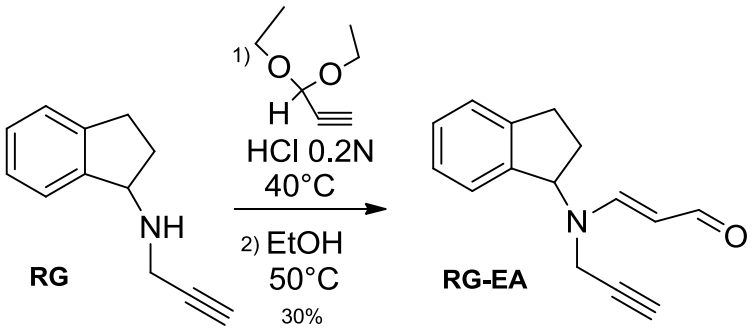

ESI-MS: calculated for $C_{15}H_{15}NO$ *M*= 225.29; Found *m/z* = 226 $[M+H]^+$

^{1}H-NMR *(300 MHz, $CDCl_3$) δ (ppm): 9.12 (d, J=7.9; 1H), 7.28-7.19 (m, 5H) 5.44 (dd, J=8.2; J=13.1; 1H), 5.06 (s, 1H), 3.79-3.77 (m; 2H), 3.03-2.87 (m; 2H), 2.54-2.51 (m; 1H), 2.28-2.15 (m; 2H).*

8.2.10.5 ***MS-PROP*** *(3-[(2-hydroxyethyl)thio]- 2-Propenal)*

To a solution of propiolaldehyde, arising from propiolaldehyde diethyl acetal (230 mg, 1.8 mmol) hydrolysis (0.2N HCl solution, 5 mL) at 40 °C for 0.5 h, 2-mercaptoethanol (140 mg, 1.8 mmol) dissolved in EtOH (5 mL) was added dropwise.

After being stirred for 2 h at 50 °C, the reaction mixture was diluted with H_2O (20 mL), and EtOH was distilled off. The pH of the aqueous phase was adjusted to 12 with 1N NaOH solution, and the reaction mixture was extracted with Et_2O. The pooled organic phases were washed with H_2O. The evaporation of the solvent gave **MS-PROP** as a yellow oil (79 mg, 33% yield).

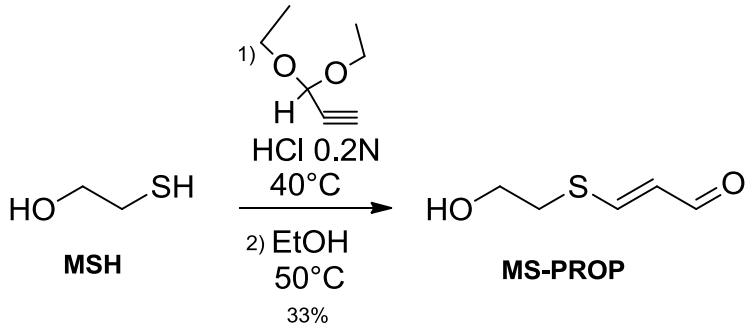

ESI-MS: calculated for $C_5H_8O_2S$ *M*= 132.18; Found *m/z* = 133 $[M+H]^+$

8.3 RESULTS AND DISCUSSION

As previously highlighted in the literature, the metabolic fate of rasagiline was reported in the Azilect® monograph only. Rasagiline is primarily metabolized by hepatic cytochrome P-450 isoenzyme 1A2-mediated *N*-dealkylation followed by renal excretion of the conjugated rasagiline and the conjugated metabolites. The major metabolite is 1-(*R*)-aminoindan, a non-amphetamine compound, lacking the deleterious activity associated with the amphetamine metabolites of the first generation MAO-B inhibitor selegiline. However, since no experimental data could be found in the rasagiline monograph as well as in literature, an *in vitro* metabolism study was undertaken to clarify, in particular, the oxidative metabolic pathways. Indeed, an *in vivo* study could not be suitable for the identification of rasagiline metabolites because of their very low plasma concentrations. The study was performed in the presence of both rat and human subcellular preparations using 500 and 100 µM rasagiline concentrations. In particular the higher rasagiline concentration has been employed to increase the formation of the metabolites allowing their structural identification. However, the incubations were also done at lower concentration (100 µM) to confirm the presence of the metabolites while avoiding the potential formation of artifacts due to the high substrate concentration. Ideally, an even lower rasagiline concentration (e.g. 1 µM) would have been more appropriate to conduct the study in conditions more similar to those *in vivo*. However the LC-MS/MS apparatus used throughout this study does not allow to detect the metabolites at such concentrations.

The LC-ESI-MS analyses of the RLM and HLM incubations, performed at 500 µM, were reported in the figures 1 and 2, revealing that rasagiline was extensively metabolized and beside the well know metabolites aminoindan and 3-hydroxy-rasagiline, four (**AI-EA**, **RG-NOH**, **RG-EA**, **3OH-RG-EA**) new metabolites, arising from oxidative biotransformation, were identified.

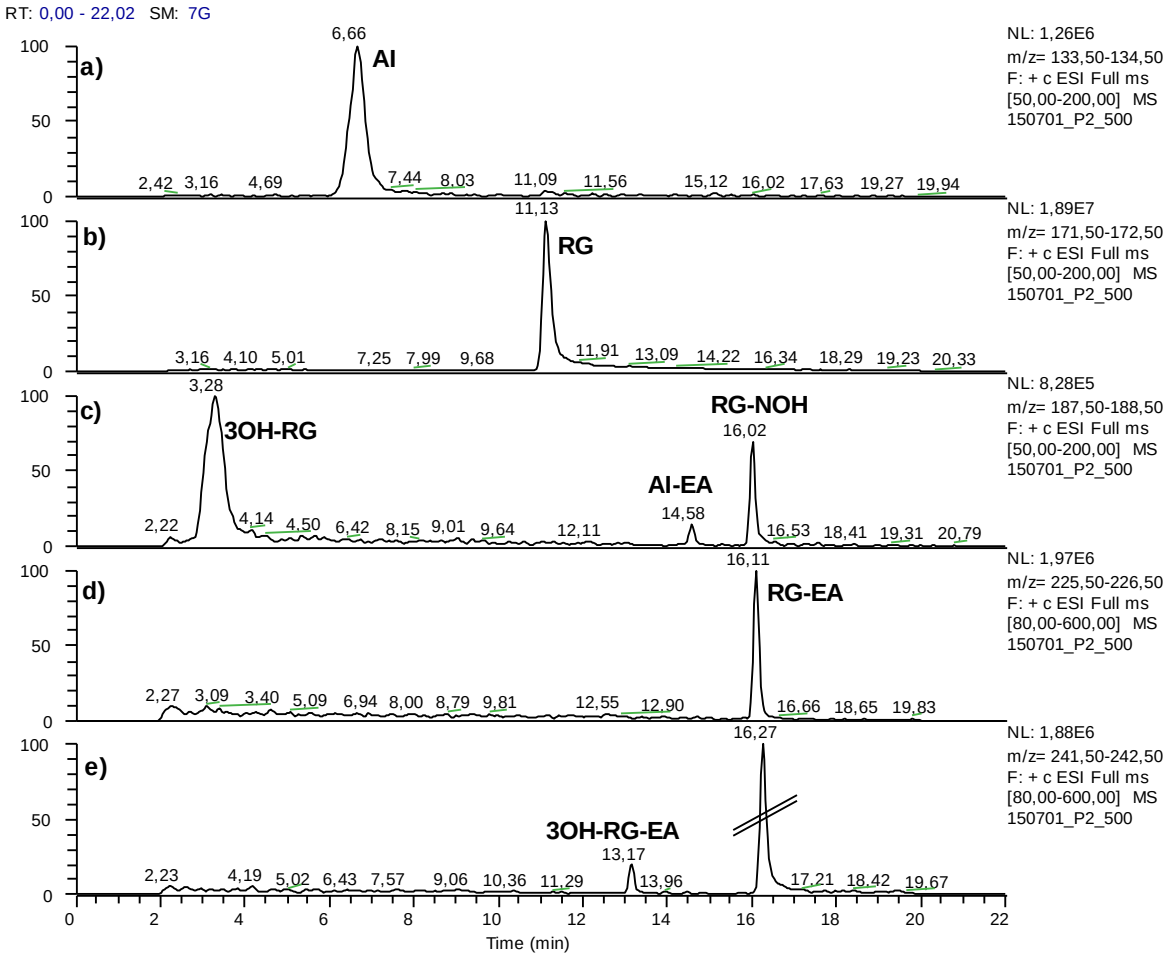

Figure 1. LC-ESI-MS chromatograms (positive mass-range screening) of RLM incubation of **RG** (500 µM): (**a**) *m/z* 134, (**b**) *m/z* 172, (**c**) *m/z* 188, (**d**) *m/z* 226, (**e**) *m/z* 242.

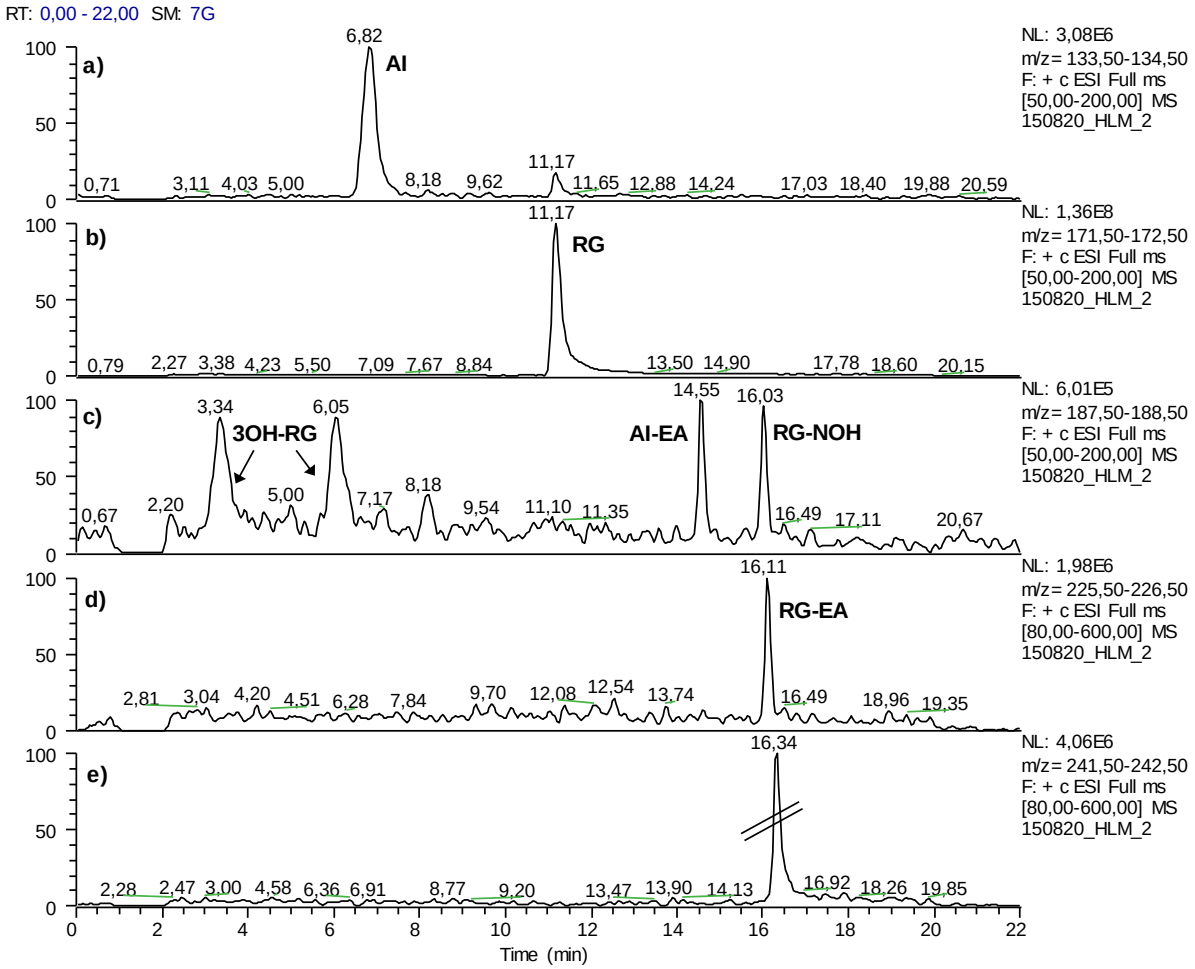

Figure 2. LC-ESI-MS chromatograms (positive mass-range screening) of HLM incubation of **RG** (500 µM): (**a**) *m/z* 134, (**b**) *m/z* 172, (**c**) *m/z* 188, (**d**) *m/z* 226, (**e**) *m/z* 242.

8.3.1 Metabolite 1-(*R*)-aminoindan (*m/z* 134)

As expected, the known metabolite, 1-(*R*)-aminoindan, arising from the oxidative *N*-dealkylation of **RG,** was detected at *m/z* 134 in LC-MS chromatograms of the incubations done in the presence of RLM and HLM preparations (Figures 1a and 2a). Moreover the retention time of the metabolite matched with that of the synthetic standard. According to literature data, **AI** represents, both in rat and human liver preparations, the main metabolite formed in *in vitro* incubations. 1-(*R*)-aminoindan, the major metabolite of rasagiline, is a non-amphetamine metabolite, thus avoiding potent deleterious activity associated with the amphetamine metabolites of the first generation MAO-B inhibitor, selegiline. Various neuroprotective studies demonstrated that **AI** possess beneficial pharmacological effects in animal and cell culture models of PD (Bar-Am et al., 2010).

8.3.2 Metabolites at *m/z* 188

LC-MS^2 analysis performed at *m/z* 188 of RLM and HLM incubations revealed the presence of 3/4 metabolites (**3OH-RG**, **AI-EA** and **RG-NOH**) depending on the species investigated: the protonated molecules (*m/z* 188) suggest that an oxidation occurred with the insertion, for each metabolite, of an oxygen atom on **RG** structure.

It is worth of mention that in the RLM incubations (Figure 1c) only one polar metabolite was formed (**3OH-RG**, peak at 3.28 min) while in HLM incubation (Figure 2c) a couple of metabolites (**3OH-RG**, peaks at 3.34 and 6.05 min) was observed instead.

All the MS^2 spectra of the metabolites **3OH-RG** showed a common fragmentation pattern, characterized by the fragment ions at *m/z* 170 $[M+H-18]^+$ and at *m/z* 133 $[M+H-55]^+$ (Figure 3a). These features suggest that metabolites eluting at 3.34 and 6.05 min are diastereomers. This hypothesis was confirmed by the synthesis of the corresponding reference standard compounds whose mass spectral and chromatographic data resulted identical to those of the metabolites. As highlighted in the introduction, the formation of **3OH-RG** was already reported in the Azilect® monograph, however no mention was done about the formation of the diastereomers by enzymatic oxidation of the indane scaffold.

LC-MS^2 spectra of metabolites **AI-EA** and **RG-NOH** showed similar fragmentation pathways, being the main fragment ions at *m/z* 117 $[M+H-71]^+$ and at *m/z* 72 $[M+H-116]^+$ (Figure 3b,c): unfortunately these ions were not sufficiently diagnostic for the attribution of the structures to the metabolites.

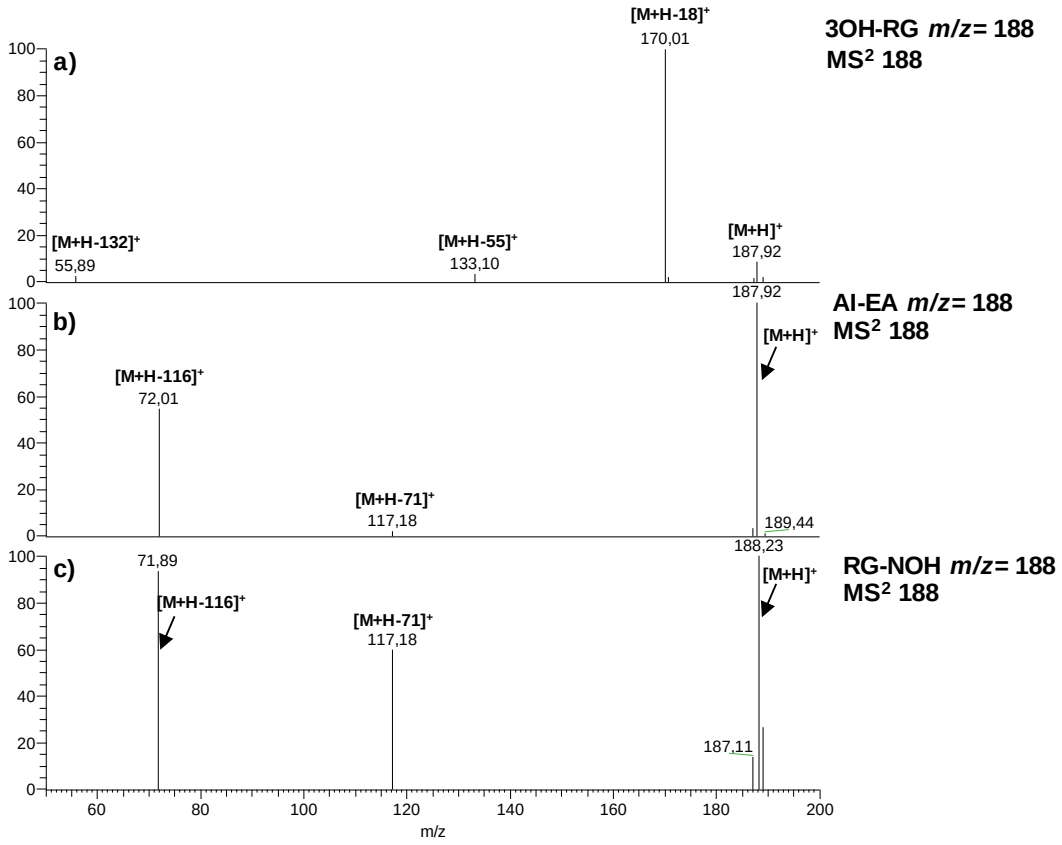

Figure 3. LC-MS^2 spectra of the metabolites **3OH-RG**, **AI-EA** and **RG-NOH**

Taking into account the presence of a benzene ring in the structure of rasagiline, the aromatic hydroxylation could form the corresponding hydroxylated metabolites 4-hydroxyrasagiline (**4OH-RG**), 6-hydroxyrasagiline (**6OH-RG**) and 7-hydroxyrasagiline (**7OH-RG**). However this hypothesis was ruled out by the synthesis of the reference standards of these putative metabolites. Their mass spectra showed the fragmentation patterns not comparable (Figure 4) with those of **AI-EA** and **RG-NOH**. In particular the presence of the fragment ion at *m/z* 133 indicated the presence of the hydroxylated benzene ring in the indane scaffold: this feature was not observed in the **AI-EA** and **RG-NOH** mass spectra.

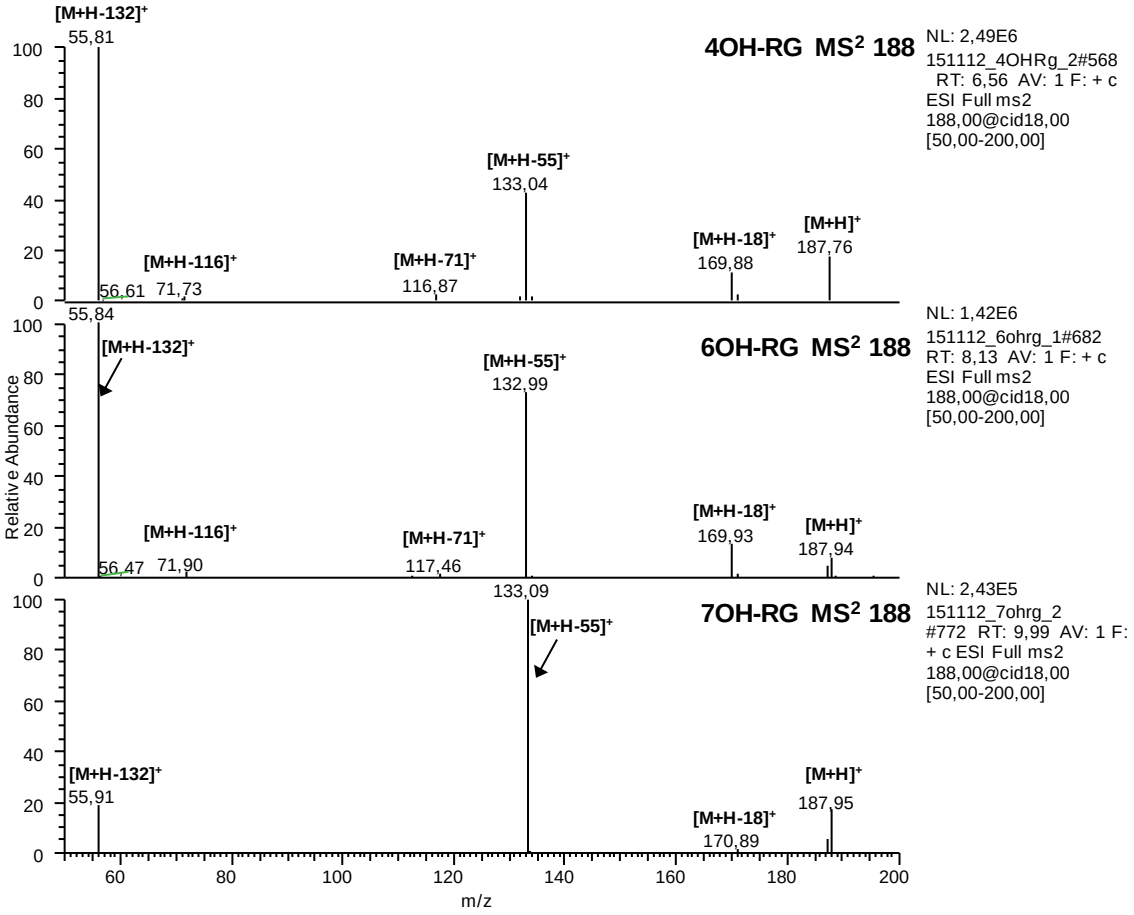

Figure 4. LC-MS^2 spectra of the putative metabolites **4OH-RG**, **6OH-RG** and **7OH-RG**

Moreover, the retention times of the synthetic standards did not match those of the metabolites formed in incubation (Figure 5). Possibly the higher retention time showed by **7OH-RG** (9.95 min) could be due to appreciable *intramolecular* H-bonding (O-H- -N) present only in this isomer as described by Herzig et al. (2006).

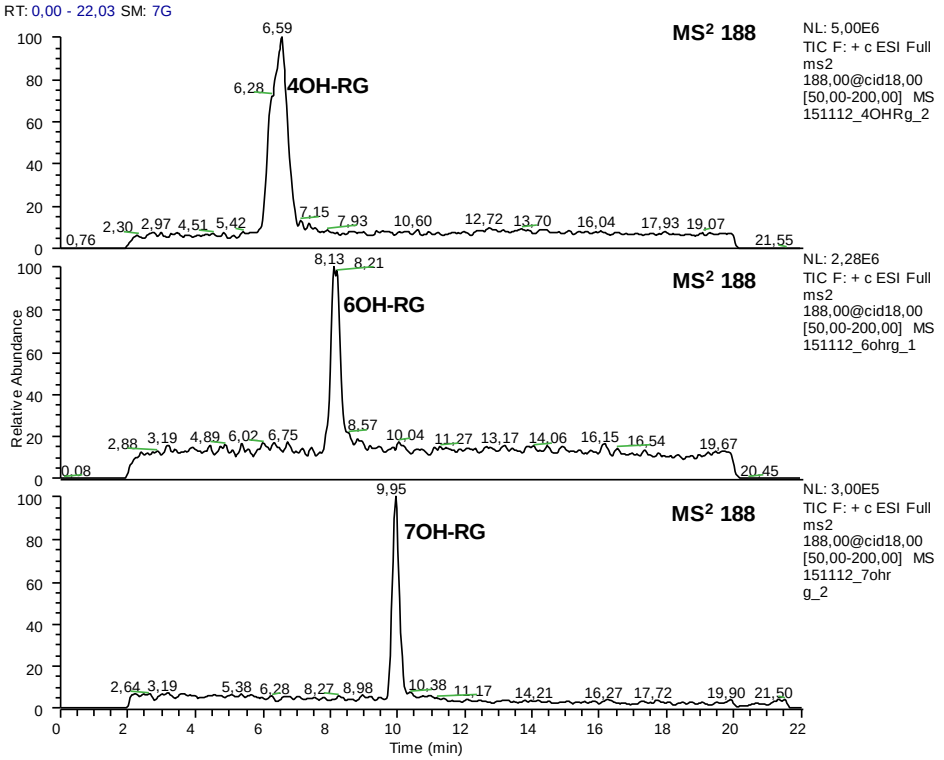

Figure 5. LC-MS^2 chromatograms of the putative metabolites **4OH-RG**, **6OH-RG** and **7OH-RG**

The synthesis of the potential metabolite **5OH-RG** has not been attempted because of the elusive nature of this compound as previously reported by Herzig et al. (2006).

The assignment of the structure to the unknown metabolites **RG-NOH** and **AI-EA** was performed by comparison of their mass spectral and chromatographic data with those of the corresponding reference standards synthetized on the basis of the following hypothesis.

8.3.2.1 ***RG-NOH***

The presence in the **RG** structure of a secondary amine function, susceptible to oxidation, suggested the formation of rasagiline hydroxylamine whose synthesis, starting from rasagiline, was performed following the method reported by Hanson et al. (2010); the procedure involved the *N*-alkylation of the secondary amine with acrylonitrile, followed by *N*-oxidation with *m*-CPBA and Cope elimination of the protecting group.

Indeed, hydroxylamine are important metabolic products of *N*-oxidation of aliphatic primary and secondary amines. However, many are unstable in aqueous solutions in the presence of oxygen, especially at alkaline pH values and in the presence of metal ions (Beckett et al., 1977). As a consequence, the fate of hydroxylamine *in vivo* and *in vitro* conditions is still not well understood. Even if, in our study, **RG-NOH** appeared stable during the incubation,

sample preparation and analysis procedures, the chemical and metabolic stability of **RG-NOH** were studied more in deep.

*Chemical stability of **RG-NOH***

The chemical stability of **RG-NOH** was evaluated, at room temperature and at 37°C, in the same buffer (50 mM TRIS·HCl, pH 7.4) used in the metabolic study; and at fixed times, aliquots were withdrawn and directly analyzed by the LC-UV method described above.

As determined by LC-UV analyses, **RG-NOH** was stable at room temperature over the time course of 96h. However, when the study was performed at 37°C, **RG-NOH** was not stable forming a degradation product, increasing over the time (Figures 6 and 7) characterized by a retention time lower than **RG-NOH** (8.1 vs 10.12 min), and an absorption maximum higher than **RG-NOH** (281 vs 210 nm): this last feature suggests the presence of a conjugated chromophore.

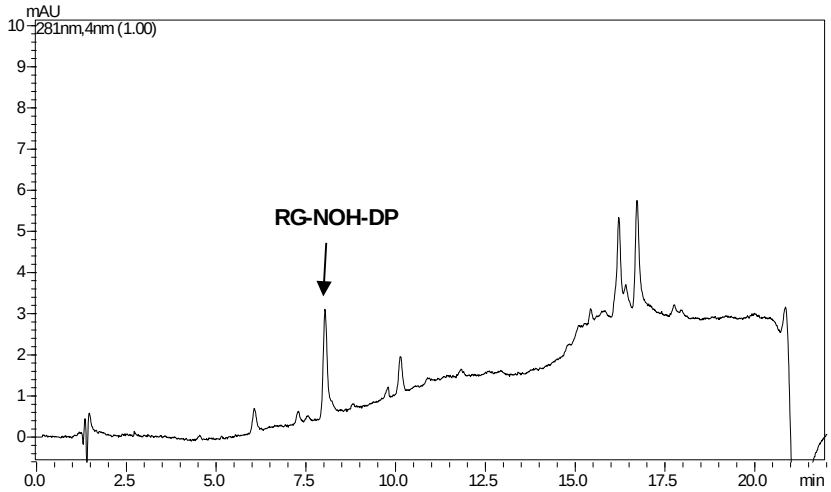

Figure 6. LC-UV chromatogram (λ_a= 281 nm) of **RG-NOH** in pH=7.4 TRIS·HCl buffer at 37°C after 1h.

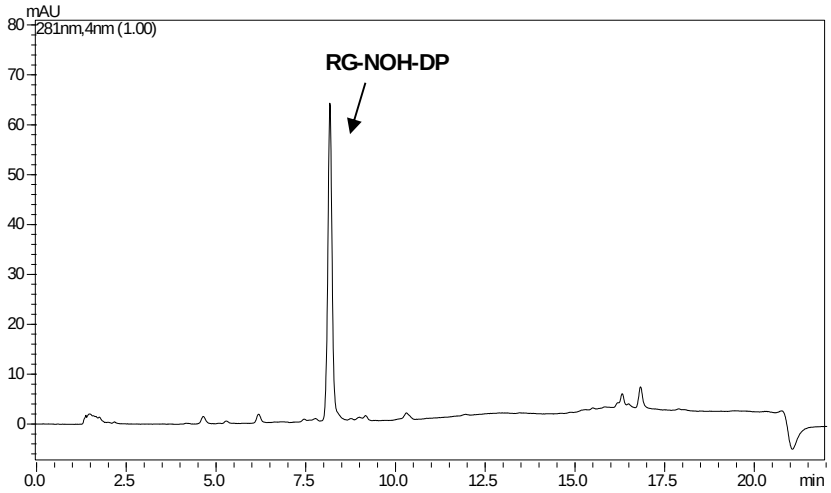

Figure 7. LC-UV chromatogram (λ_a= 281nm) of **RG-NOH** in pH=7.4 TRIS·HCl buffer at 37°C after 23h.

To obtain further information regarding the structure of the degradation product a LC-MS analysis was performed showing the presence of a peak at t_R= 15.02 having a protonated molecule at *m/z* 186 with a loss of 2 amu compared to **RG-NOH** (Fig. 9). The MS/MS spectrum of peak at *m/z* 186 showed a fragment ion at m/z 169 (loss of OH) and a main fragment ion at *m/z* 117 (indane scaffold) corresponding to the neutral loss of 69 Da (the enamine aldehyde moiety). On the basis of these data and of the results obtained in the structure assignment of **AI-EA** (dealing with the structure assigned to **RG-EA**), we tentatively propose for **RG-NOH-DP** the structure reported in the figure 8.

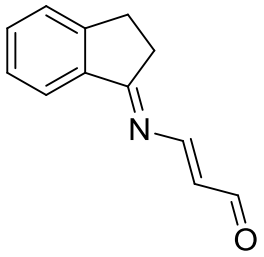

Figure 8. Proposed structure for **RG-NOH-DP**

Since the chemical reactivity of the metabolites and of the degradation products is of relevance in the field of drug stability studies, we evaluate the reactivity of **RG-NOH-DP** in the presence of 2-mercaptoethanol; the LC-MS analysis showed that **RG-NOH-DP** disappeared giving an adduct characterized by a protonated molecule at *m/z* 264 corresponding to the addition of 2-mercaptoethanol to **RG-NOH-DP**.

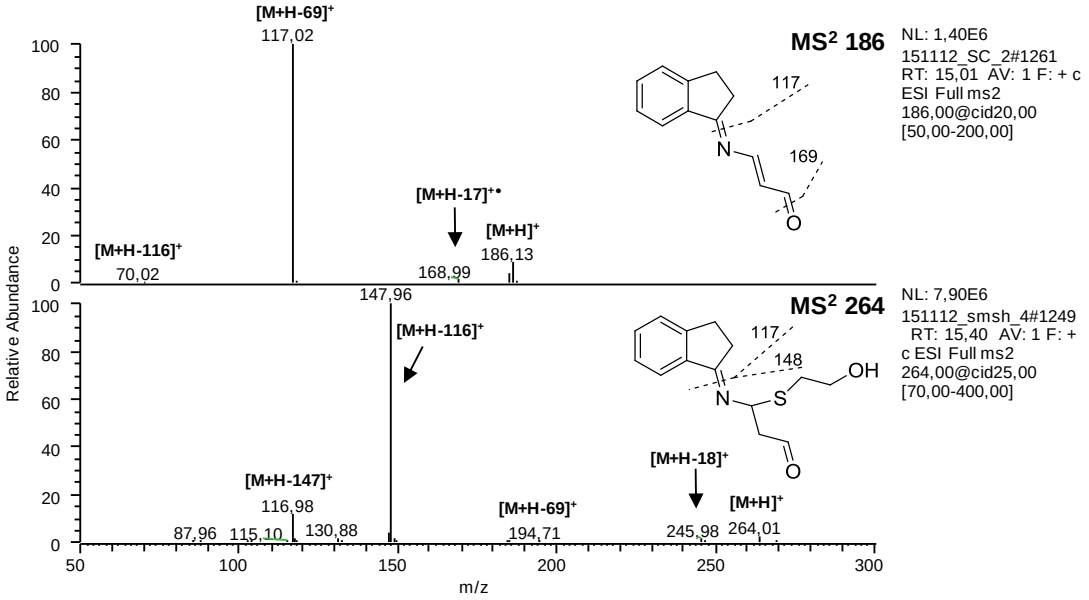

Figure 9. MS^2 spectra of **RG-NOH-DP** and the corresponding 2-mercaptoethanol adduct

Indeed, the mass spectrum of ion at *m/z* 264 (Figure 9) gave a main fragment ion at *m/z* 148 and a minor one at *m/z* 117 both arising from N=C cleavage. Furthermore, the mass spectrum of **RG-NOH-DP** did not show the presence of the fragment ion at *m/z* 148. It is of relevance to note that, per se, **RG-NOH** did not form any adduct in the presence of 2-mercaptoethanol. A search in literature revealed that the stability of primary and secondary hydroxylamines has been studied. In particular, the chemical stability of amphetamine hydroxylamine and methamphetamine hydroxylamine was investigated in pH 8.4 potassium phosphate buffer (Cashman et al., 1999) showing their instability. Amphetamine hydroxylamine, a primary amine, was converted to the corresponding oxime with a half-life of 3.5 h, whereas the half-life of methamphetamine hydroxylamine was significantly longer being approximately of 13h; however the degradation product arising from methamphetamine hydroxylamine has not been defined.

*Phase I metabolic stability of **RG-NOH***

The metabolic stability of **RG-NOH** was assessed by its incubation in the presence of RLM in the same conditions (37°C, 1h) used for rasagiline metabolism. In addition, parallel experiment without the presence of RLM was conducted as control.

The presence of **RG-NOH-DP** was observed both in the incubations with or without microsomes. This result confirmed that the formation of **RG-NOH-DP** is due to the chemical instability of **RG-NOH**. Moreover it is worth of mention that in the incubation of rasagiline in RLM, the formation of **RG-NOH-DP** was not detected over 1h period.

This result could be explained taking into account the fact that **RG-NOH** was formed at low concentration in the incubation mixture and the presence of its degradation product was not detected in this condition.

*Phase II metabolic stability of **RG-NOH***

Glucuronidation and sulfation

To assess the formation of the potential conjugate metabolites of **RG-NOH**, the incubations were carried out in the presence of RLM with UDPGA as cofactor for the glucuronidation and in the presence of rat liver cytosol (RLC), with PAPS as cofactor, for sulfation. The analyses of all the incubations were done by a LC-ESI-MS method in full-scan negative-ion mode. As shown in figure 10, in the presence of RLM/UDPGA, the formation of a metabolite with retention time of 12.7 min was observed, which is not found in control incubations. The metabolite is characterized by a protonated molecule $[M-H]^-$ at *m/z* 362, corresponding to the addition of 175 Da to the mass of the parent drug, suggesting the formation of the glucuronide of rasagiline hydroxylamine. The product ion scan spectra of peak at *m/z* 362 showed the diagnostic fragment ions at *m/z* and 175 $[Gluc-H]^-$ and 157 $[Gluc-H-H_2O]$ whereas the ion at *m/z* 193 is attributable to neutral loss of glucuronic acid (Figure 10).

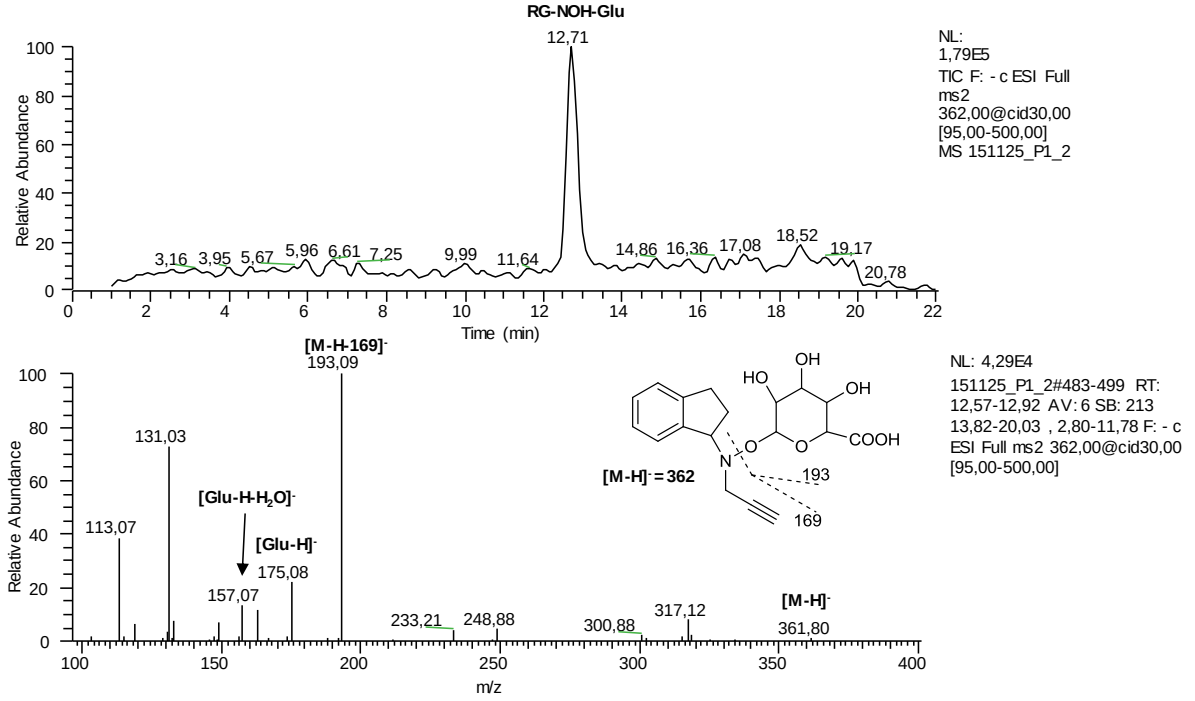

Figure 10. Negative LC-ESI-MS chromatogram of RLM/UDPGA incubation of **RG-NOH** and negative ESI-MS-MS spectrum (*m/z* 362) of peak at t_R= 12.71 minutes

In the case of the incubations performed in the presence of RLC/PAPS, LC-ESI-MS analysis in full-scan negative-ion mode revealed that no sulphate metabolites were formed.

8.3.2.2 ***AI-EA***

Some hypotheses were advanced to clarify the mechanism of formation of the metabolite **AI-EA** (*m/z* 188). According to the well described mechanism of prototropic rearrangement of tertiary propargylamine *N*-oxides (Szabó and Hermecz, 2001), and taking into account the formation in the incubation of **RG-NOH**, it is possible to hypothesize that after the oxidation of rasagiline to **RG-NOH,** the latter could undergo to a rearrangement forming the enamino aldehyde moiety found in the structure of **AI-EA** (Figure 11).

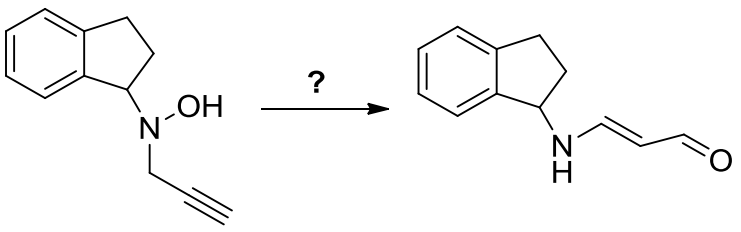

Figure 11. Hypothesis for the formation of **AI-EA** through the rearrangement of **RG-NOH**

However this hypothesis was not confirmed because, as reported above, **RG-NOH** in TRIS buffer (pH 7.4, 50 mM) at 37°C did not form **AI-EA** but the degradation product **RG-NOH-DP** instead. Even if the hypothesis of the rearrangement did not appear correct, nonetheless it suggested the synthesis of the enaminoaldehyde derivative of **AI**. This was easily accomplished by reacting the in situ generated propiolaldehyde with **AI**. The product obtained showed the same mass spectral data and chromatographic characteristics of the metabolite **AI-EA**. The reactivity of propiolaldehyde with amine derivatives to form enaminoaldehyde suggested also another hypothesis to explain the metabolic formation of **AI-EA**. Since the propiolaldehyde was formed during the enzymatic *N*-dealkylation of **RG**, it could react with **AI**. This hypothesis was supported also by the high concentration (500µM) of rasagiline used in the incubation: indeed, in this condition, it is reasonable to postulate that propiolaldehyde and **AI** reach a sufficient concentration to react each other forming eventually **AI-EA**.

However the incubation performed in the presence of 2-mercaptoethanol did not cause a decrease in the formation of **AI-EA**. Indeed 2-mercaptoethanol reacts with propiolaldehyde to give the corresponding addiction compound and preventing the reaction with rasagiline. Similarly, the incubation of rasagiline performed at lower concentration (100µM) did not cause the expected decrease of **AI-EA** formation. Interestingly this result is the opposite of that observed in the case of the metabolites **RG-EA** and **3OH-RG-EA**. Taking together these experimental data allowed to exclude the involvement of propiolaldehyde in the metabolic formation of **AI-EA**. Further investigation is required to establish the mechanism of formation for the metabolite **AI-EA**.

8.3.3 Metabolites RG-EA (*m/z* 226) and 3OH-RG-EA *(m/z* 242)

The formation of metabolite **RG-EA** (*m/z* 226) was observed in RLM and HLM incubations performed at 500µM rasagiline concentration (Figura 1d,e and 2d,e), whereas at 100µM rasagiline concentration **RG-EA** was not detected.

The protonated molecule $[M+H]^+$ at *m/z* 226 (+54 Da more than **RG**) suggested the addition of propiolaldehyde to the structure of rasagiline. The rationale of this hypothesis was based on the known reactivity of propiolaldehyde with the amine derivatives to form the enaminoaldehyde. Indeed, since the propiolaldehyde was formed during the enzymatic *N*-dealkylation of **RG**, it could react with another molecule of **RG** to give **RG-EA**; the high concentration (500µM) of rasagiline used in the incubation could favour this reaction. This

hypothesis was supported by the lack of **RG-EA** in the incubations carried out at lower concentration (100 µM) of rasagiline.

To confirm our attribution, we synthetized the reference standard of **RG-EA,** exploiting the reaction of in situ generated propiolaldehyde with rasagiline; the retention time and the mass spectrum of the synthetic standard corresponded with those of the metabolite.

The metabolite **3OH-RG-EA** (*m/z* 242) was observed only in the incubations with RLM at higher concentration of rasagiline (500µM). The protonated molecule at $[M+H]^+$ at *m/z* 242 (+70 Da more than **RG**) and its mass spectrum (Figure 12), showing the presence of the diagnostic fragment ion at *m/z* 224 $[M+H-18]^+$ (H_2O loss), suggested the addiction of propiolaldehyde to the primary metabolite **3OH-RG**.

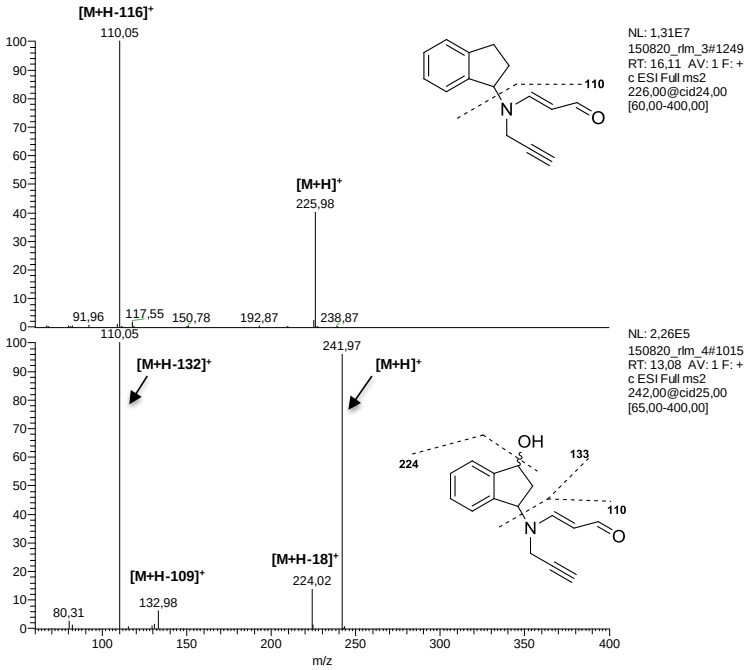

Figure 12. MS^2 spectra of the metabolites **RG-EA** and **3OH-RG-EA**

The proposed mechanism of formation of **RG-EA** and **3OH-RG-EA** was also confirmed by trapping of propiolaldehyde in RLM and HLM incubations using 2-mercaptoethanol as nucleophilic trapping agent; accordingly, in LC-MS^2 chromatograms the metabolites **RG-EA** and **3OH-RG-EA** were not detected in the presence of 2-mercaptoethanol (figures 13b and 14b).

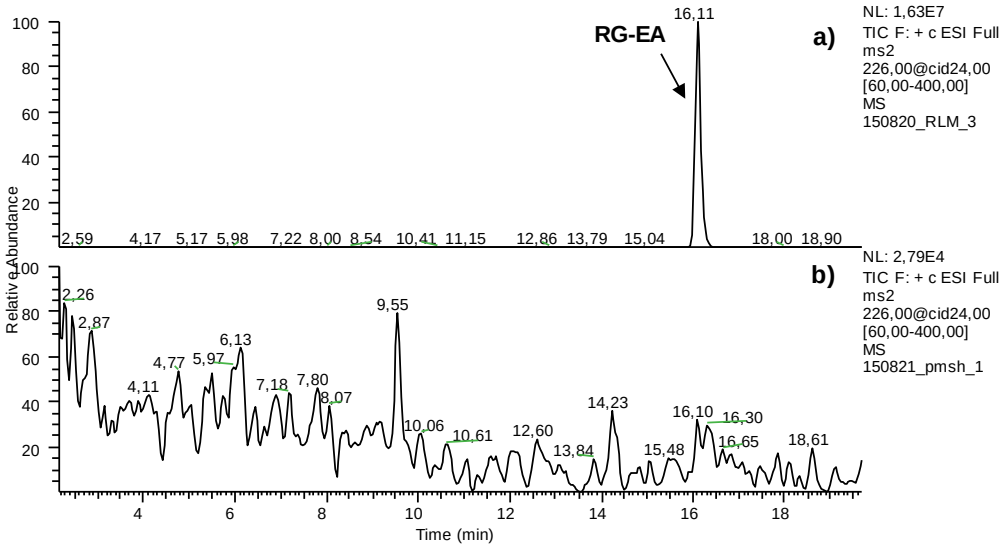

Figure 13. Positive LC-MS^2 chromatograms of RLM incubation (RG:500µM): (a) incubation without 2-mercaptoethanol, (b) incubation with 2-mercaptoethanol (3mM), monitoring the ion at *m/z* 226.

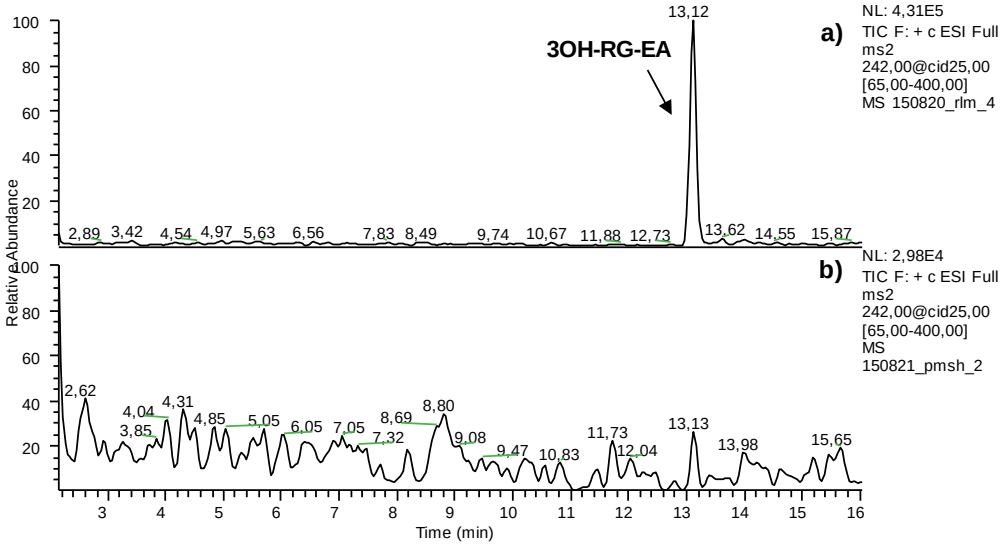

Figure 14. Positive LC-MS^2 chromatograms of RLM incubation (RG:500µM): (a) incubation without 2-mercaptoethanol, (b) incubation with 2-mercaptoethanol (3mM) monitoring the ion at *m/z* 242.

Finally, in the **RG** incubations, done in the presence of 2-mercaptoethanol, the expected formation of the adduct of 2-mercaptoethanol and propiolaldehyde (**MS-PROP**; Figure 15) was observed by LC-UV analysis exploiting its absorption maximum at 291 nm (Figure 16). Indeed, the addiction of 2-mercaptoethanol to propioaldehyde caused a bathochromic spectral shift from 213 to 291 nm as previously highlighted by Demaster et.al (1982) regarding the glutathione-propiolaldehyde-adduct .

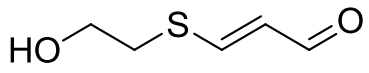

Figure 15. Structure of **MS-PROP**

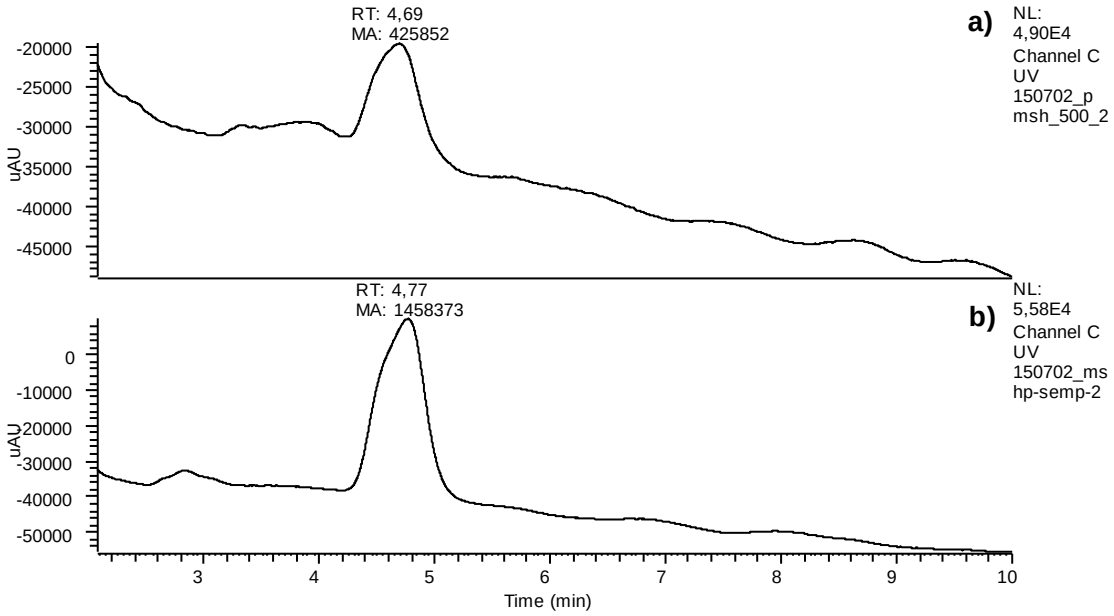

Figure 16. (a) LC-UV chromatogram (λ_a= 291) of RLM incubation (RG: 500µM) in the presence of 2-mercaptoethanol (b) LC-UV chromatogram (λ_a= 291) of the synthetic standard of 2-mercaptoethanol-propioladehyde adduct.

Overall these data suggested that **RG-EA** and **3OH-RG-EA** should not be considered as metabolites but artifacts due to the high concentration of the rasagiline substrate used in the incubations; as a consequence, their formation *in vivo* conditions could be excluded.

Moreover, to complete the investigation, HIM incubations were performed to evaluate the oxidative metabolism of rasagiline: no metabolites were formed in this condition.

8.4 CONCLUSION

The metabolic scheme for the *in vitro* metabolism of **RG** was shown in Figure 17 and was elucidated in presence of both rat and human microsomes. The structural characterization of unknown metabolites was performed by means of LC-MS and LC-UV analysis. Beside the well-known 1-(*R*)-aminoindan and 3-hydroxy-rasagiline some new metabolites arising from oxidative metabolism were identified. Rasagiline underwent *N*-oxidation giving the corresponding hydroxylamine **RG-NOH** and possibly **AI-EA** whose mechanism of formation is still under investigation. The presence of **RG-NOH** was confirmed by glucuronidation of hydroxylamine function and by means of its synthesis. Moreover the metabolite **AI-EA** was observed even if the mechanism of its formation was not clarified. The metabolites **RG-EA** and **3OH-RG-EA** formed by the addition of propiolaldeide were considered artifacts since their presence was detected in incubations performed at 500µM of **RG**.

The pharmacological activity of rasagiline metabolites will be evaluated studying the potential activity of these compounds as MAO enzyme inhibitors. Besides, **AI-EA**, **RG-NOH** and **RG-EA** will be tested on indoleamine 2,3-dioxygenase (IDO) enzyme, since the indan scaffold could have a favourable role in its inhibition. This is relevant since IDO enzyme is involved in pathological immune escape and has recently become an attractive target for anti-cancer therapy.

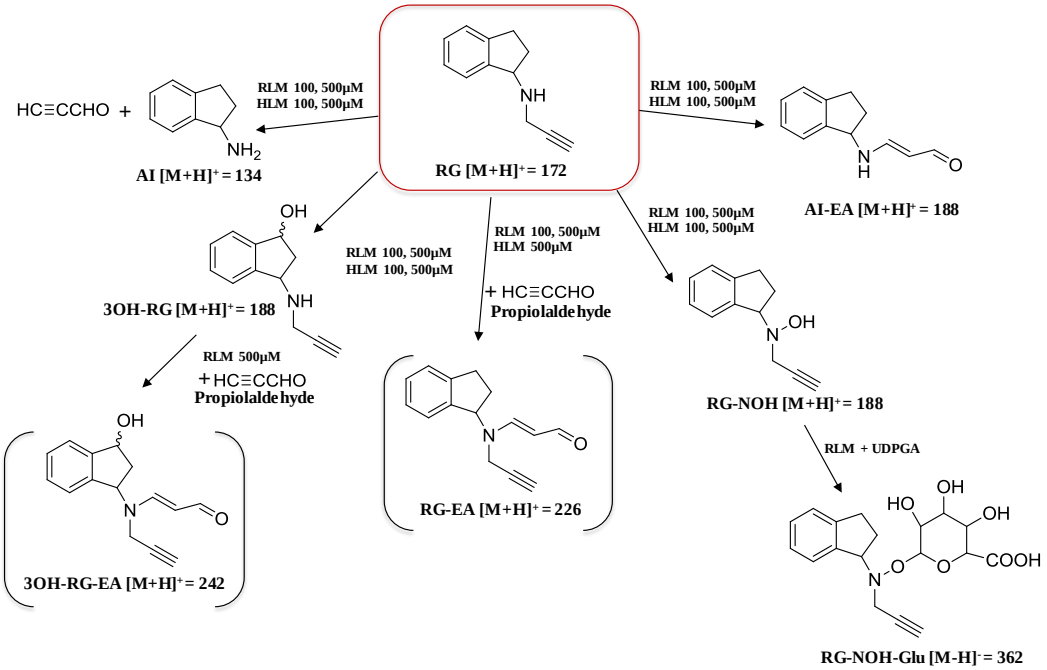

Figure 17. *In vitro* metabolic scheme of rasagiline. The structures in parentheses indicate the artifacts

8.5 REFERENCES

Azilect® rasagiline mesylate (package insert), 2006 Kansas City, MO: TEVA neuroscience.

Bar-Am, O., Weinreb, O., Amit, T., and Youdim, M. B. H. (2010). The neuroprotective mechanism of 1-(*R*)-aminoindan, the major metabolite of the anti-parkinsonian drug rasagiline. *Journal of Neurochemistry*, *112*, 1131–1137.

Beckett A.H., Purkayastha A.R., Morgan P. H. (1977). Oxidation of aliphatic hydroxylamines in acqueos solutions. *Journal of Pharmacy and Pharmacology*, *29*, 15–21.

Cashman, J., Xiong, Y. N., Xu, L., & Janowsky, A. (1999). *N*-Oxygenation of Amphetamine and Methamphetamine by the Human Flavin-Containing Monooxygenase (Form 3): Role in Bioactivation and Detoxication. *The Journal of Pharmacology and Experimental Therapeutics*, *288*(3), 1251–1260.

Chen, J.J., Swope, D. M. (2005). Clinical Pharmacology of Rasagiline: A Novel, Second-Generation Propargylamine for the treatment of Parkinson Disease. *Therapeutic Review*, *45*, 878–894.

Chen, J. J., Swope, D. M., & Dashtipour, K. (2007). Comprehensive Review of Rasagiline, a Second-Generation Monoamine Oxidase Inhibitor, for the Treatment of Parkinson's Disease. *Clinical Therapeutics*, *29*(9), 1825–1849.

Demaster Eugene G., Sumner Hatton W., Kaplan Eli, Shirota Frances N., Nagasawa H. T. (1982). Pargyline-induced hepatotoxicity: possible mediation by the reactive metabolite, propiolaldehyde. *Toxicology and Applied Pharmacology*, *65*, 390–401.

European Medicines Agency, Product information, http://www.ema.europa.eu/docs/en_GB/document_library/EPAR__Product_Information/human/000574/WC500030048.pdf , 2009; last accessed 28th December 2015

European Medicines Agency, Scientific discussion, http://www.ema.europa.eu/docs/en_GB/document_library/EPAR__Scientific_Discussion/human/000574/WC500030046.pdf, 2005; last accessed 28th December 2015

Finberg, J. P. M. (2010). Pharmacology of Rasagiline , a New MAO-B Inhibitor Drug for the Treatment of Parkinson's Disease with Neuroprotective Potential. *Rambam Maimonides Medical Journal*, *1*(1), 1–10.

Gong B., Boor PJ., (2006). The role of amine oxidases in xenobiotic metabolism. *Expert Opinion on Drug Metabolism & Toxicology*, 2, pp.559–71.

Hanson, K. L., Vandenbrink, B. M., Babu, K. N., Allen, K. E., Nelson, W. L., & Kunze, K. L. (2010). Sequential Metabolism of Secondary Alkyl Amines to Metabolic- Intermediate Complexes : Opposing Roles for the Secondary Hydroxylamine and Primary Amine Metabolites of Desipramine, (S)-Fluoxetine, and N- Desmethyldiltiazem. *Drug*

Metabolism and Disposition, *38*, 963–972.

Herzig, Y. et al., (2006). Hydroxy-1-aminoindans and derivatives: preparation, stability, and reactivity. *Journal of Organic Chemistry*, *71*(11), pp.4130–40.

Lecht, S., Haroutiunian, S., Hoffman, A., & Lazarovici, P. (2007). Rasagiline - A novel MAO B inhibitor in Parkinson's disease therapy. *Therapeutics and Clinical Risk Management*, *3*(3), 467–474.

Luan, F. et al., (2013). TOPS-MODE model of multiplexing neuroprotective effects of drugs and experimental-theoretic study of new 1,3-rasagiline derivatives potentially useful in neurodegenerative diseases. *Bioorganic and Medicinal Chemistry*, 21(7), pp.1870–1879.

Ma, J., Chen, X., Duan, X., Deng, P., Wang, H., & Zhong, D. (2008). Validated LC–MS/MS method for quantitative determination of rasagiline in human plasma and its application to a pharmacokinetic study. *Journal of Chromatography B*, *873*, 203–208

Song, M., Wang, L., Zhao, H., Hang, T., Wen, A., Yang, L., & Jia, L. (2008). Rapid and sensitive liquid chromatography-tandem mass spectrometry: assay development, validation and application to a human pharmacokinetic study. *Journal of Chromatography. B, Analytical Technologies in the Biomedical and Life Sciences*, *875*(2), 515–21.

Sterling, J. et al., (2002). Novel Dual Inhibitors of AChE and MAO Derived from Hydroxy Aminoindan and Phenethylamine as Potential Treatment for Alzheimer's Disease. *Journal of Medicinal Chemistry*, 45, pp.5260–5279.

Szabó, A. & Hermecz, I. (2001). Novel intramolecular rearrangement of tertiary propargylamine N-oxides. *Journal of Organic Chemistry*, 66(21), pp.7219–22.

Tabakman R., Lecht S., Lazarovici, P., (2004). Neuroprotection by monoamine oxidase B inhibitors: a therapeutic strategy for Parkinson's disease? *Bioessays*, 26, pp.80–90.

Youdim, M.B.H., Gross, A. & Finberg, J.P.M. (2001). Rasagiline [*N*-propargyl-1R(+)-aminoindan], a selective and potent inhibitor of mitochondrial monoamine oxidase B. *British Journal of Pharmacology*, 132(2), pp.500–506.

CHAPTER 9. Conclusion

In this work, the study of the chemical and metabolic stability of oxybutynin, selegiline and rasagiline has been addressed and new degradation products and metabolites were identified. Overall, the results and, in particular, the similarity observed in the chemical and metabolic degradation of these drugs, confirmed the rationality in conducting the study in an integrated manner. Indeed, oxybutynin, selegiline and rasagiline underwent to extensive *N*-oxidation, both in chemical and metabolic stability studies. The *N*-oxidation of tertiary propargylamines (**Oxy** and **SG**) is characterized by the formation of unstable *N*-oxides which are involved in the generation of their rearrangement products, **Oxy-EK** and **SG-EA**.

Contrary to **Oxy** and **SG** *N*-oxides, the stability of **Oxy-EK** and **SG-EA** allow their use as the indicator of stability in the development and validation of stability-indicating analytical methods used in drug substance and drug product stability studies. Similarly, the formation of *N*-oxides of **Oxy** and **SG** and the corresponding metabolites **Oxy-EK** and **SG-EA** were also observed in microsomal incubations: their mechanism of formation was the same found in the chemical stability study.

The chemical oxidation of the secondary propargylamine **RG** give rise to the corresponding rasagiline hydroxylamine (**RG-NOH**) or the enaminoaldehyde derivative **RG-EA** depending on the stressor used (hydrogen peroxide or **ACVA** respectively). While the mechanism of formation of **RG-NOH** in the presence of hydrogen peroxide could be easily attributed, the formation of **RG-EA** remains to establish. Moreover, the presence of **RG-NOH** and **AI-EA** was found in the *in vitro* metabolism: interestingly, while the enzymatic oxidation of **RG** to **RG-NOH** corresponds to a known metabolic pathway, the formation of **AI-EA** through **RG** enzymatic oxidation was not fully understood at the present time.

As expected, the oxidative chemical degradation of propargylamines is dependent on the pH and the unionized form results more prone to oxidation than the protonated one. This feature should be taken into account in the stability study of drug products (e.g. transdermal delivery system) containing **Oxy**, **SG** and **RG** in their unionized forms.

The presence in the structure of **Oxy-EK**, **SG-EA** and **RG-EA** of a α,β-unsaturated carbonyl function, which could behave as a Michael acceptor reacting with nucleophilic functions of biological macromolecules, suggest to test these compounds for their potential toxicity/genotoxicity. At present time, the mutagenic power of **Oxy-EK** was evaluated indicating a lack of mutagenic effects for this compound. Moreover, the potential pharmacological activity of metabolites found in the present study will be investigated

(antimuscarinic activity, monoamine-oxidase (MAO) and indoleamine 2,3-dioxygenase (IDO) enzyme inhibition and neuroprotective activity).

At the end of this study on chemical and metabolic stability studies of **Oxy**, **SG** and **RG** a complete scenario on the reactivity of these compounds was achieved.

CHAPTER 10. *In vitro* phenotyping: new insights with the cocktail approach

The following study was carried out during my PhD term abroad at the University of Geneva (Laboratory of Pharmaceutical Analytical Chemistry, School of Pharmaceutical Sciences) under the supervision of Prof. Serge Rudaz.

10.1 INTRODUCTION

Cytochromes P450 (CYPs) are the major phase I metabolic enzymes involved in the biotransformation of xenobiotics and endogenous compounds. The activity of CYPs is characterized by a high interindividual variability due to environmental factors (e.g., diet, drug therapy, toxic substances) and/or genetic polymorphisms, which are part of the individual CYP phenotype. Certain major isoforms of the CYP superfamily involved in the metabolism of marketed drugs (CYP2C9, CYP2C19, and CYP2D6) are recognized as highly polymorphic. According to the type of allelic variant affecting these CYPs, genetic polymorphism can significantly alter their metabolic activity, thus modifying the clinical response and/or increasing the risk of drug-drug interactions (DDI).

The evaluation of genetic polymorphism can be performed by sequencing the DNA of the CYP genes (genotyping) or by determining the CYP expression/activity (phenotyping). In certain cases, owing to the genetic and epigenetic regulations, the relationship between the CYP gene and the enzymatic activity is not trivial, which makes the test selection (e.g., constitutional or functional) for predicting the drug's clinical response difficult.

Currently, *in vitro* phenotyping of CYPs has been successfully used to enhance the background understanding of the behavior of polymorphic CYPs involved in xenobiotic metabolism and DDI. The cocktail approach is an advantageous strategy used to monitor the activities of several cytochromes P450 (CYPs) in a single test to increase the throughput of *in vitro* phenotyping studies.

The Geneva cocktail assay was developed with eight CYP-specific probe substrates to simultaneously evaluate the activity of the most important CYPs, namely, CYP1A2, CYP2A6, CYP2B6, CYP2C9, CYP2C19, CYP2D6, CYP2E1, and the CYP3A subfamily. After cocktail incubation in the presence of human liver microsomes (HLMs), the eight selected substrates and their specific metabolites were analyzed by ultra-high-pressure liquid

chromatography and electrospray ionization quadrupole time-of-flight mass spectrometry. The cocktail was previously tested on HLMs with different allelic variants and in presence of selective inhibitors. The results were in agreement with the genetic polymorphisms of the CYPs and the expected effect of the alterations, confirming the reliability of this cocktail assay for phenotyping of the microsomal CYPs (Spaggiari et al., 2014).

In this work the cocktail was tested in presence of oxybutynin (**Oxy**) and oxybutynin metabolites (*N*-desethyloxybutynin (**Oxy-DE**) and **Oxy-EK**) studying the effect of these metabolites as potential inhibitor of CYPs. This application was suggested by considering that metabolites, as novel chemical entities, may be involved in unpredicted drug-drug interactions.

10.2 EXPERIMENTAL

10.2.1 Materials and methods

Methanol (MeOH), acetonitrile (ACN), and water of ultra LC–MS grade were purchased from Biosolve (Valkenswaard, Netherlands). Formic acid (98–100 %) was obtained from Merck (Darmstadt, Germany). Chlorzoxazone (98 %), 6-hydroxychlorzoxazone (97 %), (±)-4-hydroxymephenytoin (98 %), 4′-hydroxyflurbiprofen (98 %), and hydroxybupropion (95 %) were purchased from Toronto Research Chemicals (Toronto ON, Canada). Potassium hydroxide, 4-(2-hydroxyethyl)piperazine-1-ethanesulfonic acid sodium salt (HEPES) (99.5 %), dextromethorphan hydrobromide (99 %), dextrorphan tartrate (98 %), bupropion hydrochloride (98 %), phenacetin (97 %), acetaminophen (99 %), flurbiprofen (99 %), coumarin (99 %), 7-hydroxycoumarin (99 %), were obtained from Sigma-Aldrich (Buchs, Switzerland), whereas methanolic stock solutions of midazolam and 1-hydroxymidazolam were purchased from Lipomed (Arlesheim, Switzerland). (S)- Mephenytoin (99 %) was obtained from Enzo Life Sciences (Lausen, Switzerland), reduced β-nicotinamide adenine dinucleotide 2′-phosphate tetrasodium salt (NADPH) (96 %) was obtained from Applichem (Darmstadt, Germany). Pooled HLMs from 30 donors were purchased from BD Biosciences (Allschwil, Switzerland). The substrate, metabolite, and inhibitor stock solutions at 1 mg/mL were prepared in MeOH and stored at −20 °C for 6 months or less.

Oxybutynin, **Oxy-DE** and **Oxy-EK** were supplied by the Laboratory of Pharmaceutical and Analytical Chemistry, Department of Pharmaceutical Sciences (Novara).

10.2.2 UHPLC-QTOF instrumentation

The chromatographic analyses were performed with an Acquity UPLC system (Waters, Milford, MA, USA) able to deliver mobile phases at a pressure of up to 1,000 bar. The equipment includes a binary solvent manager with a maximum delivery flow rate of 2 mL/min, an autosampler with a 2-µL loop operating in full-loop injection mode, and a column manager composed of a precolumn eluent heater and a column oven set to 40 °C. The UPLC system was coupled in an optimized configuration with a Xevo® QTOF mass spectrometer (Waters, Milford, MA, USA) fitted with a Z-spray electrospray ionization (ESI) source. The samples were stored at 4 °C in the autosampler prior to and during the analysis. Data acquisition, data handling, and instrument control were performed by MassLynx version 4.1 (Waters, Milford,MA, USA). The reversed-phase LC separations were performed on a Waters 100 mm×2.1 mm XBridge™ BEH C_{18} XP column with 2.5-µm particle size and a flow rate of 400 µL/min in gradient mode (solvent A, water with 0.1 % formic acid; solvent B, ACN with 0.1 % formic acid, 2–75 % solvent B in 15 min, up to 95 % solvent B in 0.2 min, held at 95 % solvent B to 0.5 min, then column reconditioning at 2 % solvent B to 18 min), with the eluate from the first 0.5 min diverted to waste.

10.2.3 MS operating conditions

The analysis were carried out in TOF detection mode. Regarding the MS operating conditions, the desolvation gas (nitrogen) flow was set to 1,000 L/h with a temperature of 500 °C, the source temperature was 150 °C, the cone gas (nitrogen) flow rate was 20 L/h, the collision gas (argon) flow rate was 0.2 mL/min, and the capillary voltage was 3.0 kV in the positive mode and 2.4 kV in the negative mode. The cone voltage and the extraction cone voltage were similar in both positive and negative mode at 30 V and 4.1 V, respectively. The data were collected in the V-optics centroid mode over an m/z range of 100–1,000 with an accumulation time of 0.2 s. An independent reference lock-mass ion was infused through the LockSpray™ interface to ensure accuracy and to decrease acquisition variability. A solution of leucine-enkephalin (m/z 556.2771) at a concentration of 0.2 µg/mL in 1:1 (*v/v*) ACN/water plus 0.1 % formic acid was used as the reference compound and was infused at a flow rate of 10 µL/min. The LockSpray frequency was set to 20 s (scan duration of 1 s) and the data were averaged over five spectra.

10.2.4 Incubation method

All of the microsomal incubations were performed in duplicate in a final incubation volume of 100 µL. The reaction medium contained 50 mM HEPES (pH 7.4), excess NADPH, 0.5 mg protein per milliliter of HLMs, and the cocktail of substrates. The final substrate concentrations were obtained by adding the required volume of the cocktail solution to the reaction medium. These concentrations were as follows: 50 µM for phenacetin, 2 µM for coumarin, 5 µM for bupropion, 5 µM for flurbiprofen, 100 µM for (S)-mephenytoin, 5 µM for dextromethorphan, 40 µM for chlorzoxazone, and 2.5 µM for midazolam. The final organic solvent (MeOH) concentration was 0.5 % (*v/v*). After preincubation for 3 min at 37 °C, the CYP-dependent phase I reactions were initiated by adding excess NADPH (2.0 mM). The incubation proceeded for 20 min at 37 °C under agitation (400 rpm). The enzymatic reaction was stopped by adding 100 µL of ice-cold ACN to the reaction medium. The precipitated proteins were removed by centrifugation (5 min at 10,000 rpm), and an aliquot (150 µL) of the resulting supernatant was transferred to a vial for LC–MS analysis.

Oxy, **Oxy-DE** and **Oxy-EK** were tested at a single concentration of 10 µM. Each reagent was incubated in duplicate with the cocktail of substrates and the pooled HLMs under the previously described incubation conditions.

10.3 RESULTS AND DISCUSSION

The eight CYP probe substrates of the cocktail, namely phenacetin (CYP1A2), coumarin (CYP2A6), bupropion (CYP2B6), flurbiprofen (CYP2C9), (S)-mephenytoin (CYP2C19), dextromethorphan (CYP2D6), chlorzoxazone (CYP2E1), and midazolam (CYP3A subfamily), were selected to monitor simultaneously the metabolic activities of clinically and toxicologically relevant cytochromes in humans. The different substrates of the cocktail and their concentration in incubation are reported in the Table 1.

After cocktail incubation in the presence of human liver microsomes (HLMs), the eight selected substrates and their specific metabolites were analyzed by the UHPLC-(Q)TOF method (Figure 1).

CYP isoform	Probe substrate	CYP-specific reaction	CYP-specific metabolite	K_m[a] (μM)	Concentration for incubation (μM)	Exact mass (*m/z*)	Polarity
1A2	Phenacetin	O-Deethylation		1.7-152	50	180.1024	ES^+
			Acetaminophen			152.0675	ES^+
2A6	Coumarin	7-Hydroxylation		0.3-2.3	2	147.0446	ES^+
			7-Hydroxycoumarin			163.0395	ES^+
2B6	Bupropion	Hydroxylation		67-168	5	240.1155	ES^+
			Hydroxybupropion			238.0998 ($-H_2O$)	ES^+
2C9	Flurbiprofen	4′-Hydroxylation		6-42	5	199.0923 ($-COO$)	ES^-
			4′-Hydroxyflurbiprofen			215.0875 ($-COO$)	ES^-
2C19	(*S*)-Mephenytoin	4′-Hydroxylation		13-35	100	219.1134	ES^+
			(±)-4′-Hydroxymephenytoin			235.1083	ES^+
2D6	Dextromethorphan	O-Demethylation		0.4-8.5	5	272.2014	ES^+
			Dextrorphan			258.1858	ES^+
2E1	Chlorzoxazone	6-Hydroxylation		39-157	40	167.9852	ES^-
			6-Hydroxychlorzoxazone			183.9801	ES^-
3A subfamily	Midazolam	1′-Hydroxylation		1-14	2.5	326.0860	ES^+
			1′-Hydroxymidazolam			342.0809	ES^+

Table 1. The substrates selected for the cocktail approach, with their cytochrome P450 (CYP)-specific metabolites and exact detection mass. (ES electrospray) (Spaggiari et al., 2014)

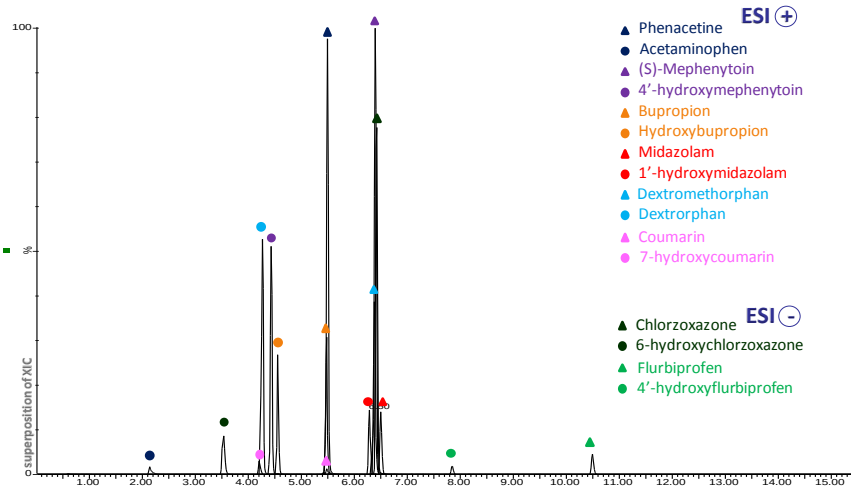

Figure 1. UHPLC-(Q)TOF analysis of substrates and their CYP-specific metabolites of the cocktail microsomal incubations.

On the one hand the mixture of the cocktail was incubated as control, on the other hand the mixture of the cocktail was exposed to inhibitor (**Oxy**, **Oxy-DE** and **Oxy-EK**) to estimate the nature and the impact of the interference on CYP activities. The CYP activity assessment was based on the metabolic ratio (area of CYP-specific metabolite to area of probe substrate). Moreover a radar plot was used as graphical representation of the profile of activity of CYPs to obtain a better comparison of the different assays. For clarity, the activities of the CYPs obtained using the cocktail approach were considered as reference values (e.g., 100 % of phase I activity, red octagon). This reference profile was represented on a radar plot in which each axis corresponds to the relative activity of the CYP. The logarithmic scale affords equivalent visual variations in cases of increasing and respective decreasing activities of the CYPs (Figure 2). For example, an activity increased by a factor of 2 (i.e. 200%) presents the same variation as that reduced by a factor of 2 (i.e. 50%).

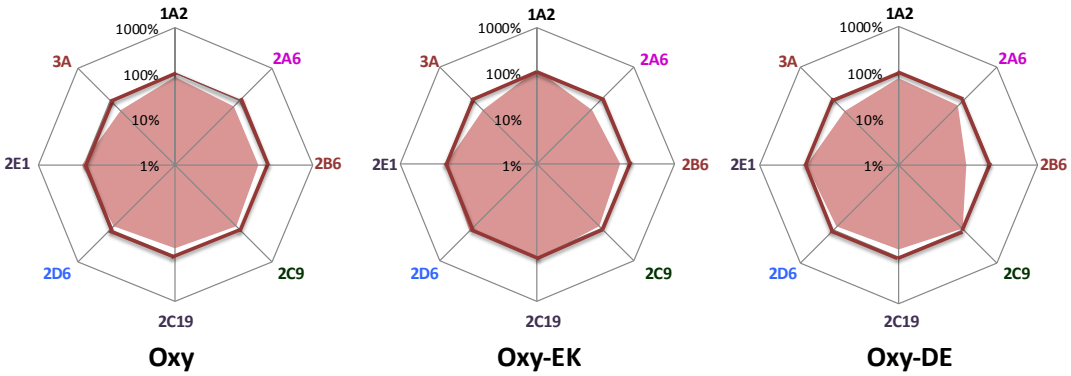

CYPs	Oxy	Oxy-EK	Oxy-DE
1A2	74%	104%	67%
2A6	61%	43%	60%
2B6	61%	59%	27%
2C9	72%	76%	84%
2C19	63%	105%	61%
2D6	73%	108%	72%
2E1	96%	89%	85%
3A subfamily	44%	45%	40%

Figure 2. Radar plot obtained after incubation of **Oxy**, **Oxy-EK** and **Oxy-DE** in presence of the cocktail. CYP metabolic ratios are expressed as a percentage of the metabolic ratios obtained using the cocktail without inhibitor (100%)

The addition of **Oxy**, **Oxy-EK** and **Oxy-DE** at a concentration of 10µM reduced the CYP3A4 activity for each compound, in addition **Oxy-EK** and **Oxy-DE** reduced the activity of CYP2A6 and CYP 2B6 respectively, whereas the activities of the other CYPs monitored were not modified compared with the original profile. These data are to be confirmed in presence of different inhibitor concentrations.

These results allowed us to obtain further information regarding the potential activity of **Oxy** and oxybutynin metabolites as inhibitor of CYP isoforms. Moreover oxybutynin is recognized in literature as inhibitor of isoenzyme 2C8 (Walsky et al., 2005), suggesting to test these compounds in presence of a new cocktail assay in which the isoform 2C8 will be included.

10.4 REFERENCES

Spaggiari, D., Geiser, L., Daali, Y., and Rudaz, S. (2014). Phenotyping of CYP450 in human liver microsomes using the cocktail approach. *Analytical and Bioanalytical Chemistry*, *406*, 4875–4887.

Walsky, R. L., Gaman, E. A., and Obach, R. S. (2005). Examination of 209 Drugs for Inhibition of Cytochrome P450 2C8, *The Journal of Clinical Pharmacology*, *45*, 68–78.

Appendix I. Effect of Oxy and Oxy-EK on the number of spontaneous revertant colonies of *Salmonella typhimurium* TA1535, TA1537, TA1538, TA98 and TA100, and of *Escherichia coli* WP2*uvr*A and WP2*uvr*A/R in the absence of the metabolic activator S9. Values are expressed as means ± SEM (*n* = 6 replicates).

Substance	[µg/plate]	Number of revertant colonies						
		TA1535	**TA1537**	**TA1538**	**TA98**	**TA100**	**WP2*uvr*A**	**WP2uvrA/R**
Oxybutynin	9	149.0 ± 5.8	39.3 ± 2.3	38.7 ± 2.3	47.7 ± 2.2	150.3 ± 9.3	50.5 ± 3.5	151.0 ± 4.5
	13	150.4 ± 7.5	39.7 ± 1.9	39.5 ± 1.7	49.3 ± 2.6	147.7 ± 6.2	49.5 ± 2.6	149.7 ± 7.6
	18	153.2 ± 4.5	42.0 ± 1.7	41.5 ± 1.4	47.0 ± 2.1	147.0 ± 4.1	51.8 ± 3.7	149.4 ± 5.5
	25	153.7 ± 6.4	41.1 ± 3.1	40.8 ± 2.9	49.3 ± 1.8	153.1 ± 7.7	50.5 ± 2.8	153.1 ± 8.6
	36	151.3 ± 8.0	40.1 ± 2.2	40.7 ± 1.6	49.7 ± 2.9	149.7 ± 8.9	50.7 ± 3.1	151.5 ± 6.0
	50	107.5 ± 11.3$^{\sim t}$	31.3 ± 3.5$^{\sim t}$	37.8 ± 1.8$^{\sim t}$	40.0 ± 2.5$^{\sim t}$	121.8 ± 12.9$^{\sim t}$	41.4 ± 5.5$^{\sim t}$	139.1 ± 9.7$^{\sim t}$
Oxy-EK	9	153.8 ± 3.6	39.1 ± 2.6	41.3 ± 1.5	48.7 ± 2.3	152.0 ± 6.1	51.3 ± 1.7	152.2 ± 7.3
	13	154.8 ± 5.6	39.6 ± 2.0	39.4 ± 2.0	48.3 ± 1.8	153.3 ± 4.4	49.4 ± 2.0	153.1 ± 9.8
	18	153.8 ± 7.9	41.2 ± 1.7	40.8 ± 1.7	48.3 ± 3.2	153.5 ± 7.5	50.7 ± 1.5	152.8 ± 8.3
	25	156.0 ± 4.3	41.7 ± 1.5	41.8 ± 1.6	48.0 ± 2.7	154.0 ± 8.5	51.4 ± 1.2	153.4 ± 6.4
	36	152.5 ± 7.4	40.8 ± 2.2	40.7 ± 1.4	49.0 ± 3.2	149.0 ± 5.2	49.9 ± 1.5	150.2 ± 5.8
	50	132.0 ± 9.5$^{\sim t}$	28.7 ± 2.0$^{\sim t}$	32.7 ± 1.4$^{\sim t}$	42.7 ± 1.8$^{\sim t}$	129.4 ± 5.8$^{\sim t}$	44.7 ± 1.4$^{\sim t}$	135.9 ± 6.0$^{\sim t}$
Vehicle		150.7 ± 9.4	39.0 ± 2.1	39.7 ± 1.8	48.0 ± 2.3	148.0 ± 7.3	50.4 ± 1.3	152.0 ± 6.9
2NF	2			164.3 ± 15.3	112.0 ± 9.5			
SA	1	513.7 ± 23.1				512.0 ± 42.6		
MMS	500						223.3 ± 12.5	529.0 ± 11.5
9AA	50		156.0 ± 17.3					

[a] DMSO 50 µl/plate. $^{\sim t}$ Early signs of cytotoxicity (evaluated as a reduction of the revertant colonies without changes in the auxotrophic background lawn).

Appendix II. Effect of Oxy and Oxy-EK on the number of spontaneous revertant colonies of *Salmonella typhimurium* TA1535, TA1537, TA1538, TA98 and TA100, and of *Escherichia coli* WP2*uvr*A and WP2*uvr*A/R in the presence of the metabolic activator S9. Values are expressed as means ± SEM (n = 6 replicates).

Substance	[µg/plate]	Number of revertant colonies						
		TA1535	**TA1537**	**TA1538**	**TA98**	**TA100**	**WP2*uvr*A**	**WP2*uvr*A/R**
Oxybutynin	9	153.2 ± 9.2	42.5 ± 2.4	41.2 ± 2.2	49.7 ± 1.8	149.7 ± 6.8	51.0 ± 3.0	151.7 ± 5.5
	13	153.0 ± 6.4	42.7 ± 2.0	41.9 ± 3.5	49.0 ± 2.1	150.0 ± 4.1	51.7 ± 2.3	152.0 ± 3.4
	18	153.2 ± 3.2	41.9 ± 2.1	42.2 ± 2.1	48.3 ± 2.3	148.3 ± 5.3	51.9 ± 2.0	153.3 ± 4.5
	25	154.8 ± 5.8	43.8 ± 3.4	42.4 ± 1.7	49.7 ± 2.5	149.8 ± 7.6	50.0 ± 1.6	152.2 ± 6.8
	36	153.2 ± 8.5	42.5 ± 2.5	42.6 ± 1.8	49.0 ± 3.2	150.3 ± 3.3	53.2 ± 1.8	152.9 ± 3.9
	50	152.4 ± 7.7	43.2 ± 1.5	41.7 ± 2.9	50.0 ± 3.2	148.8 ± 7.1	51.7 ± 2.2	153.8 ± 3.5
Oxy-EK	9	153.0 ± 5.3	42.2 ± 2.6	41.3 ± 1.5	49.0 ± 1.7	149.0 ± 6.7	50.6 ± 4.1	152.5 ± 4.3
	13	152.5 ± 7.1	42.4 ± 3.5	41.1 ± 2.8	49.5 ± 2.2	149.5 ± 5.2	51.2 ± 5.7	151.9 ± 6.2
	18	154.6 ± 9.5	43.0 ± 2.2	42.4 ± 3.5	49.7 ± 2.3	149.7 ± 3.3	52.4 ± 2.5	151.5 ± 4.4
	25	153.9 ± 8.3	43.7 ± 2.9	42.2 ± 2.6	49.4 ± 3.0	149.3 ± 3.7	52.2 ± 2.6	153.7 ± 5.1
	36	154.7 ± 5.3	43.0 ± 2.7	41.7 ± 1.9	48.2 ± 2.6	149.8 ± 4.9	51.5 ± 1.9	153.1 ± 6.6
	50	153.3 ± 6.0	41.4 ± 2.2	42.6 ± 2.2	50.1 ± 2.7	150.2 ± 6.4	49.5 ± 2.2	149.1 ± 5.2
Vehicle		152.0 ± 5.1	42.0 ± 3.7	40.8 ± 2.9	49.3 ± 2.9	149.2 ± 5.3	51.5 ± 3.7	151.0 ± 4.6
2AA	10	434.8 ± 19.3	423.7 ± 18.5				236.7 ± 9.6	380.3 ± 23.2
2AA	1			438.3 ± 23.5	121.3 ± 11.1	334.8 ± 14.1		

[a] DMSO 50 µl/plate.

Publications

I. Rossana Canavesi, Silvio Aprile, Elena Varese, Giorgio Grosa. Development and validation of a stability-indicating LC–UV method for the determination of pantethine and its degradation product based on a forced degradation study, *Journal of Pharmaceutical and Biomedical Analysis* 2014; 97:141-150

II. Rossana Canavesi, Silvio Aprile, Giovanni B. Giovenzana, Antonella Di Sotto, Silvia Di Giacomo, Erika Del Grosso, Giorgio Grosa. New insights in oxybutynin chemical stability: identification in transdermal patches of a new impurity arising from oxybutynin *N*-oxide rearrangement, *European Journal of Pharmaceutical Sciences* (in press)

Oral communication

- Rossana Canavesi, Giorgio Grosa "Chemical and metabolic stability studies of propargylamine-containing drugs" Summer School on Pharmaceutical Analysis (SSPA) 2015 "Advanced analytical methodologies for medicinal plants characterization", Rimini, September 2015